

CLIMATE CHANGE IMPACT ASSESSMENTS FOR REGIONS OF THE UNITED STATES

By

Ying Tang

A DISSERTATION

Submitted to
Michigan State University
in partial fulfillment of the requirements
for the degree of

Geography--Doctor of Philosophy

2015

ABSTRACT

CLIMATE CHANGE IMPACT ASSESSMENTS FOR REGIONS OF THE UNITED STATES

By

Ying Tang

The Earth's climate is projected to change significantly in the future, which will greatly impact many natural and human systems. Climate projections are important components of climate change impact, vulnerability, and adaptation assessments, and this research aims to examine several issues related to climate models and model projections and the use of these projections in impact assessment studies. The research is composed of three individual studies. The first study compares various methods in generating climate change projections for use in agriculture assessment studies at several lake-modified sites in the Great Lakes region of the United States. By producing climate change projections using different data sources and methods and comparing their similarities and differences, the study hopes to inform impact researchers and decision makers about the various choices for generating climate change projections and their advantages/disadvantages. The second study assesses the skill of regional climate models (RCMs) in simulating low-level wind maxima, often referred to as low-level jets (LLJs). As a pronounced climate feature in central United States, the LLJs have their impacts ranging from wind energy, to precipitation, and to bird migration. Knowing how well RCMs simulate the climatology of LLJ is a necessary first step towards a better understanding of RCMs as a powerful tool for generating regional climate change projections through dynamical downscaling for central US and other regions affected by LLJs. Finally, the third study applies RCM projections to assess the potential risk of

extreme wildfires in the United States. Climate change is expected to alter the frequency and severity of atmospheric conditions conducive to wildfires. Using outputs from a suite of RCMs, this study examines the changes of an operational fire weather index, the Haines Index, between the current climate and the projected future climate. The results are expected to be used to inform fire managers that future summers might be more conducive to extreme and erratic wildfires.

ACKNOWLEDGMENTS

I would like to express the deepest appreciation to my advisor, Dr. Shiyuan Zhong, for her excellent guidance, patience, and for providing me with an excellent atmosphere for doing research. I would like to thank Dr. Julie A. Winkler, for her generous support, caring, and patience in guiding my research and correcting my writing. I would like to thank Dr. Lifeng Luo, who patiently taught me programming with Fortran and bash. I would also like to thank my committee members Mr. Warren E. Heilman and Dr. Pang-Ning Tan for guiding my research and helping me to develop my research background in forestry and computer science. I would also like to thank Mr. Xindi Bian, who always seeks new research ideas, and thank Malgorzata Liszewska and Lydia Rill for providing data for my research.

Many thanks to Mr. Jim Brown and Mr. Wilson Ndovie for computational support, and Ms. Sharon Ruggles, Ms. Judy Reginek, Ms. Claudia Brown, and Ms. Becky Young for administrative support.

I thank my geography colleagues, especially members of the climate group, for providing a pleasant environment for research and life.

Finally, I would like to thank my mother, Danying Shou, and my grandparents, Peifang Xuan and Guangdi Shou, who are always supporting me and encouraging me.

TABLE OF CONTENTS

| | |
|---|-----|
| LIST OF TABLES..... | vi |
| LIST OF FIGURES..... | vii |
| Chapter 1 Background and Research Objectives..... | 1 |
| 1.1 Overview..... | 1 |
| 1.2 Research Objectives..... | 6 |
| 1.2.1 Guidance for Selecting Climate Projections for Assessments..... | 6 |
| 1.2.2 An Evaluation of RCM Simulations of the Low Level Jet Climatology..... | 7 |
| 1.2.3 An Assessment of Lower Atmospheric Conditions Conducive to Extreme Fires.... | 9 |
| 1.3 Dissertation Structure..... | 9 |
| Chapter 2 Guidance for Selecting Climate Projections for Assessments..... | 11 |
| 2.1 Introduction..... | 11 |
| 2.1.1 Overview and General Objectives..... | 11 |
| 2.1.2 Climate Projections for Agricultural Impact Assessments..... | 13 |
| 2.2 Data..... | 18 |
| 2.3 Methods..... | 20 |
| 2.3.1 Dynamical Downscaling Scenario..... | 21 |
| 2.3.2 Delta Method for CMIP5 and NARRCAP..... | 22 |
| 2.3.3 Multiple Linear Regression for NARCCAP..... | 23 |
| 2.3.4 Multiple Linear Contour Regression for NARCCAP..... | 24 |
| 2.3.5 Agricultural Indices..... | 25 |
| 2.4 Results..... | 26 |
| 2.4.1 Monthly Change Factors for Delta Method..... | 26 |
| 2.4.2 Hybrid Downscaling Methods..... | 27 |
| 2.4.3 Growing Degree Days..... | 29 |
| 2.4.4 Growing Season Length..... | 29 |
| 2.5 Discussions..... | 33 |
| 2.6 Conclusions..... | 36 |
| Chapter 3 Evaluation of the Southerly Low-level Jet Climatology in the Central United States as Simulated by NARCCAP Regional Climate Models..... | 39 |
| 3.1 Introduction..... | 39 |
| 3.2 Data and Methods..... | 43 |
| 3.3 Results..... | 47 |
| 3.3.1 Jet Frequency..... | 47 |
| 3.3.1.1 Cold Season S-LLJ Frequencies..... | 47 |
| 3.3.1.2 Warm Season S-LLJ Frequencies..... | 48 |
| 3.3.1.3 Annual Cycle of S-LLJ Frequency..... | 50 |
| 3.3.2 Jet Height..... | 52 |
| 3.3.3 Jet Speed..... | 54 |

| | |
|--|-----|
| 3.4 Discussion | 54 |
| 3.5 Conclusions | 62 |
| Chapter 4 The Potential Impact of Regional Climate Change on Fire Weather in the United States | 65 |
| 4.1 Introduction | 65 |
| 4.2 Data and Methods | 70 |
| 4.2.1 Data | 70 |
| 4.2.2 Haines Index Calculation | 70 |
| 4.3 Results | 73 |
| 4.3.1 Percentage of days with $HI \geq 5$ | 74 |
| 4.3.1.1 GCM-Induced Biases in Current Climate Simulations | 74 |
| 4.3.1.2 Spatial and Seasonal Variations in Frequency for the GCM-Driven Current Climate | 75 |
| 4.3.1.3 Projected Future Changes | 78 |
| 4.3.2 The A and B components | 80 |
| 4.3.3 Persistence of high HI events | 81 |
| 4.4 Discussion | 83 |
| 4.5 Conclusions | 86 |
| Chapter 5 Summary | 88 |
| APPENDIX | 93 |
| REFERENCES | 164 |

LIST OF TABLES

| | |
|---|----|
| Table 2-1. CMIP5 models used in the current study | 94 |
| Table 4-1. NARCCAP model combination outputs used in the current study | 95 |
| Table 4-2. Calculation of the Haines Index A and B components for the three elevation variants (temperature and dewpoint are in Celsius unit) | 96 |

LIST OF FIGURES

| | |
|--|-----|
| Figure 1-1. Framework for top-down climate change impact assessment study | 97 |
| Figure 2-1. Change of monthly average of daily maximum temperature compared to baseline period (1980-2000) for CMIP5 models. The columns are the RCP 4.5, RCP 6.0, RCP 8.5, respectively. The rows are time slices of 2010-2030, 2040-2060, and 2070-2090, respectively. The unit is Celsius. | 98 |
| Figure 2-2. Same as Figure 2-1, but for daily minimum temperature. | 99 |
| Figure 2-3. Same as Figure 2-1, but for daily precipitation. The change factor for precipitation is a ratio and unitless. | 100 |
| Figure 2-4. Change of monthly average of daily maximum temperature compared to baseline period (1978-1998) for NARCCAP models. The unit is Celsius. | 101 |
| Figure 2-5. Same as Figure 2-4, but for daily minimum temperature. | 102 |
| Figure 2-6. Same as Figure 2-4, but for daily precipitation. The change factor for precipitation is a ratio and unitless. | 103 |
| Figure 2-7. Empirical cumulative distribution function for daily maximum temperature for observation, NARCCAP NCEP run, and NARCCAP control run. | 104 |
| Figure 2-8. Empirical cumulative distribution function for daily maximum temperature for observation, NARCCAP control run, NARCCAP MLR projection, and NARCCAP MCR projection during current period. | 105 |
| Figure 2-9. Empirical cumulative distribution function for daily maximum temperature for NARCCAP future run, NARCCAP MLR projection, and NARCCAP MCR projection during future period. | 106 |
| Figure 2-10. Same as Figure 2-7, but for daily minimum temperature. | 107 |
| Figure 2-11. Same as Figure 2-8, but for daily minimum temperature. | 108 |
| Figure 2-12. Same as Figure 2-9, but for daily minimum temperature. | 109 |
| Figure 2-13. Median values of GDDs from CMIP5 delta projections for time slice 2010-2030. | 110 |

| | |
|--|-----|
| Figure 2-14. Same as Figure 2-13, but for 2040-2060. | 111 |
| Figure 2-15. Same as Figure 2-14, but for 2070-2090. | 112 |
| Figure 2-16. Differences of median GDDs from CMIP5 delta projections for time slice 2010-2030 and median observed GDDs for 1980-2000. | 113 |
| Figure 2-17. Same as Figure 2-16, but for 2040-2060. | 114 |
| Figure 2-18. Same as Figure 2-16, but for 2070-2090. | 115 |
| Figure 2-19. Median values of GDDs from NARCCAP delta projections for time slice 2040-2060. | 116 |
| Figure 2-20. Differences of median values of GDDs from NARCCAP delta projections for time slice 2040-2060 and median observed GDDs for 1978-1998. | 117 |
| Figure 2-21. Median values of GDDs from NARCCAP NCEP simulations for time slice 1978-1998. | 118 |
| Figure 2-22. Median values of GDDs from NARCCAP raw control simulation, NARCCAP MCR projections, NARCCAP MLR projections for control period 1978-1998. | 119 |
| Figure 2-23. Same as Figure 2-22, but for future period of 2040-2060. | 120 |
| Figure 2-24. Differences of future and control period median values of GDDs from NARCCAP raw control simulation, NARCCAP MCR projections, NARCCAP MLR projections. | 121 |
| Figure 2-25. Median values of growing season length from CMIP5 delta projections for time slice 2010-2030. | 122 |
| Figure 2-26. Same as Figure 2-25, but for 2040-2060. | 123 |
| Figure 2-27. Same as Figure 2-25, but for 2070-2090. | 124 |
| Figure 2-28. Differences of median values of growing season length from CMIP5 delta projections for time slice 2010-2030 and median observed growing season length for 1980-2000. | 125 |
| Figure 2-29. Same as Figure 2-28, but for 2040-2060. | 126 |
| Figure 2-30. Same as Figure 2-28, but for 2070-2090. | 127 |

| | |
|--|-----|
| Figure 2-31. Median values of growing season length from NARCCAP delta projections for time slice 2040-2060..... | 128 |
| Figure 2-32. Differences of median values of growing season length from NARCCAP delta projections for time slice 2040-2060 and median observed growing season length for 1978-1998..... | 129 |
| Figure 2-33. Median values of growing season length from NARCCAP NCEP simulations for time slice 1978-1998..... | 130 |
| Figure 2-34. Median values of growing season length from NARCCAP raw control simulation, NARCCAP MCR projections, NARCCAP MLR projections for control period 1978-1998..... | 131 |
| Figure 2-35. Same as Figure 2-31, but for future period of 2040-2060..... | 132 |
| Figure 2-36. Differences of future and control period median values of growing season length from NARCCAP raw control simulation, NARCCAP MCR projections, NARCCAP MLR projections..... | 133 |
| Figure 3-1. Study domain, the topography (shading) as resolved by the CRCM and the locations (circles) and evaluations (shading) of the 36 rawinsonde stations used in the study..... | 134 |
| Figure 3-2. Percentage of useable soundings (numbers next to the stations) for the cold and warm seasons at 00 UTC and 12 UTC. The background shading is CRCM model elevation..... | 135 |
| Figure 3-3. Cold-season 00 UTC RCM-simulated (shading) and rawinsonde observed (shading and number next to the station circle) jet frequency. The percentages are rounded. White regions represent places with no jet..... | 136 |
| Figure 3-4. Same as Figure 3-3, but for 12 UTC..... | 137 |
| Figure 3-5. Same as Figure 3-3, but for warm season..... | 138 |
| Figure 3-6. Same as Figure 3-5, but for 12 UTC..... | 139 |
| Figure 3-7. Jet frequency at 12 UTC during April to September for the four RCMs. ... | 140 |
| Figure 3-8. Percentage of jet number in each month of the year at each of the 36 stations. At each station, the percentages from all 12 months sum up to 100%..... | 141 |
| Figure 3-9. Difference of RCM simulated and observed percentage of jet number in each | |

| | |
|--|-----|
| month of the year at each of the 36 stations..... | 142 |
| Figure 3-10. Cold-season 00 UTC RCM-simulated (shading) and rawinsonde observed (shading and number next to the station circle) jet height. Units in meters AGL..... | 143 |
| Figure 3-11. Same as Figure 3-10, but for 12 UTC..... | 144 |
| Figure 3-12. Same as Figure 3-10, but for warm season..... | 145 |
| Figure 3-13. Same as Figure 3-12, but for 12 UTC..... | 146 |
| Figure 3-14. Cold-season 00 UTC RCM-simulated (shading) and rawinsonde observed (shading and number next to the station circle) jet speed. Units in ms^{-1} | 147 |
| Figure 3-15. Same as Figure 3-14, but for 12 UTC..... | 148 |
| Figure 3-16. Same as Figure 3-14, but warm season..... | 149 |
| Figure 3-17. Same as Figure 3-16, but for 12 UTC..... | 150 |
| Figure 4-1. Burned area (left axis) and number of wildland fires (right axis) in United States from 1984 to 2012 (NIFC). The National Interagency Coordination Center at NIFC compiles annual wildland fire statistics for federal and state agencies. 2004 fires and acres do not include state lands for North Carolina..... | 151 |
| Figure 4-2. Differences in percentage of days for $\text{HI} \geq 5$ in the US for six model combinations between current and NCEP climate for March (left column), August (center column) and October (right column)..... | 152 |
| Figure 4-3. Percentage of days for $\text{HI} \geq 5$ in the US for six model combinations under current climate for March (left column), August (center column) and October (right column)..... | 153 |
| Figure 4-4. Percentage of days for $\text{HI} \geq 5$ in the US for six model combinations under future climate for March (left column), August (center column) and October (right column)..... | 154 |
| Figure 4-5. Change in percentage of days for $\text{HI} \geq 5$ in the US for six model combinations between current and future climate for March (left column), August (center column) and October (right column)..... | 155 |
| Figure 4-6. Mean (contour) and standard deviation (shading) of percentage of days for $\text{HI} \geq 5$ in the US for six model combinations for current climate (upper), future climate (center), and difference between current and future climate (lower) during August. The | |

mean is contoured from 0 to 100 by 10 intervals for current (upper) and future (center) climate and from -10 to 20 by 3 intervals for the change between current and future climate (lower). The standard deviation is colored from -5 to 50 by 5 intervals for current (upper) and future (center) climate, and from -1 to 15 by 1 intervals for the change between current and future climate (lower). 156

Figure 4-7. Change in percentage of days for A=3 in the US for six model combinations between current and future climate for March (left column), August (center column) and October (right column). 157

Figure 4-8. Change in percentage of days for B=3 in the US for six model combinations between current and future climate for March (left column), August (center column) and October (right column). 158

Figure 4-9. Change of average length of events with $HI \geq 5$ for August between current and future climate. 159

Figure 4-10. Mean (contour) and standard deviation (shading) of change of average length of events with $HI \geq 5$ for August between current and future climate for six model combinations. The mean is contoured from -2 to 5 by 1 intervals. The standard deviation is shaded from 0 to 5 by 0.5 intervals. 160

Figure 4-11. Change of average length of events longer than five days with $HI \geq 5$ for August between current and future climate. 161

Figure 4-12. Change of average length of events longer than thirteen days with $HI \geq 5$ for August between current and future climate. 162

Figure 4-13. Change of average length of events longer than twenty-one days with $HI \geq 5$ for August between current and future climate. 163

Chapter 1 Background and Research Objectives

1.1 Overview

The Earth's climate is projected to change in the future with increasing greenhouse gas (GHG) emissions to the atmosphere. The Intergovernmental Panel on Climate Change (IPCC, Collins et al. 2013) suggested a general warming in North America and increasing precipitation in the northern half of North America. The projected climate change will likely affect many aspects of our environment (droughts, wildfires, etc) and many sectors of our economy (energy, agriculture, etc) (Westerling et al. 2003; Yang et al. 2012; Rosenzweig et al. 2014).

In most climate impact studies, the starting point of analyses is climate projections, which are simply defined as plausible future climate (Carter et al. 2001). As shown in Figure 1-1, these climate projections are produced using general circulation models (GCMs) driven by alternative GHG emissions scenarios (Nakicenovic et al. 2000); it can be further downscaled dynamically using regional climate models (RCMs) or empirically using statistical methods such as linear regression and quantile mapping. These downscaled climate change projections form the basis for impact studies. In carrying out a climate change impact studies, scientists often have the freedom to choose the set of GCM outputs to work with, along with different types of downscaling methods.

As a climate impact study is often an inter-disciplinary effort with researchers coming from different fields, the choice of climate projections and approaches may be overwhelming in some if not all cases. Understanding the processes involved in generating climate change

projections and the pros and cons associated with different methods and products is a necessary first step towards a better interpretation and use of climate change projections. Thus, the overarching goal of this research is to provide some insights into impact assessment studies for multiple fields while providing detailed impact assessment examples for regions of North America.

This goal is achieved by examining three aspects of the climate impact assessment framework shown in Figure 1-1, using three sample studies. The first study focuses on selecting an ensemble of climate projections for an assessment and is illustrated using an example for the agriculture sector, specifically the impact of climate change on the conditions for fruit growth in the Great Lakes region of North America. The second study provides an the evaluation of regional climate models, one of the primary tools used for dynamical downscaling, particularly the accuracy of RCMs in simulating the southerly low-level jet or LLJ, which is a prominent weather and climate phenomenon in the North American Great Plains. Finally, the third study is an application of dynamically-downscaled climate projections to assess the impact of climate change on the potential for erratic or extreme wildfires in the United States. The following provides a brief background for the three studies.

The first study is concerned with the choice of climate downscaling approaches in an agricultural impact assessment application for the Great Lakes region. It is part of a larger project, which involves the assessment of regional climate change on tart cherry production over the Great Lake Region and several other large tart cherry production regions in eastern and central Europe. As the latest IPCC report pointed out, price and demand are dynamically balanced internationally and impact studies for agriculture should broaden their scope by

including the trade relationships with other regions instead of only assessing local economic impacts (Porter et al. 2014). Agricultural impact assessments are essential endeavors as climate change along with increasing population pose a great threat to food production and security. Given the importance of agricultural impact assessments, their starting point – climate projections – should be chosen with great caution. Specifically, agricultural assessment tools such as crop models often use daily weather data at a location as inputs (e.g. maximum temperature, minimum temperature, daily mean temperature, and daily precipitation). The spatial and temporal mismatches with the coarse resolution gridded output of GCMs are typically addressed using downscaling approaches. Furthermore, a bias correction also is often needed to adjust for biases in the climate models. In sum, obtaining climate projections for agricultural impact assessment poses a great challenge with many options. The current study aims to illustrate a number of considerations when selecting a climate projection including the uncertainty associated with the future projections.

The second study examines the ability of RCM to capture the climatological characteristics of the Great Plains southerly low-level jet. The ability of RCMs to simulate the climatology of prominent weather features such as the LLJ builds confidence in the appropriateness of the RCM simulations and their use for climate change assessments. A LLJ is a maximum in the lower troposphere vertical wind profile. As a prominent weather phenomenon in the central United States, LLJs have a large impact on local weather (Kapela et al. 1995). For example, southerly LLJs can contribute to nighttime precipitation maxima in central United States (Pitchford and London 1962; Bonner 1966). LLJs have also been related to fire spread, insect migration, blizzards, etc. (Sjostedt et al. 1990; Arritt et al. 1997; Zhong

et al. 1996). Traditionally, studies of LLJ have relied on rawinsonde soundings launched twice daily from a network of upper-air stations at about 300 km spacing across the US. In addition to having coarse spatial coverage, the sounding data, although the best representation of real-world LLJs, may also suffer from discontinuities in data introduced by changes in instrumentation, measurement locations and recording procedures as well as changes in local land use (Walter et al. 2014). The heterogeneous distribution of observational stations may also influence spatial analysis. Gridded models or reanalysis data overcome some of these shortcomings and have been used to study LLJs. Higgins et al. (1997) studied the impact of Great Plains LLJ on summertime precipitation and moisture transport using the National Centers for Environmental Prediction/National Center for Atmospheric Research (NCEP/NCAR) and the National Aeronautics and Space Administration Data Assimilation Office (NASA/DAO) reanalysis data, and found favorable results using the reanalysis. Given their higher spatial (~30-50 km) and temporal (hourly) resolution, RCMs are a valuable alternative to rawinsonde data or coarse resolution gridded data for understanding the spatial and temporal variability of LLJs (Todd et al. 2008). Also, because LLJs are meso-scale phenomena, RCMs may be better tools compared to GCMs for understanding LLJ characteristics in future climate. Previously, Doubler et al. (2015) produced a long-term LLJ climatology based on the North America Regional Reanalysis (NARR). Their study revealed LLJ frequency maxima not present in some other coarse resolution observation data. The archived RCM simulations provided by the North American Regional Climate Change Assessment Program (NARCCAP) provide an alternative means for investigating the current LLJ climatology and to extend to the analysis to future changes in the jet climatology. As a

preliminary step, the second study of this dissertation evaluates the NARCCAP RCM simulations for the current climate with rawinsonde observations to assess the capability of an ensemble of RCMs to provide a detailed and realistic LLJ climatology. The use of an ensemble also provides insights on the uncertainty associated with the RCM simulations.

The third study illustrates the use of an ensemble of climate projections in a climate change impact assessment base on a case study related to wildfires (Figure 1-1). Wildfires endanger life and property in many regions of the United States. Large and mega-fires cause most of the damage and costs of wildfires, even though they are not the largest portion of fire incidents (Williams 2004). Large, extreme fires are causes for great concerns due to their potential to burn large areas. Natural factors, which may be affected by climate change (Westerling et al. 2003), play a significant role in affecting fire danger (i.e. the combination of both constant and variable factors that influence the initiation, spread, and difficulty to control a wildfire on an area, Bradshaw et al. 1984). In the future, the locations of the key regions of fire danger might change, as well as fire frequency, fire duration, and other characteristics. Most previous studies on this topic examined a fire-weather index using climate projection from either a single high-resolution regional climate model or multiple coarse-resolution general circulation models (Flannigan et al. 2005). As a result, these assessments of climate change impacts on fire weather suffer from large uncertainties. The case study presented here instead calculates a fire-weather index using an ensemble of finer-resolution RCM simulations and consequently provides greater insight on the spatial variations of fire hazard and on the surrounding uncertainty.

1.2 Research Objectives

The overarching goal of this research is to examine several aspects of climate change impact assessments for North America while shedding light on the complex issues involved in impact studies. More specifically, three case studies are conducted, each focusing on a specific aspect of a climate change assessment. For each topic, the study objectives and research questions are outlined below.

1.2.1 Guidance for Selecting Climate Projections for Assessments

This particular study aims to generate and compare climate change projections obtained using different climate models run with different greenhouse emissions scenarios, and different methods to downscale the model simulations to a local scale. The example provided is for fruit crops in the Great Lakes region of North America. Several downscaling methods, which differ considerably in their complexity and the effort needed for development, are adopted to generate climate change projections for locations within the Great Lakes region, and the resulting climate change projections are compared. In addition to primary climate variables (e.g., maximum and minimum temperature and precipitation), derived indices important to fruit crops (e.g., growing degree days, growing season length) are compared. The results shed light on the influence of the choices of initial model simulations and downscaling methods on the interpretation of the potential impacts of climate change, in this case the projected impacts on fruit production. The specific objectives are to:

- generate downscaled climate change projections for three locations along Lake

Michigan shoreline where fruit production is concentrated using downscaling procedures that range from the simple to complex including: a) projections obtained from GCM simulations in the Coupled Model Intercomparison Project Phase 5 (CMIP5, Taylor et al. 2012) database using the simple delta method; b) hybrid downscaling method whereby the delta method is applied to dynamically-downscaled RCM simulations obtained from the NARCCAP (Mearns et al. 2007, 2009) database; c) a complex hybrid approach where multiple linear regression or multiple linear contour regression is applied to the simulations from the NARCCAP dataset to both downscale and debias the RCM simulations;

- compare downscaled projections obtained from different method to evaluate the influence of the different projections on the ensemble range and uncertainty estimation and the interpretation of future impacts of climate change on regional fruit production, and to the assess the efficacy of different downscaling methods given the differences in resources needed to develop the various projection types.

This study will provide insights on the advantages and disadvantages of the choices regarding what climate change projections to include on the outcomes of agriculture impact assessments. The main goal is to provide general guidelines for selecting climate projections for assessment studies.

1.2.2 An Evaluation of RCM Simulations of the Low Level Jet Climatology

RCMs are an important tool in the study of regional climates. By examining the

climatology of regional-scale significant weather phenomena as produced by RCMs, more confidence can be placed in using RCMs in assessment studies. An evaluation of how well RCMs can produce the long-term climatology of southerly LLJs, which are a frequently-occurring feature in the Great Plains, currently does not exist. This study will fill this gap by evaluating the ability of an ensemble of four RCMs from the NARCCAP archive to simulate the characteristics of southerly LLJs for the current climate as compared to rawinsonde (sounding) observations. The specific objectives are to:

- examine the spatial, diurnal and seasonal variations of the southerly LLJs as simulated by the RCMs, including jet frequency, elevation, and speed; investigate spatial variation of the annual cycle of LLJ frequency;
- examine the agreement and disagreement among models in the climatological patterns;
- evaluate the LLJ climatology produced by the RCM current climate simulations against sounding observations and the climatological patterns identified in previous observation-based LLJ climatological analyses;

A detailed evaluation of RCM-simulated LLJ climatologies is necessary for understanding the usefulness and limitations of RCMs in simulating LLJs. Because LLJs play a crucial role in the hydrological cycle over the central United States, understanding the strengths and weakness of RCMs in simulating LLJs will be very useful for a better interpretation of RCM simulated current and future climate of the central United States.

1.2.3 An Assessment of Lower Atmospheric Conditions Conducive to Extreme Fires

A case study is presented to illustrate the use of an ensemble of downscaled climate projections in a climate change assessment study. The Haines fire weather index, or HI, is computed for the current and future climate to assess the impact of climate change on lower atmospheric conditions conducive to extreme or erratic fires. The assessment of the HI climatology provides insight into future changes of lower atmosphere stability and moisture content, which are both important components of fire weather. The specific objectives are to:

- produce HI climatologies for the NARCCAP RCM current and future climate simulations;
- estimate the projected changes in the HI climatologies between the current and future climate including changes in the probability and persistence of weather favorable for extreme, erratic wildfires.

The main hypothesis is that the frequency, duration, and severity of fire weather in most regions of the United States will increase as a result of global climate change, but that the amount and type of increase would vary significantly across different regions and periods of time. This impact assessment will assist fire and resource managers in designing climate change adaptation strategies (Millar et al. 2007).

1.3 Dissertation Structure

This dissertation is divided into five chapters. The first chapter provides a brief

background of the study, the rationale of the research, and the research objectives.

Chapter 2 discusses a framework for obtaining climate projections for impact studies, including data sources, downscaling and bias-correction methods, ensemble analysis, and the uncertainty associated with such choices. Projections produced by the GCM (CMIP5) delta method, RCM (NARCCAP) delta method, raw RCM simulations, and hybrid downscaling (multiple linear regression and multiple linear contour regression) are analyzed in relation to climate variables important for agricultural productions.

Chapter 3 presents an evaluation of the ability of RCMs to simulate regional-scale circulation features. LLJ climatologies developed from RCM simulations for the current climate from the NARCCAP archive are compared with the long-term rawinsonde sounding data from a network of stations in central and eastern United States. The strengths and weakness of each RCM in simulating jet frequency, height, and speed as well as the LLJ spatial and temporal distributions are examined.

Chapter 4 presents a case study of a climate change impact assessment concerning wildfires. HI climatologies are generated for RCM simulations from the NARCCAP archive, in order to analyze whether the future climate will be more or less favorable for extreme or erratic fire behavior. The frequency of days with large HI values and the duration of consecutive high HI events are examined.

Chapter 5 summarizes findings from Chapter 2 to Chapter 4, discusses the contributions of the current work, and outlines needed future research.

Chapter 2 Guidance for Selecting Climate Projections for Assessments

In collaboration with

Julie A. Winkler, Shiyuan Zhong, Pang-Ning Tan, Malgorzata Liszewska, and Lydia Rill

2.1 Introduction

2.1.1 Overview and General Objectives

Climate projections are often produced using GCMs driven by a series of GHG emissions scenarios (Nakicenovic et al. 2000). A GCM is a mathematical model built upon fundamental conservation laws governing the circulation of the earth's atmosphere and ocean. GCMs have been shown to successfully simulate historical and current climate of the earth (Kushnir et al. 2002; Cai et al. 2009). However, GCMs often have coarse resolutions that are inadequate for local/regional impact assessments. For example, for lake-modified locations such as Michigan, GCMs may not resolve the lakes and coastlines well (or simply does not include the Laurentian Great Lakes), which in turn affects local feedback mechanisms in climate modeling.

Regional climate models are often used to dynamically downscale results from GCMs, better resolve coastlines, terrains, or other features of a local nature (e.g., land use) and provide higher-resolution climate projections for regional or local impact studies. Many studies suggest that RCM add value to GCM simulations in complex coastal areas and at high temporal scales (Feser et al. 2011; Di Luca et al. 2013; Castro et al. 2005). However, because RCMs are not error/bias free, climate projections developed using dynamical downscaling are subject to errors and biases associated with both the GCMs and RCMs. Statistical

downscaling has often been utilized for providing higher-resolution climate projections directly from GCM outputs. It is also possible to combine the two approaches, known as hybrid downscaling. Some dynamically-downscaled projections have been produced by various agencies and programs, e.g. the NARCCAP, and ENSEMBLES (Hewitt 2005), for use by the climate science community and other stakeholders for climate impact assessments.

Despite the popularity of climate change impact studies, the uncertainties associated with such studies are not well addressed in most applications. To account for the uncertainty in impact assessments, ensemble modeling is often used. Instead of simulating the future climate projections using only one climate model, an ensemble can be constructed using different models and for a particular model with different initial conditions and parameterizations (i.e., perturbed physics) (Parker 2013). Ensemble members can also include the same model run with different greenhouse gas emissions scenarios. In addition, a group of climate models forced with various emissions scenarios can be included in an ensemble. Even though agreement among models does not necessarily mean correctness, if the ensembles members perform well in simulating the current climatology, it builds more confidence in applying the ensembles to climate change impact assessments.

The interpretation of ensemble results calls for great attention. One way to display a large number of ensemble members is to present the average of the outcomes. However, as shown in the recent IPCC report (Collins et al. 2013), different GCMs project long term climate change significantly different from each other. For example, FIO-ESM and GFDL-CM3 respectively show negative and positive changes in temperature for 2081-2100 under RCP 4.5 in west Europe (Collins et al. 2013). By simply taking the average of the two models,

it's likely the projected change will be close to zero, which understates the possibility of change. On the other hand, displaying the full range of simulated results using classic “spaghetti plots” or multi-panel plots may cause other issues such as overwhelming readers or misinterpreting of uncertainty. An example for the latter could be that readers would assume that the range of uncertainty obtained from the ensemble encompasses the whole range of uncertainty in climate impact analysis, which is seldom true in reality.

Nowadays scientists have the freedom of using climate simulations from various archival sources or conducting their own climate simulations. They have leeway in the selection of GCM or RCM models, choice of downscaling method, size of ensemble, degree of bias correction, and choice of greenhouse gas emissions scenarios, etc. Frequently, researchers from fields other than climate science find themselves in need of climate projections, but can be overwhelmed by the different options and approaches. Thus, the current study provides an illustrative example for an agricultural impact assessment of the consequences of different choices in developing climate projections, which can also help serve as general guidance for others using climate projections for climate change assessments, particularly agricultural assessments. The current study is part of a larger project aimed at developing climate projections using multiple downscaling approaches based on available archives of GCM and RCM simulations for the United States and Europe.

2.1.2 Climate Projections for Agricultural Impact Assessments

Assessments of the potential impacts of climate change on agriculture are important

undertakings. Even though crop yields generally tend to increase with elevated CO₂ concentration, this effect may be modified or compensated by future temperature or precipitation change (Tubiello et al. 2007). In the assessment of climate change impacts on agriculture, daily weather data at a specific location are often needed. Downscaling approaches can be used to obtain daily data at a specific location. On one hand, as mentioned earlier, GCMs are generally too coarse and inadequate to account for meso-scale processes such as land-sea breeze or lake-effect precipitation that are resolved by RCMs. On the other hand, RCMs are resource-intensive and may suffer from additional errors introduced by RCMs or the subgrid-scale parameterizations they use. Thus, for regional climate impact assessments, one of the first decisions to be made is whether to adopt GCM only or to further downscale dynamically or statistically. Another decision is whether to obtain available climate projections produced by others or to generate climate projections targeted specifically for a project. Moreover, given that GCMs and RCMs are not free of biases/errors, a decision on whether and how to perform bias correction is also necessary.

In agricultural impact assessments, commonly used variables are daily average temperature, maximum daily temperature, minimum daily temperature, and daily precipitation (Olesen et al. 2007; Xiong et al. 2009; Knox et al. 2010; Laux et al. 2010; Ruane et al. 2013). During the growing stage of crops, temperatures too high or too low may cause irreversible damage to them, the same as flooding or drought conditions (Wahid et al. 2007; Li et al. 2009). Thus, monthly mean temperature and monthly mean precipitation are generally too coarse for crop modeling. For example, crop process models such as Crop Environment REsource Synthesis (CERES), Cropping Systems Simulation Model (CropSyst),

and the Sirius crop simulation model all require daily weather inputs (Singh et al. 2008; Semenov 2009). Furthermore, agricultural impact assessments are often localized and usually involve station data, whereas a grid point from GCM or RCM outputs represents a much larger geographical area compared to that of a station (Mall et al. 2004; Laux et al. 2010; Richter and Semenov 2005).

Downscaling methods are often applied in agricultural impact assessments to address discrepancies in spatial and/or temporal scale. As the name implies, downscaling fulfills the need of obtaining variables at a finer spatial resolution and/or temporal resolutions. Three categories of downscaling were summarized by Winkler et al. (2011): dynamical downscaling, which commonly refers to an RCM driven by a GCM; empirical or statistical downscaling, which relates local surface variables to large scale atmospheric state variables; and disaggregation downscaling, which aims at interpolating coarse spatial or temporal resolution variables to finer resolutions. Additionally, hybrid downscaling is simply the combination of dynamical downscaling with one or more empirical methods.

Bias correction is often a necessary component of downscaling. A widely used bias adjustment method is the delta method (Fischer et al. 2005; Yao et al. 2007; Lhomme et al. 2009; Knox et al. 2010; Ruane et al. 2013). The delta method is simple and less computationally intensive than many other downscaling methods. To apply the delta method, a change factor, or delta, for a variable, such as temperature, is calculated by subtracting, usually for a model gridpoint, the GCM or RCM simulated current climate average temperature from the GCM or RCM simulated future climate average temperature (for precipitation, ratios are used) (Winkler et al. 2011). The change factor is often interpolated to

finer resolutions or applied to observed time series of climate variables at a station in consideration of scale difference. The change factor usually is calculated as monthly, seasonal, or annual averages rather than daily averages. One disadvantage of the delta method is that only the mean is corrected, rather than the distribution of the climate variable. This disadvantage can be addressed by the quantile mapping (QM) method, which adjusts both the mean and variance (Wood et al. 2004; Themeßl et al. 2011). The QM method establishes a relationship between the distribution of the observations and the distribution of the model-simulated current climate for the same period as observations, and corrects the distribution produced by models based on the transfer functions. The QM method can also bridge the gap between the spatial scale of the GCM or RCM simulations to finer resolution grids or a site, and thus downscale the model simulations.

Previous agriculture impact assessment studies have adopted various downscaling approaches. Although GCM simulations have rarely been directly used for agricultural assessments, numerous examples have shown the direct use of RCM outputs as daily weather inputs for crop modeling (e.g., Challinor and Wheeler 2008; Chavas et al. 2009; Xiong et al. 2007). For example, Xiong et al. (2007) and Xiong et al. (2009) used daily weather simulations from the PRECIS (Providing REgional Climates for Impacts Studies) RCM as input to the CERES-Maize model to analyze maize and future cereal production, respectively, for China. The statistical downscaling of GCM outputs has been widely adopted in the literature, particularly the use of disaggregate downscaling. Examples include Zhang (2005) who used quantile mapping and a stochastic weather generator (CLIGEN) to temporally downscale monthly data to a daily resolution as input to a crop production and soil erosion

model. Similarly, Thornton et al. (2009) used statistically downscaled GCM outputs and a weather generator (MarkSim) to study the response of bean and maize crops to climate change in East Africa.

The delta method is the most popular method used in the agricultural assessment literature, mainly because it is straightforward and easy to adopt (Fischer et al. 2005; Lhomme et al. 2009; Masutomi et al. 2009; Tubiello and Fischer 2009; Schlenker and Lobell 2010; Knox et al. 2010; Ruane et al. 2013). Also, the simplicity of this method facilitates the inclusion of a large number of climate projections within an ensemble. The change factors are most often calculated from monthly mean values (typically for a 30-year period) from current and future climate simulations. Popular future periods include the end of the century (2071-2100) or multiple non-overlapping periods such as 2011-2040, 2041-2070, and 2071-2100.

Many studies used more than one downscaling method in order to compare projections produced by different methods. Wood et al. (2004) applied linear interpolation (LI), spatial disaggregation (SD), and bias-correction and spatial disaggregation (BCSD) on GCM and RCM outputs. Themeßl et al. (2011) applied an ensemble of downscaling and error correction methods, including multiple linear regression (MLR), multiple linear regression with randomization (MLRR), the analogue method (AM), the nearest neighbor analogue method (NNAM), local intensity scaling (LOCI), and QM to precipitation downscaling over the European Alpine region and compared with raw RCM outputs. The comparison among methods is often location- or model- based and thus will not apply to every case.

The specific goal of this study is to compare ensembles developed using different methods and from different sources in order to provide a guidance to further assessments.

Outcomes of this study will help guide the choice of downscaling methods, especially those for geographic locations modified by large water bodies. Several common downscaling methods frequently used in the climate change impact studies are adopted to generate climate change projections for the Great Lakes region.

2.2 Data

The current study uses both simulated and observational data. Model data include RCM outputs from NARCCAP (Mearns et al. 2007, 2009) and GCM outputs from CMIP5 (Taylor et al. 2012).

NARCCAP performed climate simulations using a suite of RCMs driven by a set of GCMs for North America, providing an ensemble of regional climate change projections for assessment studies (Mearns et al. 2007, 2009). The horizontal grid spacing used in all the RCM simulations was 50km. Simulations with the different model combinations were produced for both a current climate period (1971-2000) and a future climate period (2041-2070). For the 21st century, the GCMs were forced with the A2 emissions scenario which describes a very heterogeneous world with continuously increasing global population and regionally oriented economic growth (Nakicenovic et al. 2000). In addition to the GCM-driven current climate simulations, another set of RCM simulations driven by the NCEP-Department of Energy (DOE) Reanalysis 2 (referred to below as NCEP, Kanamitsu et al., 2002) for the period 1979-2004 were also produced for the purpose of RCM evaluations. Reanalysis-driven simulations are often referred to as perfect boundary condition simulations

(Giorgi 2006).

The set of RCMs used in the current study includes the Canadian Regional Climate Model (CRCM) (Laprise et al. 1998; Caya and Laprise 1999), the Weather Research and Forecasting Grell configuration (WRFG, Skamarock et al. 2005; Grell and Devenyi 2002), the Regional Climate Model version 3 (RCM3, Pal et al. 2007), and Hadley Centre Regional Climate Model version 3 (HRM3, Wilson et al. 2005). The driving GCMs include the NCAR Community Climate System Model (CCSM, Collins et al. 2006), the Canadian Climate Centre's Canadian Global Climate Model version 3 (CGCM3, Flato 2005), the Geophysical Fluid Dynamics Laboratory GCM (GFDL, Delworth et al. 2006), and Hadley Centre Coupled Model version 3 (HadCM3, Gordon et al. 2000).

CMIP5 is another important data source for the current study. CMIP5 aims at filling in the gaps in the understanding of past and future climate with inputs from more than 20 groups running more than 50 models (Taylor et al. 2012). Both long-term (century scale) and near-term (decadal scale) experiments are included in CMIP5, although the current study will only focus on long-term experiments. The GCMs were forced with a family of representative concentration pathways (RCPs) including the RCP 2.6, RCP 4.5, RCP 6.0, RCP 8.5 (the number roughly represent the radiative forcing in 2100 compared to pre-industrial values) (Moss et al. 2010).

In order to compare downscaled outputs of CMIP5 to NARCCAP (forced with A2 scenario), the experiments with the RCP 4.5, the RCP 6.0, and the RCP 8.5 scenarios will be used in the analysis. In terms of radiative forcing (RF) relative to pre-industrial conditions, the RCP 8.5 scenario has the highest RF until near 2100, while the A2 scenario is just below

RCP 8.5. The A2 scenario is close to the RCP 4.5 and the RCP 6.0 scenarios before 2030 and has higher RF after 2030. On the other hand, the RCP 4.5 has a higher RF than the RCP 6.0 scenario before 2060 and a lower RF after that. For the long-term experiments in CMIP5, a historical experiment forced by observed changes in anthropogenic greenhouse gases is also included in CMIP5.

The historical experiment is also used in the current study. The simulation periods vary from model to model, with historical experiments starting generally in 1850 and ending in 2005 and with RCP experiments starting in 2006 and ending in 2100 or beyond. A list of models used in the current study and institutions involved in CMIP5 obtained from the website of the Program for Climate Model Diagnosis and Intercomparison (PCMDI) is shown in Table 2-1. Only model simulations with all three of the RCP 4.5, RCP 6.0, RCP 8.5 experiments and containing all four of the monthly average of daily temperature maximum, daily temperature minimum, daily average temperature, and daily precipitation are adopted in the current study.

In addition to the RCM and GCM simulations, observed data for three Michigan stations (Maple City, Hart, and Eau Claire) are also used. The observation data are from the National Weather Service Cooperative Network (COOP) and Global Historical Climatology Network (GHCN), and missing data are filled by nearby stations (Haylock et al. 2008).

2.3 Methods

The downscaling approaches include simple statistical downscaling (application of

the delta method to the CMIP5 data), dynamical downscaling (raw NARCCAP output), and hybrid downscaling (application to the NARCCAP simulations of the simple delta method and empirical-dynamical downscaling approaches including multiple linear regression and multiple linear contour regression). Downscaled projections were generated at three sites along Lake Michigan shore, namely Eau Claire, Hart, and Maple City; only the results for Maple City are presented here. The three sites are selected because they are all located in the production region for perennial crops and because all three have long-term climate records. In addition, the proximity of these stations to the lake represents one type of challenge downscaling often faces in areas of surface heterogeneity. The nearest land grid point approach is used for both the GCM and RCM simulations and for all downscaling methods.

2.3.1 Dynamical Downscaling Scenario

Dynamically-downscaled projections were produced at the three sites using outputs from NARCCAP RCM suite. Specifically, raw model outputs from eight RCM-GCM model combinations (CRCM-CCSM, CRCM-CGCM3, WRFG-CCSM, WRFG-CGCM3, RCM3-GFDL, RCM3-CGCM3, HRM3-GFDL, and HRM3-HadCM3) were extracted for the time slice of 1978-1998, representing current climate, and the time slice of 2040-2060, representing the climate of the mid-century. Three primary climate variables (daily maximum temperature, daily minimum temperature, and daily total precipitation) from these time periods were obtained for the three stations using the nearest grid point approach. Daily total precipitation or simply daily precipitation was obtained by accumulating the three hourly

precipitation data in the NARCCAP archive.

2.3.2 Delta Method for CMIP5 and NARCCAP

For the GCM delta method, the daily observation data at the three stations for the period of 1980-2000 were used to represent the current climate at the stations. Data for the same period were extracted from the control runs for the GCM historical experiments. For the future climate, multiple 21-year periods with a 1-year lag were extracted from the GCM future experiments beginning with 2010 (2010-2030, 2011-2031, 2012-2032, ..., 2080-2100). The change factors, or deltas, were calculated at the nearest land grid point to each station, for each calendar month, each variable, and each pair of future and control periods. The monthly change factors were then applied to daily observations for the selected period to obtain daily series. For the analyses presented below, three time slices, 2010-2030, 2020-2040, and 2070-2090, were chosen to represent the early-, mid-, and late-century.

For RCM delta method, a similar period of observations and control climate was used (1978-1998, due to missing data near the end of 1999 and 2000), and the future period is the 21-year mid-century time slice from 2040 to 2060. Daily maximum and minimum temperature were taken directly from the NARCCAP simulations, while daily average temperature is the average of the 8 times daily of the archived 3-hourly temperature data. Similarly, daily precipitation is the sum of the 8 times daily 3-hourly precipitation data. Again, the land grid point closest to each station was used in the downscaling. The change factor was calculated for each calendar month as the difference (ratio) for temperature

(precipitation) variables between the monthly averages for control and future climate. The daily series were obtained by applying change factor to the observations.

A subset of 16 GCM simulations from the CMIP5 dataset was used in the analyses. The subset of model runs, summarized in Table 2-1, was chosen based on the criteria in which all four variables (monthly averaged daily maximum temperature, daily minimum temperature, daily mean temperature, and precipitation) are available for the three RCPs (RCP 4.5, RCP 6.0, RCP 8.5). For the NARCCAP dataset, 8 RCM-GCM combinations were used (CRCM-CCSM, CRCM-CGCM3, WRFG-CCSM, WRFG-CGCM3, RCM3-GFDL, RCM3-CGCM3, HRM3-GFDL, and HRM3-HadCM3).

2.3.3 Multiple Linear Regression for NARCCAP

Multiple linear regression (MLR) is a common downscaling approach (Thiemeßl et al. 2011). MLR aims to model the relationship of multiple explanatory variables and a response variable, and seeks to fit a linear equation which minimizes the sum of squared residuals. In the current study, the nine explanatory variables obtained from the NARCCAP simulations are zonal surface wind speed (uas), meridional surface wind speed (vas), maximum daily surface air temperature (tasmax), minimum daily surface air temperature (tasmin), surface air temperature (tas), precipitation (pr), specific humidity (huss), surface pressure (ps), and 500hPa geopotential height, while three response variables are maximum temperature (tasmax), minimum temperature (tasmin), and precipitation (pr) at a station. Daily averages (or sums in the case of precipitation) were calculated for those variables that are in 3-hourly

time steps. The regression functions were developed based on the NARCCAP NCEP-driven runs and the observations for the period of 1980 to 2004 and then applied to the RCM control (1978-1998) and future climate (2040-2060) runs to generate downscaled daily tasmax, tasmin, and pr projections for the three stations.

2.3.4 Multiple Linear Contour Regression for NARCCAP

Multiple linear contour regression (MLCR) was proposed by Abraham et al. (2013) to simultaneously minimize the residuals of the projected variables and preserve the overall shape of distribution. The MLCR method aims to minimize the sum squared error, as shown below:

$$\min \sum_{i=1}^n ((y - X\beta)^2 + \gamma(z - \hat{X}\beta)^2)$$

where γ is set to 5, y is the observation data, z is the rank-ordered observation value, X is the training data from NARCCAP NCEP simulation, and \hat{X} is the ordered training data from NARCCAP current simulation. The same sets of predictors were used by MLCR as in MLR.

The solution is:

$$\beta = (X^T X + \gamma \hat{X}^T \hat{X})(X^T y + \gamma \hat{X}^T z)$$

The MLCR projection consists two parts: the first part tries to build linear regression relationship between the observation and the output from the NARCCAP NCEP-driven runs; and the second part aims to correct NARCCAP control run distribution to observation distribution. By setting γ to 5, the second part is prioritized. The solution is then applied to future NARCCAP raw projection to generate future MLCR projection.

2.3.5 Agricultural Indices

The downscaled climate variables were used to derive several agricultural indices including growing degree day (GDD) and growing season length. The GDDs were calculated using Baskerville-Emin method (Baskerville and Emin 1969) with a base temperature of 4 °C. For any given day, if t_{max} is lower than the base temperature, the GDD for that day equals 0. Mean temperature is calculated by averaging t_{max} and t_{min} . If t_{min} is greater or equal to the base temperature, the GDD equals the difference of average temperature and base temperature. If not, the GDD is calculated as follows:

$$W = (t_{\text{max}} - t_{\text{min}})/2$$

$$A = \arcsin((\text{base} - t_{\text{ave}})/W)$$

$$\text{GDD} = ((W * \cos(A)) - (\text{base} - t_{\text{ave}}) * ((3.14/2.0) - A))/3.14$$

Where t_{ave} is the mean temperature, t_{max} is daily maximum temperature, and t_{min} is daily minimum temperature.

The growing season length is measured as the length of last spring frost to first fall frost. The dates when daily minimum temperatures fall below 0 °C are recorded as frost days. Then the duration of frost-free period is calculated. If there is no frost during the year, then the growing season length is defined as 274 days (total number of days during spring, summer, and fall).

2.4 Results

2.4.1 Monthly Change Factors for Delta Method

The change factors for the three stations (Eau Claire, Hart, and Maple City) are very similar because they share similar geographic characteristics (only results for Maple City are shown). The spread of the monthly average change factor becomes larger from time slices 2010-2030 to 2070-2090 (Figure 2-1 to 2-2). The changes in maximum temperature generally range from 0 to 5 °C for mid-century for all three RCPs, and about 1 to 6 °C for late-century for the RCP 4.5 and RCP 6.0 scenarios, while for the RCP 8.5 scenario the change factors range from 1 to 9 °C, with two exceptions. The month of April and May tend to have the smallest spread among all models for all time periods and RCP scenarios. The MIROC-ESM and MIROC-ESM-CHEM model have largest change factor for maximum temperature in February and March among 16 models, which significantly contribute to the spread within these two months. August and September are two other months with a larger spread; but the spread was not dominated by one or two models as in the case of February and March. For minimum temperature, the spread of change factors is larger during winter and smaller during summer, compared to maximum temperature. The change factors remain very similar for mid-century and late-century periods for the RCP 4.5 and RCP 6.0 scenarios, while the RCP 8.5 scenario is more different in terms of value and spread. The change factors for precipitation generally range from 0.8 to 1.5 with more consistency among models during the warm season (May to September) for all RCP scenarios (Figure 2-3). In sum, CMIP5 models projected a general increase in temperature and precipitation in the future climate for all three

RCPs at Maple City at the shore of Lake Michigan.

The change factors derived from the NARCCAP RCM simulations are very close to those derived using CMIP5 for the three stations (Figure 2-4 to 2-6). The spread of maximum temperature is larger in warm season and the spread of minimum temperature is larger during cold season, with both ranging from 0 to 5 °C. The precipitation change factor has large variation across months. Similar to CMIP5 results, the change factor for precipitation also ranges from 0.8 to 1.5 with values above 1 (increased precipitation in the future) during the cold season, and with values around 1 (small changes in precipitation in the future) during the warm season (Figure 2-6). The projected change factors from NARCCAP (2040-2060) have smaller range compared to CMIP5 projections, which is not surprising given smaller number of models included. For both CMIP5 and NARCCAP projections, no model shows consistently higher or lower values across months compared to other models. One disadvantage of the delta method is that each calendar month of future projections is created by adding to or multiplying by the same value for the 21-year period. Thus, the inter-annual variability of future projections produced by the delta method is introduced only by the inter-annual variability in the observations for the current climate period, which may require further treatment for agricultural impact assessment.

2.4.2 Hybrid Downscaling Methods

The overall r-squared values are over 0.8 for daily maximum temperature prediction and over 0.7 for daily minimum temperature prediction, but are very low for precipitation. In

Figure 2-7, the empirical cumulative distribution function (ECDF) for daily maximum temperature from observations, NARCCAP control runs, and NARCCAP NCEP runs are presented. Both the NCEP and control runs tend to underestimate observations for a large portion of daily maximum temperature, and the NCEP runs tend to overestimate the upper end of temperature while this situation varies for control runs. The MLR and MLCR outcomes for the current climate period (1978-1998) are shown in Figure 2-8. After bias-correction, the distribution of MLCR outcomes is close to the distribution of the observation data, while the MLR method does not necessarily improve the distribution of the control run. The ECDFs of future projections of daily maximum temperature maximum based on MLR and MLCR are shown in Figure 2-9. The MLR and MLCR transformations tend to increase values in the lower end. The MLCR outcome curves are almost always below the raw future projection curve except for the CRCM-CCSM run, which indicates a positive adjustment to temperature values. The MLR curves for the HRM3 runs are similar to the raw future projections, while the MLR projections for other models adjust raw future projections of daily maximum temperature below 20 °C to higher values. The same sets of analysis for daily minimum temperature are shown in Figure 2-10 to Figure 2-12. The NCEP runs for all models tend to underestimate daily minimum temperature on for smaller values (below 0 °C), which is also found for the control runs of CRCM-CCSM, CRCM-CGCM3, WRFG-CCSM, and RCM3-CGCM3. The MLCR resulted in a distribution that is more similar to the distribution of the observations, compared to the MLR outcomes that correct the mean but not the distribution of the data. Additionally, the MLR transformations even increase the distribution differences from the observations at higher temperature values for the RCM3 and

HRM3 runs. The ECDFs for future projections are shown in Figure 2-12. The MLR and MLCR methods tend to increase values on the lower end for the two CRCM runs and the WRFG-CCSM run, while the MLR method generally decreases values at the higher end of temperature for all models except for the two CRCM runs.

2.4.3 Growing Degree Days

For the baseline (1980-2000) period, the observed median GDD is about 2480. According to the CMIP5 projections, the median GDDs for the 2010-2030 time slice for Maple City are around 2700, while the differences among models are smaller than 300 (Figure 2-13). During 2040-2060, the median GDDs are round 3000 with the RCP 8.5 scenarios having the highest GDDs, followed by the RCP 4.5 and the RCP 6.0 scenarios. The median GDDs are slightly higher in the RCP 4.5 than the RCP 6.0 scenario, which correspond to the increasing GHG concentration over time. The RCP 4.5 and RCP 6.0 scenarios have GHG concentration peaking at mid-century and end-of-century, respectively, while RCP 4.5 has higher GHG concentrations before 2060. Thus it is not surprising that GDDs for RCP 4.5 are higher during 2040-2060 compared to RCP 6.0 (Figure 2-14). Near the end of the century, the RCP 8.5 GDDs for some models can be as high as 4500 (Figure 2-15). On the other hand, the RCP 4.5 and 6.0 scenarios increased slightly in GDD, but remain close to each other.

Compared to the baseline period, the differences in GDD are relatively small for all RCP scenarios (below 500) during 2010-2030 (Figure 2-16). During 2040-2060, the

differences in GDD for RCP 4.5 and RCP 6.0 range from 300 to 900, while the differences for RCP 8.5 have a much larger range of 500 to 1300 (Figure 2-17). Near the end of the century, the change in GDD for the RCP 8.5 scenario ranges from 800 to 2000. The changes of GDD for the RCP 4.5 and 6.0 scenarios have small differences for both periods with the former higher during 2040 to 2060 and the latter higher during 2070 to 2090 (Figure 2-18). The models which projected higher GDDs compared to other models are consistently higher in all periods. The results appear to be more model-dependent, with models from the same center producing results that are more similar compared to results from other models in most cases. For example, the MIROC model family is near the upper bound of the ensemble, same as Hadley Centre models. On the other hand, the GFDL and GISS models are near the lower bound. The FIO-ESM and MRI-CGCM3 models are also lower compared to others.

For the NARCCAP delta projections, the GDDs for the future periods are around 3000 for all models (Figure 2-19). The change in GDDs for the NARCCAP models are generally around 500, similar to the average of the CMIP5 models, but with smaller intra-model variations (Figure 2-20). Comparing among models with the same driving GCM (e.g. CRCM-CGCM3 and RCM3-CGCM3) and same RCM (e.g. CRCM-CCSM and CRCM-CGCM3), the differences in projections do not appear to be dominated by either RCM or GCM. The WRF-CGCM3 model has the smallest increase (around 300) of GDD during 2040-2060.

Driving by NCEP reanalysis, the GDDs for the four RCM simulations during 1978-1998 are around 2000, while HRM3-NCEP has somewhat higher values of 2500 (Figure 2-21). The NARCCAP simulated GDDs based on raw RCM simulations, the MLCR

downscaling method, and the MLR downscaling method for the current and future period are presented in Figure 2-22 to Figure 2-23. The GDDs for the current period for the RCM raw and NARCCAP MLR projections are around 2000, while the NARCCAP MLCR projections for the current climate are around 2300 (Figure 2-22). For the future period, the GDDs range from 2000 to 3000 and average around 2500 for the NARCCAP raw and MLR projections, while the values are about 3000 for the NARCCAP MLCR projections (Figure 2-23). The differences within the ensemble are much smaller for the MLCR projections, which is understandable given the distribution correction based on observations (increased temperature for a large portion of the distribution). The differences between future and current simulations are shown in Figure 2-24. The changes in GDD mostly stay in the 400 to 600 range, with changes in the MLCR projections being the highest. The range of changes is largest for the MLR method, followed by the raw projections and the MLCR method.

2.4.4 Growing Season Length

For the baseline period of 1980-2000, the observed median growing season length is 134 days. The growing season length is defined as the period from last spring frost to first fall frost. If there is no frost during this period, the growing season length is defined as 274 days which simply indicates the total days of spring, summer, and fall during a year. The median growing season length for CMIP5 projections increases from 140 days at 2010 to 2030 for all three RCP scenarios to as high as 230 days for the RCP 4.5 and the RCP 6.0 scenarios and almost 240 days for the RCP 8.5 scenario during 2070-2090 (Figure 2-25 to 2-27). The

differences in growing season lengths (simulation minus observation) are shown in Figure 2-28 to Figure 2-30. The growing season length increases about 5 to 30 days (averaged about 10 days) for the period 2010-2030, and 10 to 50 days (averaged about 20 days) for the RCP 4.5 and the RCP 6.0 scenarios, and 20 to 70 days (averaged about 40 days) for the RCP 8.5 scenario during the 2040-2060 period. For the period 2070-2090, the range of the changes becomes even larger: the smallest increase is from the FIO-ESM in RCP 4.5 scenario (less than 10 days), the largest increases are for MIROC-ESM in the RCP 4.5 scenario (~70 days), MIROC-ESM and MIROC-ESM-CHEM in the RCP 6.0 scenario (~70 days), and MIROC-ESM and MIROC-ESM-CHEM in the RCP 8.5 scenario (~100 days). The average change in the median growing season length is about 40 days, 40 days, and 60 days in for the three emissions scenarios, respectively.

For the NARCCAP delta projections, the median growing season lengths are close to 150 to 160 days with WRFG-HadCM3 and RCM3-GFDL being the lowest and HRM3-HadCM3 being the highest (Figure 2-31). The changes in growing season length are around 30 days, as shown in Figure 2-32.

In Figure 2-33, the growing season lengths for the NARCCAP NCEP simulations are presented. The variation within the ensemble is reasonably small. The median growing season lengths for the control and future periods of for the NARCCAP with RCM raw projection, MLCR, and MLR downscaling methods are shown in Figure 2-34 to 2-35. For the control period, the MLR results show more variations among models. The median growing season lengths range from 120 to 170 days for the control period and 130 to 200 days for the future period. The projected growing season lengths have the largest variation among models

in the MLR simulations, followed by the MLCR and the RCM raw simulations. The differences of the future and control periods are shown in Figure 2-36. The averaged median change in growing season length is about 20 days for all projections. The RCM raw projections and the MLR projections have a smaller range of changes compared to the MLCR projections. On the contrary to the GDD projection, the MLCR method does not reduce the within-ensemble difference. Given that the GDD is an accumulated temperature index, the GDDs are more closely related to distribution of temperature than is growing season length. On the other hand, growing season length is more related to the distribution portion that is below 0 °C. For example, the RCM runs in Figure 2-11 has have MLR curves above the raw simulation curves and MLCR curves below the raw simulation curves, which corresponds to increased/decreased portion below 0 °C for the MLR/MLCR projections, which corresponds to longer growing season length in MLCR and lower growing season length in MLR for the two RCM3 runs.

2.5 Discussions

A large number of future climate projections were produced from two data sources (CMIP5 and NARCCAP) and downscaled and/or bias-corrected using a variety of methods. The projections include CMIP5 delta projections, NARCCAP delta projections, NARCCAP raw data projections, NARCCAP MLR projections, and NARCCAP MLCR projections. For the CMIP5 projections, three RCP scenarios are included, i.e. RCP 4.5, RCP 6.0, and RCP 8.5. For the NARCCAP projections, the simulations are forced with the A2 emission scenario.

Additionally, for the CMIP5 projections, 16 GCMs are used to form an ensemble, while for NARCCAP 8 members are adopted. Using Maple City as an example, the climate projections for lake-modified locations in Michigan and their potential agricultural impact are discussed. Even though the projected direction of changes is largely consistent among models, the differences within the ensemble are still very large, especially towards the end of the 21st century. At mid-century, the change in average temperature can vary by 7 °C among models, while this value can be as large as 12 °C towards the end of century. Given such uncertainty in projections, using only one model in agricultural impact analysis may be problematic. Additionally, taking the average of the ensemble may also underestimate or overestimate the magnitude of future changes, and thus misinform the stake holder or public about the potential danger of extremes climate conditions.

Even though the averaged changes in temperature for the models may only differ by a few degrees, the resulting differences in the impact on agriculture can be significant. For example, a one to two degree increase accumulated throughout a year may induce a GDD increase of a few hundred units. Such uncertainty cannot be neglected in any agricultural impact analysis.

In terms of the range of the ensembles, the NARCCAP ensemble has a smaller range in monthly change factors than CMIP5. However, given the uneven number of models included in the ensemble, a conclusion cannot be made on whether the GCM projections are associated with larger uncertainty compared to the RCM projections. The downscaling methods like MLCR tend to shrink the range of the changes in GDD compared to raw simulations, as multiple models are bias-corrected first based on observations, NCEP

simulations, and control simulations, and then applied to future projections. However, the range of the changes in growing season length is not necessarily reduced, given GDDs rely on the distribution of the projections of daily maximum and minimum temperature while growing season length is more related to daily minimum temperature with a critical threshold of 0 °C.

For most of the GCMs in CMIP5, the Great Lakes region are identified in the model as land, which does not take into consideration the effects caused by existence of large water surface such as lake effect precipitation, or temperature adjustments of a large water body. On the other hand, the RCMs generally resolve the coastlines of the lakes, which may present added value of dynamical downscaling compared to raw GCM outputs. For the statistical downscaling like the delta method, the effects of the lakes are partially accounted for, as observation data are used as a baseline.

The RCP 4.5 and RCP 8.5 scenarios currently receive more attention than the RCP 6.0 scenario (in terms of data simulation archive). In the analysis of the change factors, GDD, and growing season length, the future changes for RCP 4.5 and RCP 6.0 scenarios are very similar for all time slices, compared to the RCP 8.5 scenario, which generates larger values in these examples. The peaking time of the greenhouse gases is earlier in RCP 4.5 than RCP 6.0 and thus producing somewhat larger changes in GDDs and growing season lengths in RCP 4.5 in the mid-century time slice, which is reversed for the end of the century time slice. In most cases, the GCMs or RCMs from the same modeling group tend to yield more similar results. Thus, if given limited time and resources in agricultural impact analyses, work load can be reduced by choosing only one scenario from RCP 4.5 and RCP 6.0 instead of both and

choosing one GCM or RCM coming from the same modeling group. However, such simplification may suffer the loss of information, e.g. the results from GFDL-CM3 are very different from GFDL-ESM2G and GFDL-ESM2M.

In sum, many choices must be carefully reviewed before adopting one or a set of climate projections in agricultural impact analyses. By including an ensemble of models, the impact assessments are likely to better capture the uncertainty under future climate situations, and for agriculture the extreme changes are as important as the mean values.

2.6 Conclusions

This study aims to provide general guidance for choosing climate projections for agricultural impact assessments. The simple delta downscaling method was applied to both GCM and RCM ensembles, and compared to dynamically-downscaled outputs (raw RCM simulations) and outputs from hybrid downscaling methods (RCM MLR and RCM MLCR), in order to examine the similarity and differences of the projections.

For Maple City, Michigan, the future climate, as simulated by both the CMIP5 and NARCCAP models, is projected to increase in temperature and a likely increase in precipitation. Compared to the baseline period, the increase in the monthly average of maximum temperature ranges from 0 to 5 degrees Celsius during 2040-2060 and 0 to 10 degrees during 2070-2090. The GDDs are projected to increase by 500 units for the RCP 4.5 and RCP 6.0 emission scenarios and increase by 700 for the RCP 8.5 scenario by mid-century, while these numbers are 700 and more than 1000 for the end-of-century time slice. The

NARCCAP delta projections exhibit similar changes in GDD to the RCP 4.5 and the RCP 6.0 scenarios, which are slightly lower than changes for the RCP 8.5 scenario. Moreover, the NARCCAP MLCR and NARCCAP MLR simulations all project about a 500 unit increase in GDDs.

On the other hand, the CMIP5 delta scenarios projected a 20-day increase in growing season length for the 2040-2060 time slice for the RCP 4.5 and RCP 6.0 scenarios, and about a 30-day increase for the RCP 8.5 scenario compared to the baseline period of 1980-2000. These values become 30 days and 60 days for the 2070-2090 time slice. Again, the NARCCAP delta projections, NARCCAP raw simulations, NARCCAP MLCR projections, and NARCCAP MLR projections also show increased growing season length around 20 days.

The bias-correction/downscaling method of MLCR tends to decrease the range of projected changes in GDD and increase the range in changes in growing season length compared to the raw RCM simulations, while that of the MLR method is more similar to the raw RCM projections. The MLR method only intends to reduce the residual errors in simulations, while MLCR method also tries to match the simulation distributions to the observed distributions. When using GDD as an indicator, the distribution of both maximum and minimum temperature plays a significant role. On the other hand, the growing season length index is more related to daily minimum temperature, as a positive adjustment in temperature is expected to increase the length of the frost-free period.

One assumption of applying transfer functions like MLR or MLCR to the future projections is that the biases of models are consistent over time, which is not always true. Extrapolations beyond the current data thresholds should be made to account for such issues.

Under this situation, dynamical downscaling may outperform statistical downscaling if there will be large changes in mechanisms that can be captured by RCMs.

Chapter 3 Evaluation of the Southerly Low-level Jet Climatology in the Central United

States as Simulated by NARCCAP Regional Climate Models

In collaboration with
Shiyuan Zhong, Julie A. Winkler, and Claudia K. Walters

3.1 Introduction

A low level jet (LLJ) is a wind maximum in the lower troposphere. Although LLJs have been observed around the world, the central part of the United States is particularly prone to frequent occurrences of LLJs (e.g., Bonner 1968; Walters et al. 2008). Southerly LLJs (S-LLJs) in this region transport warm, moist air from the Gulf of Mexico northward (Means, 1954; Helfand and Schubert 1995), and have been related to nighttime precipitation maxima (Pitchford and London 1962; Bonner 1966). Although much less frequent than S-LLJs, northerly LLJs (N-LLJs) in the central United States advect continental polar air southward from Canada (Kapela et al. 1995). Because of the high wind speeds and strong wind shear associated with LLJs, their influence extends beyond weather and climate to include air pollution transport and dispersion (Banta et al., 2002), forest fires (Charney et al. 2003), transportation safety (Sjostedt et al. 1990), insect outbreaks (Song et al. 2005; Stensrud 1996) and wind energy (Storm et al. 2009).

The characteristics of LLJs in the central United States have been examined using observational data and numerical models. Most observational studies employed data from rawinsonde networks, although a few have used data from various other sources, including the National Oceanic and Atmospheric Administration (NOAA) profiler network (Mitchell et

al. 1995) and the National Centers for Environmental Prediction (NCEP) and the National Center for Atmospheric Research (NCAR) reanalyses (Anderson and Arritt 2001). Bonner's (1968) analysis of two years of twice-daily wind data from 47 rawinsonde stations across the United States provided the first comprehensive climatology of LLJs and laid the foundation for future studies. Mitchell et al. (1995) developed a warm-season LLJ climatology at a higher temporal resolution using hourly wind profiler observations over the central Great Plains for 1991 and 1992. Whiteman et al. (1997) analyzed high vertical and temporal resolution rawinsonde observations for two years from a site in north-central Oklahoma, which provided a detailed climatology of LLJs in the southern Great Plains. Song et al. (2005) developed a LLJ climatology for a site in Kansas using hourly, high-resolution vertical profiles of wind velocity from a combination of a minisodar and a wind profiler. Although these studies significantly advanced our understanding of the vertical structure and evolution of LLJs, they were limited in space and time by relying on data from either a handful of stations or for short periods of time (one month to two years). In contrast, Walters et al. (2008), using a 40-year time series of wind observations from the rawinsonde network, provided a long-term climatology of LLJ frequency, direction, speed and elevation for the central United States, although at a relatively coarse (~300 km) spatial scale.

Gridded reanalysis data have also been used to understand the climatological properties of LLJs. Doubler et al. (2015) developed a climatology of LLJs over North America and coastal environs using the North American Regional Reanalysis (NARR, Mesinger et al. 2006) with 3-hourly output and 32 km resolution, and evaluated jet characteristics such as frequency, speed and elevation against prior sounding-based studies.

They found strong agreement with existing LLJ climatologies and provided additional insights on the spatial extent and seasonal shifts of jet frequencies. Walters et al. (2014) compared LLJs identified from NARR and rawinsonde wind profiles for 12 stations in the central United States for four representative years and found general agreement between the two data sources, although jet frequencies are smaller for NARR at most locations.

General circulation models (GCMs) have also been used to study the LLJ climatology over the central United States. For example, Helfand and Schubert (1995) employed a GCM to simulate Great Plains LLJs and their contribution to the moisture budget for two springtime months. Ghan et al. (1996) studied LLJs using two GCMs, and found that LLJs were generally well simulated despite the differences between models, although both models failed to simulate the physical connection between clouds and LLJs. Cook et al. (2008) examined simulations of LLJs over the Great Plains from 18 atmosphere-ocean GCMs during the 21st century and projected more intense Great Plains LLJs during April, May, and June. As illustrated by these studies, an advantage of using GCM simulations to investigate LLJs is more uniform spatial coverage and more frequent temporal coverage compared to observational data. The relatively coarse spatial resolution, on the other hand, is a disadvantage. Other limitations include simulated LLJs that are either too weak or too strong, misplacement of a frequency maximum for LLJs, or weak association with physical processes (Cook et al. 2008; Ghan et al. 1996).

Because a LLJ is a regional phenomenon, the use of regional models is likely to provide “added value” to the GCM-based LLJ studies by better resolving features important for LLJ formation such as terrain heterogeneity (the Rocky Mountains and the High Plains),

coastlines (the Gulf of Mexico) and nocturnal surface-based inversions. Regional models have been primarily used to simulate an individual LLJ event (Zhong et al. 1996; Storm et al. 2009) or a series of jet events during a short time period, usually a few weeks or less (Werth et al., 2011; Vanderwende et al. 2015). Rarely have regional models been used to simulate the climatology of LLJs in the central United States.

Before regional climate models (RCMs) can be used as a viable tool for LLJ climatological studies, their ability in capturing the vertical structure of LLJs and the spatial and temporal variability of the LLJ climatology should be assessed. To date, there has not been a systematic evaluation based on multiple models of how well RCMs simulate the LLJ climatology of the central United States. RCM representations of LLJs often are only broadly compared with observations, usually with the goal of seeking possible factors contributing to biases in simulated regional precipitation (e.g., Liang et al. 2004) rather than as an evaluation of a climatological phenomenon that merits its own in-depth assessment.

In this study, we aim to compare RCM results against sounding observations to provide an initial evaluation of how well RCMs simulate the long-term LLJ climatology of the central United States. Understanding the ability of RCMs to simulate LLJs under the current climate is critical for interpreting results from RCM future climate simulations and assessing the impact of climate change on LLJs. In order to examine the usefulness of RCM results, the spatial patterns of the characteristics (frequency, height, and speed) of LLJs are analyzed for a suite of four RCM simulations that were driven by the NCEP-Department of Energy (DOE) Reanalysis 2 (referred to below as NCEP, Kanamitsu et al. 2002) for the current climate and produced for the North American Regional Climate Change Assessment

Project (NARCCAP, Mearns et al. 2012). This suite of RCM simulations was selected because of the wide use of the NARCCAP output in impact studies as evidenced by over 100 published papers and reports (Mearns et al. 2015), including many for the central United States (e.g., Takle et al. 2010; Zhang et al. 2011; Li et al. 2012; Qiao et al. 2014).

The analyses below are limited to S-LLJs in the central United States, given their much greater frequency compared to LLJs from other compass directions (Walters et al. 2008). The specific objectives of the current study are to 1) examine the S-LLJ climatology simulated by the NARCCAP RCMs driven by the NCEP reanalysis for the current climate and 2) compare the simulated climatology with that of rawinsonde observations. The analyses will focus on the spatial distribution and diurnal, seasonal and annual variations of S-LLJs. As mentioned above, previous LLJ climatologies are limited either by the number of stations used in the analysis, the coarse resolution of the observing networks or GCM simulations, and/or the length of the study period. RCMs may serve as a viable alternative for LLJ studies. The detailed LLJ climatology produced by a RCM ensemble, when evaluated against observations for an extended period, will significantly enhance our understanding of finer-scale spatial and temporal variations of LLJ characteristics and their representation in regional climate models.

3.2 Data and Methods

The most commonly-used definition of a LLJ was introduced by Bonner (1968), who defined a LLJ as a wind maximum $\geq 12 \text{ ms}^{-1}$ at or below 1.5 km above ground level (AGL),

with a decrease by at least 6 ms^{-1} to the next higher minimum or 3 km AGL, whichever was lower. In the current study, the height range for the wind maxima is extended to 3 km and the height of the next higher minimum is extended to 5 km to account for synoptically-driven LLJs that often slope upward with latitude. Following Walters et al. (2008), an additional criterion of a decrease below the jet nose of at least 6 ms^{-1} is prescribed. Jets with a direction between 113° - 247° are considered southerly jets, while jets originating between 293° - 67° are classified as northerly jets. Only the results for southerly jets are presented here due to the limited space, and the very different mechanisms leading to the formation of N-LLJs and S-LLJs.

The LLJ climatology is generated from model simulations provided by the NARCCAP (Mearns et al. 2007; Mearns et al. 2009; Mearns et al. 2012). This study analyzes the set of RCM simulations driven by the NCEP reanalysis for the period 1979-2004. A 50 km horizontal grid spacing was used in all the RCM simulations. The archived data contains 28 vertical levels from 1050 hPa to 50 hPa, with a vertical resolution of 25 hPa below 700 hPa and 50 hPa above 700 hPa. Three-hourly data are available for NARCCAP outputs.

Four model runs are included in the current study, namely CRCM, WRF, RCM3, and HRM3. The other two RCMs in the NARCCAP suite, the Scripps Experimental Climate Prediction Center Regional Spectral Model and the fifth-generational Pennsylvania State University-National Center for Atmospheric Research Mesoscale Model, are not included in the analysis because wind data at multiple vertical levels was not archived for these models. LLJs are extracted from the simulated vertical wind profiles based on the criteria described above.

The RCM-simulated LLJ climatology is compared to a sounding-based LLJ climatology as described in Walters et al. (2008) that was derived from a network of 36 rawinsonde stations across the central United States. The simulated and observed climatologies are produced for the 21-year period, October 1979 - September 2000, which is the period of overlap between the RCM simulations and the database of jet occurrences developed by Walters et al. (2008). The locations of the rawinsonde stations along with the station elevations are shown in Figure 3-1. Also shown in Figure 1 is representative topography as resolved by one of the RCMs. There are only small variations in topography across the four models because the same horizontal grid spacing was adopted for all the NARCCAP simulations. The difference between the model topography and the station topography is relatively small for most stations except for a few near the western border of the rawinsonde network where the 50-km model grid spacing is too coarse to resolve the mountainous terrain.

To compare with the twice-daily soundings, only 00 UTC and 12 UTC are considered for the RCM data analysis. Although only twice per day, these two times capture the LLJ diurnal variation rather well (Walters et al. 2008). At either 00 or 12 UTC, jet frequency and average jet speed and height are calculated for each month of the year to enable an examination of sub-seasonal variations. The results are further grouped into warm (April – September) and cold (October – March) seasons for the analysis of seasonal variability. The jet frequency for a particular month of the year is calculated simply as the ratio of the number of S-LLJ wind profiles to the total number of available wind profiles for that month over the entire 21-year study period. Similarly, the jet speed and jet height for a particular month of

the year are calculated by averaging the LLJ speed and the LLJ height using all S-LLJ wind profiles for that month and over the 21-year period. The same procedures are used to calculate the climatological values for the rawinsonde locations, although the number of available soundings is somewhat smaller because of missing observations or erroneous measurements. The percentage of useable soundings for each rawinsonde station at 00 UTC or 12 UTC during the warm and cold seasons is shown in Figure 3-2. Most stations have over 90% useable soundings, with the lowest percentage just over 70%. Generally, the warm season has more useable soundings compared to the cold season, while 00 UTC has more useable soundings than 12 UTC.

The calculations are carried out at each RCM grid point and rawinsonde location and the spatial distribution of jet frequency and average jet height and speed are shown in 4-panel figures with sounding results overlaid on the RCM results. The color scale for observations and RCM model simulations are identical for better visual comparison. In addition, the monthly S-LLJ frequencies at the rawinsonde stations and the RCM grid points nearest each station are used to compare the annual cycle of S-LLJ frequency. The annual cycles are displayed on cross-sectional plots, with the stations generally grouped from west to east and from north to south for visual comparison.

3.3 Results

3.3.1 Jet Frequency

3.3.1.1 Cold Season S-LLJ Frequencies

At 00 UTC during the cold season (Figure 3-3), the observed jet frequency for the 21-year evaluation period ranges from approximately 0-14%, which broadly is the range of the RCM simulations. Higher observed frequencies are found over the southern and central plains, with the highest value (14%) at the southernmost rawinsonde station (Brownsville, Texas (BRO)), followed by 7-8% at other stations in Texas and in Oklahoma, Kansas and eastern Nebraska. The RCM simulations generally capture the observed spatial distribution as well as the magnitude. The WRFG and HRM3 simulations, and to a lesser extent the CRCM simulation, display weak frequency maxima in the central plains (Kansas, Oklahoma, and Missouri), similar to the observed pattern, whereas relatively uniform frequencies are observed over the northern and central plains and the Midwest for the RCM3 model. The higher observed jet frequencies at Corpus Christi (CRP) and BRO are missed by the model simulations except for HRM3, although the HRM3 percentage is lower than the observed value. In contrast, RCM3 places somewhat higher frequencies to the west of BRO in northeastern Mexico. RCM3 is the only simulation with a frequency maximum (>12%) over southeast Arizona, although this area falls outside of the extent of the rawinsonde locations in the Walters et al. (2008) dataset.

The RCM simulations capture the generally higher jet frequencies at 12 UTC compared to 00 UTC during the cold season (Figure 3-4). The largest S-LLJ frequencies at 12

UTC in the observations are found across the central and southern plains from approximately Omaha, Nebraska (OAX) to Midland, Texas (MAF) and also over CRP and BRO. The RCM simulations reproduce the overall spatial pattern of S-LLJ frequencies, although the areal extent of the frequency maximum for the CRCM simulation is smaller than that of the observed maximum. Also, the jet frequencies, especially in Oklahoma and northern Texas, are underestimated by all of the RCM simulations. All four RCMs correctly place a frequency maximum over the southern tip of Texas, although again jet frequencies are somewhat underestimated and the maximum is displaced westward, especially for the CRCM and RCM3 simulations. The RCM3 and WRFG simulations present somewhat greater frequency values over the western Appalachian Highlands, which capture the higher observed frequency (11%) at Nashville, Tennessee (BNA). All four model simulations produce a frequency maximum in southeast Arizona, which is most obvious in the RCM3 simulation. Additionally, a frequency maximum over northern Mexico is seen for two of the models (WRFG and RCM3). Both of these areas fall outside the extent of the evaluation dataset.

3.3.1.2 Warm Season S-LLJ Frequencies

Warm season S-LLJ frequencies at 00 UTC are less than 10% across most of the study domain for both observations and model simulations with the exception of HRM3 (Figure 3-5). An area of higher jet frequencies centered on eastern Kansas and Oklahoma is evident for both HRM3 and WRFG. This frequency maximum is considerably more pronounced in the HRM3 simulation with jet frequencies exceeding 12%, which is almost

twice the magnitude of observed values. HRM3 is the only model that presents a frequency maximum in southern Texas at 00 UTC. A comparable maximum is not seen in the observations.

S-LLJ frequencies increase dramatically from 00 to 12 UTC during the warm season for all the RCM simulations (Figure 3-6). However, the spatial pattern of jet frequency, and its coherence with observations, differs considerably between RCMs. The broad area of frequent S-LLJ occurrences from approximately South Dakota to central Texas, as simulated by WRFG, agrees most closely with the observed spatial extent, whereas relatively high jet frequencies extend farther northward and eastward than observed for HRM3 and RCM3, respectively. HRM3 best captures the area of highest frequencies in the central plains (Kansas, Oklahoma, northern Texas). Jet frequencies are underestimated in this area by RCM3 and even more so by WRFG. All three models simulate a separate area of high jet frequency over extreme southern Texas, although RCM3 and HRM3 considerably overestimate the magnitude of this frequency maximum. In contrast, for the CRCM simulation the higher jet frequencies are generally confined to the central plains where S-LLJ frequencies are substantially underestimated, particularly in Kansas, Oklahoma, and northern Texas. Additionally, this model fails to simulate a frequency maximum over extreme southern Texas, although a weak maximum is seen farther west in northeastern Mexico.

Intra-seasonal (i.e., monthly) plots of S-LLJ frequency at 12 UTC further highlight the differences between models during the warm season (Figure 3-7). Beginning with April, all four RCMs place a frequency maximum in central Texas with a separate maximum in extreme southern Texas, although the magnitude and spatial extent of elevated S-LLJ

frequencies varies. The frequencies further increase during May. Between-model differences are somewhat larger in June and July, when the frequency maximum initially in central Texas shifts northward to northern Texas and Oklahoma for all models except RCM3, and a maximum over southern Texas is no longer evident for CRCM. Model differences are greatest in August when high jet frequencies for the CRCM are confined to a relatively small area centered over Kansas. The largest frequencies for WRFG are also found in the central plains (Kansas and northern Oklahoma), although high frequencies are seen over a much larger area compared to the CRCM simulation. In contrast, the frequency maximum remains in northern Texas and Oklahoma for HRM3 and in central Texas for RCM3. Additionally, only RCM3 and HRM3 display a distinct frequency "hotspot" over southern Texas. The RCMs are in greater agreement in September. By September, the frequency maximum has shifted northward into Kansas for all models. Also, the spatial extent of higher jet frequencies has shrunk. Relatively high jet frequencies persist over southern Texas for RCM3 in September.

3.3.1.3 Annual Cycle of S-LLJ Frequency

To evaluate how well the RCM models simulated the annual cycle of jet frequencies, the percentage of S-LLJs for each month was calculated at the RCM grid point nearest each rawinsonde station as the ratio of the number of S-LLJs found in that particular month over the 21-year period to the total number of S-LLJs (all months and all years) and then compared with observations (Figure 3-8). Only the results for 12 UTC are shown given the

much larger frequency of jets at this hour. For the observations, the stations located over the western and central plains (left side of the figure) display a strong annual cycle with most S-LLJs occurring during the warmest part of the year from May through September, while those located farther east have more jets during spring and autumn. The CRCM simulation has the most similar annual cycle compared to the observations. The annual cycle for WRFG, RCM3, and HRM3 also diverges from a warm season maximum to spring and autumn maxima along a west to east transect, but the shift is not as obvious as in CRCM or in the observations and occurs considerably farther east toward the Great Lakes and Appalachian Highlands. Differences also exist between stations located north and south, which is particularly obvious in the CRCM, WRFG, and HRM3 simulations. For stations in the Great Plains (station 6 to station 25), those located farther south tend to have higher S-LLJ frequencies earlier in the year than those located farther north. Furthermore, the simulations have generally darker shades of red during the warm season compared to the observations, indicating a general overestimation of the strength of the annual cycle. Additionally, the WRFG simulation generated higher frequencies during the winter months for stations located along the easternmost boundary of the study region, compared to the other simulations and to observations.

The differences between the model simulations and observations highlight the times of the year with positive and negative biases in the frequency of S-LLJs at 12 UTC (Figure 3-9). In general, the RCMs tend to underestimate S-LLJ frequency during the cold season and to overestimate the frequency during the warm season. More specifically, HRM3, as well as RCM3, consistently underestimate the warm season frequency. WRFG seems to

underestimate the frequency from October to December and overestimate it for other months. Overall, the stations located in a narrow zone from north to south in the Great Plains (stations 6-17) seem to have smaller differences compared to other stations located farther east, as indicated by the lighter shades on the left side of Figure 3-9 compared to the darker colors on the right side. The somewhat random discrepancies at the westernmost locations (stations 1-5) are probably due the lower total number of jets at these locations.

3.3.2 Jet Height

At 00 UTC during the cold season, the observed elevations of S-LLJs are higher above the ground level (AGL) over the central plains and the Gulf States (Figure 3-10). The highest observed values of as much as 1500 m AGL are found in Arkansas, northern Louisiana and Alabama, which is followed by stations along the Gulf Coast that have average jet heights around 1100 m AGL. In contrast, the stations along the western edge of the study area have jet heights of 900 m AGL or lower. The four model simulations capture this general pattern of jet height variation. The simulations are closer to observations at locations where jet heights are lower. This might be related to the vertical resolutions of the archived model outputs that are much coarser compared to the rawinsonde observations, especially farther away from the ground level. The four simulations generally underestimate the average jet heights in the southeastern portion of the study area and are closer to the observations farther west. The CRCM simulation is in closer agreement with the observations, especially for those areas where jet elevations are higher.

The observed average jet heights are lower at 12 UTC for the cold season, with the highest values of 900-1000 m AGL found along the Gulf of Mexico, and decrease to around 600-800 m AGL over the western portion of the study area (Figure 3-11). Compared to 00 UTC, the model simulations show a similar spatial pattern at 12 UTC, but with lower jet heights. The simulated heights over much of the study area are in good agreement with observed values except for RCM3, which underestimates the jet height, especially in the northern and central plains. The diurnal variation in the average jet height is more pronounced in the observations for the Gulf region than in the model simulations, which can be attributed to the underestimation of jet heights at 00 UTC.

Similar spatial patterns are observed in the warm season. However, the average warm-season jet heights are generally above 1000 m at 00 UTC (Figure 3-12), which is somewhat elevated from the cold-season 00 UTC jet heights. On the other hand, the heights at 12 UTC are generally within 400-800 m AGL except for stations along the Gulf Coast or in Ohio and Michigan's Lower Peninsula (Figure 3-13). At 00 UTC, the RCM3 simulation seems to have the highest heights while the HRM3 run has the lowest. At 12 UTC, WRFG seems to be the closest to the observed values, while RCM3 generally underestimates heights in the northern portion of the study area. The diurnal variation is stronger during the warm season than the cold season according to the observations. This diurnal fluctuation in the warm season is also better simulated by the models than during the cold season.

3.3.3 Jet Speed

During the cold season, the observed average S-LLJ speed reached 20 ms^{-1} in the central plains and the Midwest (Figures 3-14 and 3-15). For both 00 UTC and 12 UTC, the four models show similar spatial patterns of average jet speed with the highest speeds over the Midwest and a gradual decrease westward and southwestward, which resembles the observed spatial pattern. The CRCM and RCM3 runs have average speeds about 2 ms^{-1} higher than those of the WRF and HRM3 runs, and the simulated values are similar to the observed speeds except for an overestimation in the Midwest. WRF, and even more so the HRM3, simulate lower-than-observed jet speeds. The diurnal variation in jet speed is modest during the cold season for both the observations and simulations.

The warm-season average jet speed is generally $2\text{-}4 \text{ ms}^{-1}$ lower than the cold season average (Figure 3-16 and 3-17). The highest observed average jet speeds are found in the northern plains and the Midwest, with somewhat lower average speeds in the Gulf states. The four models again simulate similar spatial patterns, although RCM3 has a larger area of higher average speed compared to the other models. For both 00 UTC and 12 UTC, the simulated values are quite close to the observations. The diurnal variation for the warm season is also modest but slightly stronger than the cold season.

3.4 Discussion

Only a modest number of previous studies have explicitly evaluated the ability of RCMs to simulate the characteristics of S-LLJs in the central United States, even though S-

LLJs are an important component of the regional climatology. Previous analyses that focused on the climatological characteristics of S-LLJs as simulated by RCMs have for the most part been limited to an evaluation of wind vectors on constant (typically 850 hPa) pressure surfaces (e.g., Cerezo-Mota et al. 2011), whereas comparisons that considered the vertical wind shear profile have largely been restricted to case studies of jet events (e.g., Zhong et al. 1996; Vanderwende et al. 2015). The model evaluations presented here considerably expand on these previous analyses, as S-LLJs are identified from the vertical wind profiles of 21-year simulations from four RCMs, using criteria similar to those employed in numerous observational studies and considering both jet speed and vertical shear. This evaluation has particular significance in that the RCM simulations are from the NARCCAP suite of RCM runs that have been widely used in climate impacts studies (Mearns et al. 2015). Thus, the evaluation helps to support the credibility of these simulations and their use in climate assessments.

An important consideration for any model evaluation is the choice of dataset for comparison. Reanalysis datasets are often used for model evaluation (e.g., Cerezo-Mota et al. 2011), in part because of the greater spatial and temporal coverage of these gridded datasets compared to observations. However, the underlying data assimilation system and forecast model, along with the resolution at which the reanalysis data are archived, can introduce biases (e.g., Mo et al. 2005; Walters et al. 2014). For this reason, we elected to use an observational dataset for comparison. Rawinsonde measurements are the only feasible observational dataset because of their greater spatial coverage and longer period of record compared to alternative sources (e.g., the recently discontinued NOAA Profiler Network),

although their coarse temporal (twice daily) and spatial (~300 km) resolutions limit the comparisons that can be made. Inhomogeneities can also exist in the rawinsonde record due to changes during the period of record in instrumentation and observation protocols (Winkler 2004; Walters et al. 2014). The evaluations presented above highlight that, in spite of these limitations, the use of rawinsonde observations as a source of comparison provides helpful insights that can complement and supplement comparisons with reanalysis datasets.

In general, the four RCM simulations capture the characteristics of the observed S-LLJ climatology. The simulations are in good agreement with the observations when the jet frequency is low (during the cold season and at 00 UTC during the warm season), but tend to underestimate the jet frequency when the observed values are relatively high (at 12 UTC during the warm season). The higher jet frequencies at 12 UTC and stronger diurnal variation during the warm season agree with the rawinsonde observations and are further supported by previous studies (Bonner 1968; Mitchell et al. 1995; Whiteman et al. 1997). The model simulations reproduced the decrease in S-LLJ mean elevation from south-southeast to north-northwest across the study area, the higher jet elevations at 00 UTC compared to 12 UTC, and the somewhat stronger diurnal variation in jet elevation during the warm season. The simulations also captured the observed westward decrease in jet speed from the Great Lakes to the High Plains and the stronger jet speeds during the cold season compared to the warm season.

Differences exist between the model simulations, however, with the most intriguing being the spatial placement and migration of the highest jet frequencies. Dating to the early climatological analyses of Bonner (1968), the "spatial core" of warm season nocturnal S-LLJ

activity has commonly been considered to be centered in Oklahoma and Kansas (Vanderwende et al. 2015). Later climatological analyses employing a variety of data sources, including profiler measurements (Mitchell et al. 1995), NCEP-NCAR reanalysis (Anderson and Arritt 2001) and rawinsonde observations (Walters et al. 2008), suggested a more southward location of the frequency maximum in northern Texas. More recently, Doubler et al. (2015), based on their climatological analysis for 1979-2009 of the 32-km resolution NARR dataset, argued for distinct centers of greater warm season nocturnal S-LLJ activity in the central plains (Kansas/Oklahoma) and in central Texas. The simulated warm season climatological patterns for the four NARCCAP RCMs suggest that, overall, nocturnal S-LLJs are most frequent in central and northern Texas, similar to recent climatological analyses, although there is a northward migration of the frequency maximum during the warm season from central Texas to Kansas/Oklahoma with the so-called "spatial core" being the primary center of jet activity only in August and September. This migration is more rapid for the CRCM simulations with S-LLJs most frequent in Kansas/Oklahoma by July, and slowest for HRCM3 with the greatest jet frequencies remaining in central Texas into August. By September all the RCMs place the frequency maximum in Kansas/Oklahoma, but a secondary maximum remains evident in northern and central Texas for all but the CRCM simulation. This migration is in general agreement with the NARR climatology (Doubler et al. 2015), which suggests that nocturnal S-LLJs are most frequent in central Texas into July, with the Kansas/Oklahoma center dominant in August and September.

Model differences also exist in the simulation of the S-LLJ frequency maximum seen over southern Texas. In the observations, this maximum is evident at 12 UTC for both the

warm and cold seasons, although frequencies are considerably larger for the warm season. A similar maximum centered along the southern Texas coastline is also evident in the NARR climatology (Doubler et al. 2015). CRCM either misses this frequency maximum entirely or underestimates its strength. In contrast, RCM3 and HRM3 overestimate the strength of this maximum, with HRM3 simulating frequent warm season S-LLJ activity in this area even at 00 UTC, which is not supported by the observations. The strength of the frequency maximum over south Texas in the RCM3 and HRM3 simulations is particularly large in July, which is later than the April-May maximum frequencies seen in the NARR climatology (Doubler et al. 2015). The magnitude and timing of the south Texas maximum appears to be best captured by WRFG.

Between-model differences and deviations from observations in the spatial patterns and timing of jet frequencies may reflect differences in the relative magnitude of the forcing mechanisms responsible for S-LLJ occurrence or even unresolved processes in some RCMs compared to others. Warm season nocturnal S-LLJ occurrences in the central plains have been attributed to two boundary-layer forcing mechanisms, differential heating over the sloping terrain of the Great Plains and Rocky Mountains (Holton 1967) and the inertial oscillation of airflow near the top of a stable nocturnal boundary layer (Blackadar 1957). Du and Rotunno (2014) recently argued, based on a simple 1-D analytical model, that both these mechanisms contribute to S-LLJ diurnal fluctuations during June-August in a narrow zone from southern Kansas to central Oklahoma, although Vanderwende et al. (2015) later demonstrated using WRF simulations of S-LLJs in Iowa that the inertial oscillation is the more important factor for locations east of largest topographic slopes. Furthermore, as shown

by Vanderwende et al. (2015), these boundary-layer mechanisms interact with broader synoptic-scale airflow, particularly the anticyclonic airflow associated with the Atlantic subtropical high (Davis et al. 1997). CRCM's focused activity in the central plains (Kansas/Oklahoma) and depressed jet frequencies may reflect weaker synoptic-scale airflow and a greater emphasis on boundary-layer forcing, whereas the southward location and higher frequencies for HRM3 and RCM3 may reflect overly strong synoptic-scale airflow. Bukovsky et al. (2013) provide some support for this contention, as they found the June-August 850-hPa resultant wind from Oklahoma to the western Gulf of Mexico to be much larger for HRM3 compared to the corresponding CRCM 850-hPa wind field, although this explanation is incomplete as the differences between the CRCM and RCM3 wind fields are small.

Other characteristics of the RCM simulations may also contribute to the between-model differences. For example, CRCM is the only one of the four models that employed internal nudging extending the large-scale influence from the boundary of the RCM domain to the center of the domain (Bukovsky 2012; Mearns et al. 2012), which may partially explain the more limited spatial extent of the S-LLJ frequency maximum seen for this model and its location in the central plains. Furthermore, as raised by Bukovsky et al. (2013) in their evaluation of the North American monsoon, the southern boundaries of the NARCCAP simulations possibly do not extend far enough south to ensure that important larger-scale forcing translates through the model boundaries. Of particular concern is whether the model domain is sufficient to capture possible interactions between the S-LLJs and the Caribbean Jet (Cook and Vizu 2010), especially in southern and central Texas, and also to capture the

expansion/contraction and latitudinal shifts in the airflow around the Atlantic anticyclone (Davis et al. 1997).

Also of note is that the RCM simulations do not capture the annual cycle of S-LLJ frequency for locations in the eastern portion of the study area, roughly east of 93° W longitude. Here, jets are most frequent in the rawinsonde observations during spring with a secondary maximum in autumn. This timing implies that S-LLJs in the eastern portion of the study area are primarily forced by synoptic-scale mechanisms, such as strong upper-level jet streaks (Uccellini and Johnson 1979) and developing extratropical cyclones (Carr and Millard 1985; Wu and Raman 1998), which are most frequent in the central United States during the transition seasons of spring and fall, although the synoptically driven jets can be enhanced by favorable boundary-layer conditions (Mitchell et al. 1995; Walters 2001). The misplacement in the RCM simulations of the annual cycle to a summer maximum at these locations suggests that the RCMs are either not capturing the synoptic-scale forcing itself or the potential boundary-layer enhancements to that forcing. Some support for the later interpretation is provided by Vanderwende et al. (2015), who found that the WRF model had difficulty simulating S-LLJs associated with strong frontal passages.

Generalization of the findings of this evaluation to the general ability of RCMs to simulate S-LLJs in the central United States should be undertaken cautiously. Although the NARCCAP RCMs were chosen to provide a variety of model physics (Mearns et al. 2012), only a limited number of possible model configurations were considered, which often differed between models. Consequently, systematic evaluations of the influence of different parameterization schemes, horizontal and vertical resolutions, and initial and boundary

conditions are not possible. Of particular note is the potential influence of the choice of global reanalysis used to drive the simulations. Comparisons by Vanderwende et al. (2015), for example, suggest that the choice of initial and boundary conditions has a greater influence on simulated jet occurrence than the choice of planetary boundary layer schemes. HRM3 appears to be particularly sensitive to boundary conditions. Mearns et al. (2012) found that temperature and precipitation biases for HRM3 were considerably greater than the biases for the other NARCCAP models when this model was driven by the NCEP reanalysis, but of similar magnitude when the ERA-Interim global reanalysis was used to drive HRM3. They cautioned against over-interpreting evaluations of model performance when lateral boundary conditions are supplied from only a single global reanalysis, and further argued that the quality of the reanalysis needs to be considered.

Earlier evaluations of the performance of the NARCCAP RCMs in simulating temperature and precipitation concluded that there is no best model (Mearns et al. 2012). The same conclusion can be drawn from the evaluation presented here of the ability of the NARCCAP RCMs to simulate the long-term climatology of S-LLJs in the central United States. One might be tempted to rank HRM3 above the other models as the simulated jet frequencies, especially during the warm season, are generally closer to observed values, whereas jet frequencies are underestimated by the other RCMs. Some underestimation is expected, however, as the archived wind profiles from the RCMs have a coarser vertical resolution than the rawinsonde observations, limiting jet detection. The higher jet occurrences for HRM3 are more likely due to overestimation of the strength of the lower-tropospheric winds, as shown by Bukovsky et al. (2013). In other words, HRM3 "got the right answer for

the wrong reason". On the other end of the spectrum, CRCM clearly deviates from the other models, missing the frequency maximum in southern Texas and substantially underestimating jet frequencies elsewhere. The greatest similarity between simulations is found for WRFG and RCM3, although RCM3 overestimates S-LLJ occurrences in south Texas compared to WRFG.

The analyses presented above are only an initial step in evaluating the ability of RCMs to simulate the long-term climatology of S-LLJs in the central United States and in assessing the credibility of these models for projecting future changes in jet occurrences. Important next steps include detailed examinations of the differences between models in the mechanisms contributing to jet formation. Also, further work is needed to evaluate the simulated jet climatology when the boundary conditions for the RCMs are obtained from GCM simulations for the current climate.

3.5 Conclusions

The goal of this study is to evaluate whether RCMs can credibly simulate the long-term climatology of S-LLJs. Specifically, NARCCAP current climate simulations from four RCMs (CRCM, WRFG, RCM3, and HRM3) driven by NCEP are utilized to derive for each model a 21-year climatology of S-LLJs, and the results are compared to the observed S-LLJ climatology obtained from rawinsonde soundings in the central United States.

All four models reproduce the overall spatial patterns of S-LLJ frequency and average jet elevation and speed. The RCM simulations also capture the seasonal (cold and warm

season) and diurnal (00 and 12 UTC) variations in jet frequency, elevation and speed. The RCM-simulated jet frequencies are similar to observations during the cold season and at 00 UTC in the warm season, times when jets are less frequent. During the warm season, all but one of the RCMs underestimate the frequency of nocturnal S-LLJs. The RCMs realistically simulate the annual cycle of jet frequency at locations in the western and central plains where S-LLJs are most frequent from approximately May-September but poorly simulate the annual cycle for locations farther east where S-LLJs are most frequent in spring with a secondary maximum in fall. No model consistently outperforms the others in all aspects of the evaluation.

The RCM simulations support the existence in the central United States of three "hotspots" of S-LLJ activity, found in the central plains (Kansas/Oklahoma), central Texas, and south Texas. The location and seasonal and diurnal variations of these frequency maxima are in agreement with similar maximum identified in previous climatological analyses using multiple data sources including rawinsonde and profiler observations and global and regional reanalyses. Differences exist between the RCM simulations in the relative strength of the three maxima and the latitudinal migration of the highest jet frequencies. The CRCM simulation emphasizes the central plains maximum and underestimates the strength of the south Texas maximum, particularly during the warm season when this model fails to simulate a frequency "hotspot" in south Texas. On the other hand, HRM3 overestimates jet frequencies in central and south Texas. All RCMs are in agreement that the location of most frequent nocturnal S-LLJ activity migrates northward from central Texas in April and May to the central plains (Kansas and Oklahoma) by August and September.

This evaluation of four RCM simulations from the NARCCAP suite demonstrates the ability of RCMs to generate the long-term climatology of S-LLJ in the central United States and the potential applications of RCMs in LLJ research. The use of a small ensemble of RCM simulations helps to identify model differences and assists with interpretation, particularly as none of the models examined here consistently outperforms others. The credibility of the simulated S-LLJ climatologies lends confidence to the use of these models in climate impacts assessments. Work is currently underway to evaluate the simulated jet climatology when the boundary conditions for the RCMs are obtained from GCM simulations for the current climate, and to estimate future changes in the LLJ climatology for the central United States.

Chapter 4 The Potential Impact of Regional Climate Change on Fire Weather in the United States

In collaboration with
Shiyuan Zhong, Lifeng Luo, Warren E. Heilman, Xindi Bian, and Julie A. Winkler

4.1 Introduction

Wildfires pose significant threats to life and property in many regions of the United States. Wildfire incidents are largely driven by natural factors including fuel availability, temperature, precipitation, wind, humidity, and the location of lightning strikes, although anthropogenic factors such as land use and fuel management practice also contribute to wildfire occurrences (Westerling et al. 2003). Long-term climate change will likely affect these natural factors, with implications for future wildfire danger. Various indices have been developed to help assess the potential for wildfires. The assumption behind these indices is that the constant and variable factors that affect the initiation, spread and difficulty of control of wildfires can be summarized into simple numerical descriptors (Deeming, Burgan, and Cohen 1977). Widely-used indices include the Keetch-Byram Drought Index (KBDI), an estimate of forest fire potential based on the daily water balance (Keetch and Byram 1968); the Burning Index (BI), a description of the effort needed to contain a fire (Bradshaw et al. 1984); the Energy Release Component (ERC), an estimate of the 24-hour total available energy per unit area within the flaming front at the head of a fire (Bradshaw et al. 1984); the thousand-hour fuel moisture (THFM), a representation of the modeled moisture content in dead fuels (Bradshaw et al. 1984); and the Haines Index (HI), a measure of how conducive

the atmosphere is to potential extreme or erratic fire behavior based on atmospheric stability and moisture (Haines 1988).

Fire weather indices are often used locally or regionally to assist decision-making, and considerable research has been conducted on the relationship between fire weather indices and actual fire occurrences (Preisler et al. 2004; Preisler and Westerling 2007; Dayananda 1977; Mandallaz and Ye 1997). Also, as the values of these indices can vary substantially at regional and continental scales (Werth and Werth 1998; Winkler et al. 2007; Lu et al. 2011), a number of studies have used fire weather indices to study wildland fire danger across the continental United States under projected future climate conditions. For example, Brown, Hall, and Westerling (2004) employed the ERC to investigate the potential impact of 21st century climate change on the number of days with high fire danger in the western United States using high-temporal resolution meteorological output from the Parallel Climate Model. Liu, Stanturf, and Goodrick (2010) applied the KDBI to simulations from several general circulation models (GCMs) to estimate future changes in fire season length for the United States.

The current study examines potential changes in the atmospheric conditions favoring extreme fire behavior as indicated by differences in the HI between the current and projected future climate. Extreme fire behavior is defined by the National Oceanic and Atmospheric Administration (NOAA) as "a level of wildfire behavior that ordinarily precludes methods of direct attack", and "predictability is difficult because such fires often exercise some degree of influence on their environment, behaving erratically, sometimes dangerously". This focus on extreme fire behavior reflects concerns that wildfires have recently have become more

extreme. Although the number of wildfires in the United States has been relatively stable since 1984 (NIFC 2013), the total area burned has increased, particularly in recent years and despite inter-annual fluctuations related to natural climate variability (Figure 4-1), suggesting larger and more extreme wildfires. Given that more erratic fire behavior may lead to increased area burned (Parisien et al. 2005), projecting future changes in extreme or erratic fire behavior would be very helpful for fire management. Furthermore, large and mega-fires are responsible for 80 percent of fire suppression costs in the United States (Williams 2004).

The HI index, originally introduced in 1988 as the “Lower Atmospheric Severity Index”, is widely used to assess the potential for a plume-dominated fire to become large or exhibit extreme fire behavior (Haines 1988; Winkler et al. 2007; Lu et al. 2011). The HI is used operationally in wildfire forecasting and monitoring, and is a standard element in the National Weather Service daily fire-weather forecasts and the USDA Forest Service’s Wildland Fire Assessment System. Considered primarily a regional index, the HI can provide a perspective on fire risk over large areas (Heilman and Bian 2007).

Another motivation for using the HI index to study future wildfire risk is that several historical climatologies of this index are available for the United States and provide a useful reference for evaluating future changes. The first comprehensive long-term and spatially extensive climatology of the Haines Index was produced by Winkler et al. (2007), who employed temperature and dewpoint data from the National Centers for Environmental Prediction (NCEP) global reanalysis for a 40-year (1961-2000) period on a 2.5° by 2.5° latitude and longitude grid for the North American domain. Before that, climatological analyses were generally confined temporally and geographically (Jones and Maxwell 1998;

Werth and Werth 1998; Croft, Watts, and Potter 2001). More recently, Lu et al. (2011) improved on the spatial resolution of the Winkler et al. (2007) climatology using 32 km resolution temperature and dewpoint fields from the North American Regional Reanalysis (NARR). In spite of the large differences in resolution, the spatial distributions of the HI for the two climatologies are similar for most of North America with generally higher HI values in the west than in the east. The largest differences between the two climatologies are found along coastlines and in areas of complex terrain.

A number of previous studies have employed simulations from GCMs and regional climate models (RCMs) to assess the impact of climate change on fire activity. For example, Golding and Betts (2008), using the McArthur Forest Fire Danger Index and an ensemble of variants of the Hadley Centre Coupled Model version 3 (HadCM3) climate model, found a significant increase over the 21st century in fire risk for Amazonia due to climate change and deforestation. Similarly, the risk of forest and grassland fires in Australia is anticipated to increase by 2050 and 2010 based on simulations from the Regional Atmospheric Modeling System (RAMS) (Pitman et al. 2007). Spracklen et al.(2009) applied a regression model built based on observed area burned and observed climate to the output from the Goddard Institute for Space Studies (GISS) GCM and estimated that increases in temperature will cause substantial increases by 2050 in the annual mean area burned in the western United States. In addition, HI values estimated from a suite of RCM simulations suggest that atmospheric environments in the mountainous regions of the western United States during August will be more conducive to erratic wildfires by the middle of the 21st century (Luo et al. 2013). A review of additional studies that used GCMs or RCMs to investigate global wildland fire

activity under climate change can be found in Flannigan et al. (2009).

The objective of our study is to investigate how atmospheric conditions conducive to extreme fire behavior will change in a changing climate. Most of the previous studies of climate impacts on fire-weather conditions have used climate projections from either a single high-resolution RCM (Liu, Goodrick, and Stanturf 2013) with no estimates of uncertainties, or multiple coarse-resolution GCMs (Flannigan, Stokes, and Wotton 2000; Flannigan et al. 2005) with poor resolution of heterogeneity in terrain and land cover. The current study attempts to overcome these limitations by examining changes in the HI between current and future climates, based on climate projections from multiple RCMs driven by multiple GCMs. Winkler et al. (2011) pointed out that no single RCM performs best all the time; the performance depends on the field examined, and the uncertainty introduced by the choice of RCMs can be as large as the choice of GCMs. By comparing results from various combinations of GCMs and RCMs, it is possible to evaluate the robustness of the model results regarding potential changes in atmospheric conditions conducive to large and extreme wildland fires. Thus, the results will provide not only information on the potential changes, but also the associated uncertainties, a key factor to consider in the decision-making process. The analysis focuses on the time of the year and the regions within the United States most likely to be affected by climate change. These findings will help fire and resource managers in designing climate change adaptation strategies.

4.2 Data and Methods

4.2.1 Data

The datasets used to generate the HI climatology were provided by the NARCCAP (Mearns et al. 2007, 2009). The set of RCMs used in the current study includes the CRCM, WRFG, and RCM3. The driving GCMs include the CCSM, CGCM3, and GFDL. The NARCCAP model combinations are shown in Table 4-1. Simulations from six RCM-GCM combinations and three RCM-NCEP combinations are analyzed. For details on the mode configurations and physics parameterizations used for these simulations, please refer to <http://www.narccap.ucar.edu/about/index.html>.

4.2.2 Haines Index Calculation

The HI consists of an atmospheric stability component (A) and a humidity component (B) (Haines 1988). The A component is calculated as the temperature difference between two pressure levels (i.e., the lapse rate or the rate at which temperature decreases with altitude) in the lower atmosphere, and the B component represents the difference between temperature and dewpoint (i.e., the dewpoint depression) for a specific pressure level in the lower atmosphere. Each component is converted to an integer value of 1, 2, or 3 based on the prescribed thresholds shown in Table 4-2. The A and B components are summed to yield a HI value ranging from 2 to 6, with 2 representing a very low potential for erratic plume-dominated fires and 6 representing a very high potential (Haines 1988).

The temperature and humidity data for calculating the HI originally came from

radiosonde observations. Although routine radiosonde observations are available two times per day at 0000 and 1200 UTC, the original HI was calculated using only the 0000 UTC soundings because this time is closer to the time of the day in most of North America when the instability is high and relative humidity is low, posing greater fire danger. Several studies have discussed the potential bias of using observations at other times, and agreed that HI values based on 1200 UTC observations may underestimate fire potential because this is the time in North America when normally the atmosphere is stable (Jones and Maxwell 1998; Kochtubajda et al. 2001). Thus, only 0000 UTC data from NARR are used in this study, despite the availability of the NARR data at 8 times per day.

In the initial index development, the United States was divided into three regions (referred to as “low”, “mid”, and “high”) to take into account variations in surface elevation. Three different variants of the HI were formulated so that the pressure layer used in the index calculation is “high enough above the surface to avoid the major diurnal variability of surface temperature and surface-based inversions” (Haines 1988, 23). Winkler et al. (2007) reproduced the boundaries for the three variants by comparing Haines’ original map to elevation contours and found that the 300 m and 1000 m contours best outline the original boundaries between the low variant and the mid variant, and between the mid variant and the high variant, respectively. In this study, the boundaries between the low, mid, and high variants are outlined, after Winkler et al. (2007), by contouring the 300 m and 1000 m elevations of the topography used for each RCM simulation.

Wildfire danger is examined for the entire year rather than for a single month (Luo et al. 2013) or only the warm season (Lu et al. 2011), as the seasonality of wildfires varies

spatially. As shown by Westerling et al. (2003), wildfires in the western United States are strongly seasonal, with 94 percent of fires and 98 percent of area burned occurring between May and October; and peak fire activity occurring during July and August. In the eastern United States, fire activity is more frequent in spring and fall (Knapp, Estes, and Skinner2009). While most states have particular time of the year for wildfires, wildfire season in Florida is year-round.

For the GCM-driven current, GCM-driven future, and NCEP-driven current climates, the spatial distributions of the probability of the HI equal to or exceeding a given category (i.e., $HI \geq 2, 3, 4, 5, 6$) are examined for each of the RCM-GCM or RCM-NCEP combinations. The probability for a specific month is simply the number of days in that month when HI values equaled or exceeded a certain category, averaged over all years in the simulation period divided by the total number of days in the month. Calculations were performed for each month of the year, but, to simplify the discussion, only the results from March, August and October, representing the spring, summer and autumn seasons, respectively, are presented. Although there are some variations within each season, the differences are much smaller compared to the inter-seasonal variability. Changes in the distribution of high ($HI \geq 5$ or $HI=6$) HI values, indicating a greater potential for large and erratic fires, are highlighted. Additionally, the percentage of days with high values of the stability component ($A=3$) and the moisture component ($B=3$) are examined separately to evaluate their relative contributions to changes in the HI.

Changes in the persistence of high (≥ 5) HI values are also considered, as long periods of consistently high HI values are of special concern for fire managers. Persistence is

quantified by the number of consecutive days with high HI values. The average length of all events as well as events longer than certain days are computed and the changes in the average length of high HI events are examined.

As not all the model combinations are in the same projection and grid setting, the HI values and probabilities for each model combination were resampled and reprojected from curvilinear grids to a common rectilinear grid based on the grid setting of the CRCM-CCSM simulations for further analysis. The weighting method used in the interpolation is the simple inverse distance squared scheme, where nearby values exert more influence on the interpolated value. The mean and standard deviation of the HI probabilities were calculated for each grid point on the standard grid. The standard deviation measures the spread of the model projections and helps to assess the consistency or the robustness of the results among model combinations. Even though the sample size is small, the resulting standard deviation maps provide an indication of where the different model combinations have the most similar or dissimilar values. However, it is important to bear in mind that model consensus should not be confused with skill or reliability, as the RCM-GCM combinations share similar numerical schemes and parameterizations and thus are not independent (Winkler et al. 2014).

4.3 Results

As a HI value of 5 or 6 indicates a higher potential of erratic fire behavior, only results for $HI \geq 5$ are presented here, even though HI values for all possible categories were calculated. Similarly, we focus on the highest category of the A and B components in the

discussion below.

4.3.1 Percentage of days with $HI \geq 5$

4.3.1.1 GCM-Induced Biases in Current Climate Simulations

As discussed earlier, RCM simulations driven by GCMs contain errors generated not only by the RCMs, but also from the GCMs through boundary conditions. On the other hand, RCM simulations driven by NCEP reanalysis data, which are often referred to as the perfect boundary condition (Giorgi 2006), are assumed to contain errors only from the RCMs. Thus, a comparison of GCM-driven current climate simulations with NCEP-driven current climate allows for an identification of errors introduced by the GCMs. Figure 4-2 shows the difference in the percentage of days with $HI \geq 5$ between the GCM-driven and NCEP-driven current climate simulations. Red shading is associated with positive GCM biases (larger simulated percentages for the GCM-driven compared to NCEP-driven model runs) and blue shading is associated with negative GCM biases (GCM-driven simulation percentages less than the NCEP-driven values).

Over most of the United States, GCM-induced biases are greater during summer, in contrast to spring and fall when biases are generally within ± 15 percent of the frequencies obtained from the NCEP-driven simulations. Simulation results obtained with the same RCM, but different GCMs, show more similarity than those obtained with the same GCM but different RCMs.

Positive biases are observed across most of the United States the CRCM-CCSM and

CRCM-CGCM3 simulations in August, with the largest biases occurring in the Intermountain West and the Southeast. The CRCM-CGCM3 simulation yielded negative biases in the northern Plains and along the Texas coast. The WRFG-CCSM and WRFG-CGCM3 simulations also produced positive biases in the Intermountain West, and negative biases in southern Texas, the Pacific Northwest, and parts of the northern Plains. In contrast, the RCM3-GFDL and RCM3-CGCM3 simulations produced negative biases in the northern half of the United States, especially in the northern Plains. Negative biases covered most of the United States, with the exception of portions of the Southeast, for the RCM3-GFDL simulation, whereas for the RCM3-CGCM3 simulation negative biases occurred in the northern half of the United States with positive biases over much of the southern half except for southern Texas, Louisiana, and Mississippi. In summary, there is considerable spatial variation in the GCM-induced biases for the different model combinations and across seasons.

4.3.1.2 Spatial and Seasonal Variations in Frequency for the GCM-Driven Current Climate

In general, the overall spatial and seasonal patterns are similar, especially those of the two WRFG simulations, to the HI climatology generated from the NCEP-NCAR and NARR reanalyses (Winkler et al. 2007; Lu et al. 2011). The simulations for all months (not shown) indicate that the highest probability of high HI values occurs in July and August across most of the United States, with the lowest frequencies in December and January.

Focusing on the frequencies of $HI \geq 5$ during March, August, and October (Figure 4-3),

the percentage of days with $HI \geq 5$ in the western United States reaches 85-90 percent in August for most of the GCM-driven simulations, and generally falls below 30 percent during March and October. Smaller seasonal variations are seen for the eastern and central United States, although, like the western United States, the highest frequencies of $HI \geq 5$ occur in July (not shown) and August.

During March and October, the frequency of $HI \geq 5$ is larger over much of the central and eastern United States compared to the western United States. The CRCM-CCSM and CRCM-CGCM3 simulations for March and October generated similar probabilities in the central and eastern United States with peak values of nearly 50 percent over the High Plains (Figure 4-3). For most of the western United States, the two CRCM runs generated probabilities ranging from 5-35 percent, with the CRCM-CGCM3 probabilities about 5-10 percent higher than those for CRCM-CCSM. The probabilities from the WRFG combinations are generally similar, although the WRFG-CCSM values are slightly lower compared to the other simulations for the western United States, and the probabilities for the central and eastern United States from WRFG-CGCM3 are approximately 5-10 percent greater than those from the CRCM-CGCM3, CRCM-CCSM, and WRFG-CCSM simulations. The simulations for RCM3 have lower percentages across the domain, especially in the Midwest, compared to those for the other two RCMs. A possible reason for this difference is the much coarser vertical resolution in RCM3 (18 levels vs. 29 in CRCM and 34 in WRFG), which would affect the accuracy of the lapse rate calculation as indicated by Factor A of the HI. The spatial patterns for the two RCM3 simulations also differ somewhat with the highest values found in March in the southern Plains (Texas and Oklahoma) and in October from the

southern Plains eastward along the Gulf Coast and northeastward into Arkansas and Missouri, whereas the highest values for the other RCM combinations are found in the High Plains, extending from eastern Montana to southern Texas.

During August, the two CRCM simulations and two WRFG simulations generally produced higher probabilities of $HI \geq 5$ than the two RCM3 runs (Figure 4-3). While all six model combinations display only modest differences for the central Rockies (western Colorado), southwestern United States, and the California coast, substantial between-simulation differences are observed for the eastern half of the United States. The CRCM simulations generated the highest percentages in the southern Plains and along and north of the Gulf Coast, whereas the WRFG simulations generated the highest probabilities in the central and northern Plains. The highest probabilities for the RCM3 simulations are found in northern Texas and Oklahoma, somewhat similar to the spatial pattern for the WRFG simulations, but the probabilities are much lower. Lower probabilities are also found for the RCM3 simulations over much of the Midwest and Gulf coastal region. For a particular RCM, the differences in probabilities were small between the simulations driven by different GCMs. For example, the probabilities generated by the CRCM-CCSM simulation were 5 to 10 percent higher over the central and eastern United States compared to those from the CRCM-CGCM3 simulation.

In short, for the same model run, the frequency of $HI \geq 5$ exhibits similar spatial patterns in spring and fall, which can differ considerably from the spatial pattern in summer. The differences among model combinations are also smaller in spring and fall than in summer when large differences among model combinations are observed, especially in the

High Plains and along the Gulf Coast. The probabilities are smaller for RCM3 simulations compared to those of the other model runs. Larger differences are produced when different RCMs are used for the simulations compared to when different GCMs are used.

4.3.1.3 Projected Future Changes

The simulated future HI climatology (Figure 4-4) for a particular RCM/GCM combination has very similar spatial patterns to the corresponding climatological pattern for the GCM-driven current climate simulation (Figure 4-3). The highest and lowest percentages are generally found in the same areas, suggesting that the regions currently experiencing atmospheric conditions most conducive to extreme or erratic fire behavior will likely experience those conditions in the future also. Seasonal variations are also similar for the future and current climates. To better illustrate changes in probability, the differences in the percentage of days with $HI \geq 5$ between GCM-driven current and future climates (GCM-driven-future minus GCM-driven-current) were calculated for the six model combinations (Figure 4-5). The red (blue) shading depicts higher (lower) future probabilities of $HI \geq 5$ compared to the current climate.

The magnitudes of the projected changes are smaller for March and October compared to August, with projected changes within ± 10 percent for both months. The only exception is the RCM_CGCM3 simulation which projects a >20 percent increase over the central United States in October. However, there are considerable differences between models in the spatial patterns of the projected change, especially for the Great Lakes region in

March, and the northern and central Plains in October, with some simulations projecting a greater future fire risk and others suggesting a smaller risk.

All the model combinations project a higher probability of $HI \geq 5$ during August over most of the United States under future climate conditions. The largest increases (25-35 percent) for the CRCM-CCSM and CRCM-CGCM3 simulations are found in Arizona and New Mexico. Most other areas have increases around 10-20 percent, although some slight decreases are observed for both simulations over parts of the northwestern United States. For the two WRFG-driven simulations, lower future probabilities are projected for the northern Plains and southern Texas, with higher risk projected elsewhere. The WRFG-CCSM simulation also suggests decreased fire risk for the Pacific Northwest, whereas lower probabilities are found in California, the Carolinas, and Georgia for the WRFG-CGCM3 simulation. Most other regions exhibit increases between 10 and 25 percent. The RCM3 simulations also project increased probabilities over most of the United States, except for the northern Plains where a decrease is simulated by the RCM3-GFDL combination.

To assess the agreement among model combinations, Figure 4-6 shows the standard deviation and mean values of the percentage of days with $HI \geq 5$ during August for all six model combinations for the GCM-driven current and future climates and the differences between them. For both the GCM-driven current and future climates, the greatest inter-model differences in the percentage of days with $HI \geq 5$ are found in the Midwest, the northern Plains, and along the Gulf Coast. The greatest disagreement in the projected future changes is found in parts of the Midwest, the Southeast, and the Southwest.

4.3.2 The A and B components

As the HI is composed of a stability factor (A) and a moisture factor (B), it is helpful to determine the relative contribution of each factor to the projected changes in the percentage of days with high HI.

Changes in the percentage of days with A=3 between the GCM-driven current and future climate simulations are presented in Figure 4-7. The projected changes in the frequency of days with A=3 for March and October are generally within ± 15 percent. During March, the two RCM3 simulations show increases over most of the United States, while the WRFG-CGCM3 projects a large-scale decrease in frequency. The other three simulations display greater regional differences in the sign of the projected changes with generally increased probability of A=3 for the Great Lakes region and the Midwest and decreased frequency in the Great Plains and the Intermountain West. For October, the CRCM-CGCM3 and RCM3-CGCM3 simulations yielded increased probabilities over most of the United States, while the other model combinations display considerable spatial variability. For August, almost all of the model combinations project an increase in the percentage of days with A=3 across much of the United States, except the primary exception being the Pacific coast. In addition, the WRFG-CCSM, WRFG-CGCM3, and RCM3-GFDL simulations project decreased probabilities over the north central United States.

Changes in the percentage of days with B=3 between the GCM-driven current and future climate simulations are presented in Figure 4-8. The projected changes for March and October are generally within ± 20 percent, although the spatial pattern of the differences varies greatly among the six model combinations. The two WRFG simulations yielded

negative changes for March across much of the United States, whereas for the other simulations a projected decrease in the frequency of days with $B=3$ was generally limited to New England, the northern Midwest, and the Intermountain West. During October, the CRCM-CGCM3, WRF3-CGCM3, and RCM3-CGCM3 simulations projected an increased frequency of days with $B=3$ across most of the United States, while the other model combinations yielded more spatial variability. The general trends in the B component in August are more consistent among the different simulations compared to March and October. All the model combinations except for WRF3-CGCM3 project an increased frequency of days with $B=3$ over most of the United States. The WRF3-CCSM simulation projects the largest positive changes (~40 percent), whereas the largest negative changes (~20 percent) are observed for the WRF3-CGCM3 simulation. These large projected changes, especially in contrast to those for the A component, suggest that the B component contributes more to the projected future increase or decrease in the probability of high HI for August.

4.3.3 Persistence of high HI events

The persistence of high HI days is also an important consideration for fire management. Here, the persistence or the length of an event is determined by the number of consecutive days with $HI \geq 5$. The average length of all events as well as events longer than 5, 13, and 21 days are computed for the GCM-driven current and GCM-driven future climate simulations and the results compared. The results are shown for August only to represent summer season, as prior climatological analyses (Winkler et al. 2007; Lu et al. 2011) indicate

that high HI values and long events are more frequent in summer.

Projected changes in the average length of all $HI \geq 5$ events in August, as generated by the GCM-driven current versus GCM-driven future climate simulations, are shown in Figure 4-9. The average length is projected to increase by 2 to 5 days for many regions of the United States. The two CRCM simulations and the WRFG-CCSM and RCM3-CGCM3 simulations project greater increases in the length of $HI \geq 5$ events compared to the WRFG-CGCM3 and RCM3-GFDL simulations. The largest increases (~9-12 days) for the CRCM-CCSM simulation are found for the Intermountain West, whereas the CRCM-CCSM, CRCM-CGCM3, and RCM3-CGCM3 simulations project substantially longer events in Texas and Oklahoma. The two WRFG simulations and the RCM3-GFDL simulation suggest decreases in the length of $HI \geq 5$ events on the order of 1 to 3 days over the northern Plains. Based on the mean and standard deviation of the future changes in HI duration (Figure 4-10), the models exhibit the largest discrepancies in the southern part of the Intermountain West and the southern Plains (Figure 4-10).

The average length of persistent high HI events that last longer than 5, 13, and 21 days (events longer than 1 to 30 days were calculated, but shown selectively) during August are presented in Figures 4-11 to 4-13, respectively. The projected changes in the average length of high HI events lasting longer than 5, 13 or 21 consecutive days exhibit similar spatial patterns despite different thresholds of consecutive days (Figure 4-11 to 4-13). For most of the United States, the average length of these long events is projected to increase by 1-4 days under future climate conditions, but as can be expected, the magnitude of the increase becomes less as the threshold of consecutive days increases. For events longer than

21 days, many areas of United States are still projected to experience slight increases (0-2 days on average) in their frequency. These results suggest that not only the percentage of high HI days may increase in the future, but also the high HI events may have a longer duration. Additionally, regions with increased number of summer days with high HI values are likely to also have longer consecutive high HI days.

4.4 Discussion

The Haines Index was selected for this study for a number of reasons. First, this fire-weather index was designed for detecting atmospheric conditions prone to extreme fire behavior. Second, HI is considered a regional scale index because it is not sensitive to local conditions and can thus be used to provide an important perspective of the risk for wildfires to become large and erratic over a large region (Heilman and Bian 2007). Third, by considering both atmospheric stability and dryness, the HI is more informative than indices that only consider stability or moisture alone. Finally, the HI is straightforward and convenient and has been widely used in operational fire weather forecasting. However, the HI also has its limitations. The lack of consideration of wind and turbulence in the lower atmosphere is a major limitation. The delineation of the boundaries of the low, mid, and high variants is rather subjective (Haines 1988; Winker et al. 2007), often resulting in unsmoothed transitions or discontinuities in HI values across the boundaries between the different variants. The HI can also become “saturated” in regions with typically hot, dry Mediterranean or arid climates (McCaw et al. 2007), prompting the recent proposal of a continuous Haines Index

(C-HAINES) (Mills and McCaw 2010). Others (e.g., Heilman and Bian 2007) have recommended that the HI be combined with other indicators of atmospheric conditions, such as turbulent kinetic energy, to increase its effectiveness.

This study features the use of simulations from multiple combinations of RCMs driven by GCMs made available recently by NARCCAP. With their finer resolution, which allows for a better representation of factors such as topography and land cover, RCMs can describe climate feedback mechanisms acting at the regional scale (Randall et al. 2007). Previous studies concerning the impact of climate change on wildfire activity have generally employed one (Brown, Hall, and Westerling 2004) or several (Flannigan et al. 2000; Flannigan et al. 2005) coarse-resolution GCMs or a single RCM (Liu, Goodrick, and Stanturf 2013). The multi-model ensemble approach (based on six model combinations, namely CRCM-CCSM, CRCM-CGCM3, WRFG-CCSM, WRFG-CGCM3, RCM3-GFDL, RCM3-CGCM3) employed in the current study was adopted to increase reliability and to better depict uncertainty. Although there is considerable spatial variation in the projected changes for March and October, all model combinations consistently project an increase in the frequency of occurrence of atmospheric conditions favoring large and erratic wildfires for most of the United States in August, building more confidence into these results. One limitation, however, is that all model combinations were forced with the A2 scenario, which is on the higher end of the greenhouse gas emissions scenarios. Additional emissions scenarios should be considered in future analyses to address uncertainty in the projected arising from different emissions trajectories.

The spatial patterns of the GCM-driven HI climatology for the current climate are

generally in good agreement with those of the reanalysis-derived HI climatology (Winkler et al. 2007; Lu et al. 2011). Furthermore, since the spatial patterns remain similar between the GCM-driven current and future HI climatologies, it is likely that the regions currently experiencing atmospheric conditions most conducive to extreme wildfires will also experience them in the future.

The results are generally dependent on which combination of RCM and GCM is used. Model combinations with the same RCMs for the most part produce more similar spatial patterns than model combinations with the same GCMs, implying that the differences among the model combinations are caused mainly by different RCMs rather than by different GCMs. Notwithstanding, the differences caused by GCMs can be large as well. The strong dependency of the regional projections on the specific RCM calls for extreme caution when interpreting results from a single RCM for a specific location. One direction for future study is to examine the similarities and differences among the model combinations more closely and to validate the current climate simulations against actual fire occurrence and fire spread data in order to assess where a certain model or model combinations perform best. Furthermore, the mechanisms driving the change in fire potential between the current and future climate need to be studied in more detail. Another future research direction is to examine for locations where climate data are available, whether the RCM simulations improve on the estimates of future change obtained from applying statistical downscaling directly to GCM output, or whether the application of statistical downscaling to the RCM simulations would help reduce the biases in the RCM simulations.

Other factors not considered in this study, such as land-use and land-cover change

(LULCC), can also directly impact fuels and thus change fire behavior. LULCC may also affect fire weather and climate by changing carbon fluxes and greenhouse gas emissions and altering atmospheric composition and radiative forcing properties (Randall et al. 2007). Climate modeling strategies for predicting future climate conditions typically treat land use and land cover as static or unchanging due mainly to the lack of reliable LULCC projections (Stanton et al. 2012). Given the substantial influence that LULCC can have on fuel and atmospheric conditions, models used to project future conditions for fire weather and fire behavior may need to incorporate the LULCC factor.

4.5 Conclusions

The HI serves as a straightforward and useful tool for indications of atmospheric conditions that are conducive to extreme or erratic fire behavior. In this study, the potential change in the frequency of occurrence of high HI values (and thus the potential for extreme fire behavior) and the length of consecutive days with high HI values over the contiguous United States are examined using the NARCCAP simulations. Specifically, the study employs NARCCAP simulations of the current climate and future climate from six different RCM-GCM combinations representing three RCMs (CRCM, WRFG and RCM3) and three GCMs (CCSM, CGCM3, and GFDL). In addition, RCM runs driven by the NCEP reanalysis for the current climate are used to help identify errors introduced by the GCMs.

The spatial patterns and seasonal variations for the percentage of days with $HI \geq 5$ across the United States for the six model combinations are found to be very similar between

the current and future climate conditions, suggesting that the regions that are currently experiencing higher potential for large and erratic wildfires due to favorable atmospheric conditions alone would continue to do so in the future. Despite GCM biases, the simulation results suggest that most regions of the United States may see an increase in the percentage of days with $HI \geq 5$ during the summer season by mid century. The simulations also suggest that the average duration of $HI \geq 5$ episodes in the summer may be longer under future climate conditions compared to current climate conditions for most of the United States. Further analysis indicates that the moisture component of the HI contributes more to the projected changes than the stability component. Several key regions (Intermountain West, High Plains, and Gulf Coast region) with high potential for large and erratic fires in the future were identified, which could be used by fire and land managers for the purpose of long-term planning and designing strategies for climate change adaptation. Discrepancies occur among the projections from the six model combinations for spring and fall, which limits confidence in future changes for these seasons. The results also show that the HI climatology patterns from simulations using the same RCM are more similar than those using the same GCM. The projected future changes need to be interpreted in terms of the limitations of the Haines Index and with respect to the limitations of the regional and global climate models.

Chapter 5 Summary

This study examines the issues encountered during climate impact assessments, including the choice of climate projections (data source, ensemble size, ensemble construction, emission scenario, bias-correction methods, downscaling methods, etc), evaluation of model simulations, and applications of climate projections in climate change assessments (Figure 1-1). These issues are illustrated using multiple examples including an agricultural impact assessment (Chapter 2), an evaluation of the climatology of southerly LLJs as simulated by RCMs (Chapter 3), and an assessment of the future hazard of extreme, erratic wildfires (Chapter 4). Chapter 2 elaborated on multiple dimensions of constructing a climate projection ensemble. Climate model simulations were gathered from the CMIP5 and NARCCAP archives. Multiple downscaling methods are adopted including the simple delta method (for both CMIP5 and NARCCAP), dynamical downscaling ("raw" NARCCAP simulations), and hybrid downscaling (MLCR and MLR downscaling applied to the NARCCAP simulations). Emission scenarios RCP 4.5, RCP 6.0, RCP 8.5, and A2 are included. The GCM (CMIP5) ensemble consisted of 16 models while the RCM ensemble consisted of 8 RCM-GCM combinations. The station of Maple City, Michigan, was chosen as representative in the analysis. Agricultural indices including GDD and growing season length were analyzed. All the climate projections present increasing GDDs and growing season length for Maple City. Given that more models were included in the GCM ensemble, the range of outcomes is reasonably larger compared to the NARCCAP ensemble. The results when using the simulations employing the RCP 4.5 and RCP 6.0 emissions scenarios are very similar for all time slices (2010-2030, 2040-2060, and 2070-2090) but considerably different

from the projections obtained under the RCP 8.5 emissions scenario. The NARCCAP raw simulations, NARCCAP MLCR projections, and NARCCAP MLR projections display similar results to RCP 4.5 and RCP 6.5, and smaller compared to RCP 8.5 scenario. The MLCR and MLR downscaling methods both try to minimize the residuals errors of the projected variables in the RCM simulations while MLCR also tries to correct the distribution of variables compared to observation. The range of projected changes in GDDs as estimated by the MLCR method is somewhat smaller compared to that for the other downscaling methods, although the range for growing season length is more comparable across methods. Of all the projections, the uncertainty range was generally greatest for the popular delta methods applied on CMIP5 dataset, partly a function of the larger number of simulations available from the CMIP5 archive. On the other hand, if only NARCCAP dataset is considered, the results from delta method present a relatively smaller uncertainty range compared to other downscaling methods. However, the delta method only considers changes in the mean, and further adjustment is needed if inter-annual variability is an important feature in the analysis. The projections from the RCP 4.5 and RCP 6.0 scenarios are very similar but are dramatically different from those obtained from RCP 8.5 scenario, which may implicate the possibility to reduce work load by only including the RCP 4.5 and RCP 8.5 emissions scenarios in an assessment. On the other hand, the advantage of dynamical downscaling is not fully presented in the calculation of simple indices like GDD or growing season length, but it may benefit quantifications of more complex mechanisms or features that require fine spatial or temporal resolution.

Chapter 3 described an evaluation of the ability of the NARCCAP RCMs to simulate

the long-term (1979-2000) climatology of southerly low level jets (S-LLJs) in the central United States. The RCM-derived S-LLJ climatologies were evaluated against rawinsonde observations for the same period. The use of a small ensemble of RCM simulations helped to identify model differences and assisted with interpretation. The RCMs generally reproduced the broad spatial patterns and temporal variations of jet frequency and average jet height and speed. No model consistently outperformed the others in all aspects of the evaluation, although differences existed between models in the placement, migration and relative strength of "hotspots" of more frequent jet activity. In particular, three of the four models placed the center of greatest nocturnal S-LLJ activity during the warm season in northern and central Texas, whereas for the other model the greatest jet activity was located in the south-central plains (Kansas/Oklahoma). The magnitude of a S-LLJ frequency maximum over south Texas also varied between models, with simulated frequencies exceeding observed frequencies for some models but substantially underestimating for others. The evaluation presented here highlights the potential applications of RCMs in LLJ research where high spatial, temporal, and vertical resolutions are necessary. The overall performance of the models in reproducing the long-term S-LLJ climatology supports the credibility of the NARCCAP RCM simulations and their use in climate assessments for the central United States where S-LLJs are an important contributor to the regional climatology.

Chapter 4 illustrated a case study of a climate change impact assessment by analyzing potential changes in fire-weather conditions for the contiguous United States using the HI, a fire-weather index that has been employed operationally to detect atmospheric conditions favorable for large and erratic fire behavior. The index summarizes lower atmosphere

stability and dryness into an integer value with higher values indicting more fire-prone conditions. A NARCCAP RCM ensemble was constructed to examine changes by mid-century in the seasonal percentage of days and the consecutive number of days with high (values \geq 5) HI across the United States. Despite differences among the six RCM-GCM combinations in the magnitude and location of the projected changes, the results consistently suggest an increase in the number of days with high HI values over most of the United States during the summer season, with the dryness factor of the HI contributing more than the stability parameter to the projected changes. In addition, the consecutive number of days with high HI is projected to increase in summer. Together, these results suggest that future summers may be more conducive to large and dangerous fires. The projections for other seasons are inconsistent among the model combinations.

Based on three studies presented in Chapter 2 to 4, the overall goal of illustrating some aspects of considerations when using climate projections for climate change assessment studies is achieved. As shown in these analyses, an ensemble of climate projections is necessary for interpretation of potential futures changes, although the design of a climate projection ensemble should be made based on the goals of the assessment. The ensemble should consider the uncertainty introduced by differences in the structure of climate models, greenhouse gas emissions scenarios, and downscaling procedures. Moreover, the biases and errors of the climate projections should be carefully evaluated. Additionally, the studies presented here illustrate the importance of going beyond ensemble mean values and displaying and interpreting all ensemble members.

The research presented here can be expanded multiple ways. First, the climate

projections produced as part of this dissertation can be shared with other research groups via pre-packed datasets or interactive GIS platform on the website (Liu et al. 2009; Li et al. 2015). Second, the geographical area of the analyses, especially that for the agricultural impact assessment, can be expanded to include telecoupling, such as the differential impact of climate change on agricultural production in different geographical regions and the resulting impact on the goal trade of agricultural products (Porter et al. 2014; Liu et al. 2013). Third, all of the climate projections (from both GCMs and RCMs) are treated equally in the assessments presented here, while it is likely that certain models may be more or less suitable for certain regions. This raises another concern of assigning weights or using models selectively for certain studies or regions. Fourth, only observational data from weather stations and outputs from climate models are used in the current study. In the future, other data sources such as remote sensing data may be included for data sparse regions (Gillies et al. 1995; Vinukollu et al. 2011). Fifth, the analyses are limited to only a few climate parameters (Chapter 2), one circulation feature (Chapter 3) and a single fire index (Chapter 4) and can be expanded to include a more climate variables, atmospheric phenomena, and impacts. In particular, the choice of impact models introduces another dimension of uncertainty, and more than one impact model can be included in the assessment to encompass a range of uncertainty rising from impact models (Asseng et al. 2013). Sixth, the current study is primarily concerned with the change of climate parameters and processes, rather than the consequences for natural and human systems, and future work should extend. Future work needs to evaluate the potential benefit or risk of climate change (Patz et al. 2005; Peel et al. 2013).

APPENDIX

Table 2-1. CMIP5 models used in the current study

| Modeling Center | Model | Institution |
|---|---|---|
| FIO IPSL | FIO-ESM IPSL-CM5A-LR IPSL-CM5A-MR | The First Institute of Oceanography, SOA, China Institut Pierre-Simon Laplace |
| MIROC | MIROC5 | Atmosphere and Ocean Research Institute (The University of Tokyo), National Institute for Environmental Studies, and Japan Agency for Marine-Earth Science and Technology |
| MIROC | MIROC-ESM MIROC-ESM-CHEM | Japan Agency for Marine-Earth Science and Technology, Atmosphere and Ocean Research Institute (The University of Tokyo), and National Institute for Environmental Studies |
| MOHC (additional realizations by INPE) | HadGEM2-ES | Met Office Hadley Centre (additional HadGEM2-ES realizations contributed by Instituto Nacional de Pesquisas Espaciais) |
| MRI | MRI-CGCM3 | Meteorological Research Institute |
| NASA GISS | GISS-E2-H GISS-E2-R | NASA Goddard Institute for Space Studies |
| NCAR | CCSM4 | National Center for Atmospheric Research |
| NIMR/KMA | HadGEM2-AO | National Institute of Meteorological Research/Korea Meteorological Administration |
| NOAA GFDL | GFDL-CM3 GFDL-ESM2G GFDL-ESM2M | Geophysical Fluid Dynamics Laboratory |
| NSF-DOE- NCAR | CESM1(CAM5) | National Science Foundation, Department of Energy, National Center for Atmospheric Research |

Table 4-1. NARCCAP model combination outputs used in the current study

| RCM | GCM-driven | | | NCEP-driven |
|------|------------|-------|------|-------------|
| | GFDL | CGCM3 | CCSM | NCEP |
| RCM3 | X | X | | X |
| CRCM | | X | X | X |
| WRFG | | X | X | X |

Table 4-2. Calculation of the Haines Index A and B components for the three elevation variants (temperature and dewpoint are in Celsius unit)

| Elevation | Stability Component (A) | | Humidity Component (B) | |
|-----------|---|---|--|---|
| | Calculation | Categories | Calculation | Categories |
| Low | 950 hPa temperature - 850 hPa temperature | A = 1 if < 4 A = 2 if 4-7 A = 3 if >= 8 | 850 hPa temperature - 850 hPa dewpoint | B = 1 if < 6 B = 2 if 6-9 B = 3 if >= 10 |
| Mid | 850 hPa temperature - 700 hPa temperature | A = 1 if < 6 A = 2 if 6-10 A = 3 if >= 11 | 850 hPa temperature - 850 hPa dewpoint | B = 1 if < 6 B = 2 if 6-12 B = 3 if >= 13 |
| High | 700 hPa temperature - 500 hPa temperature | A = 1 if < 18 A = 2 if 18-21 A = 3 if >= 22 | 700 hPa temperature - 700 hPa dewpoint | B = 1 if < 15 B = 2 if 15-20 B = 3 if >= 21 |

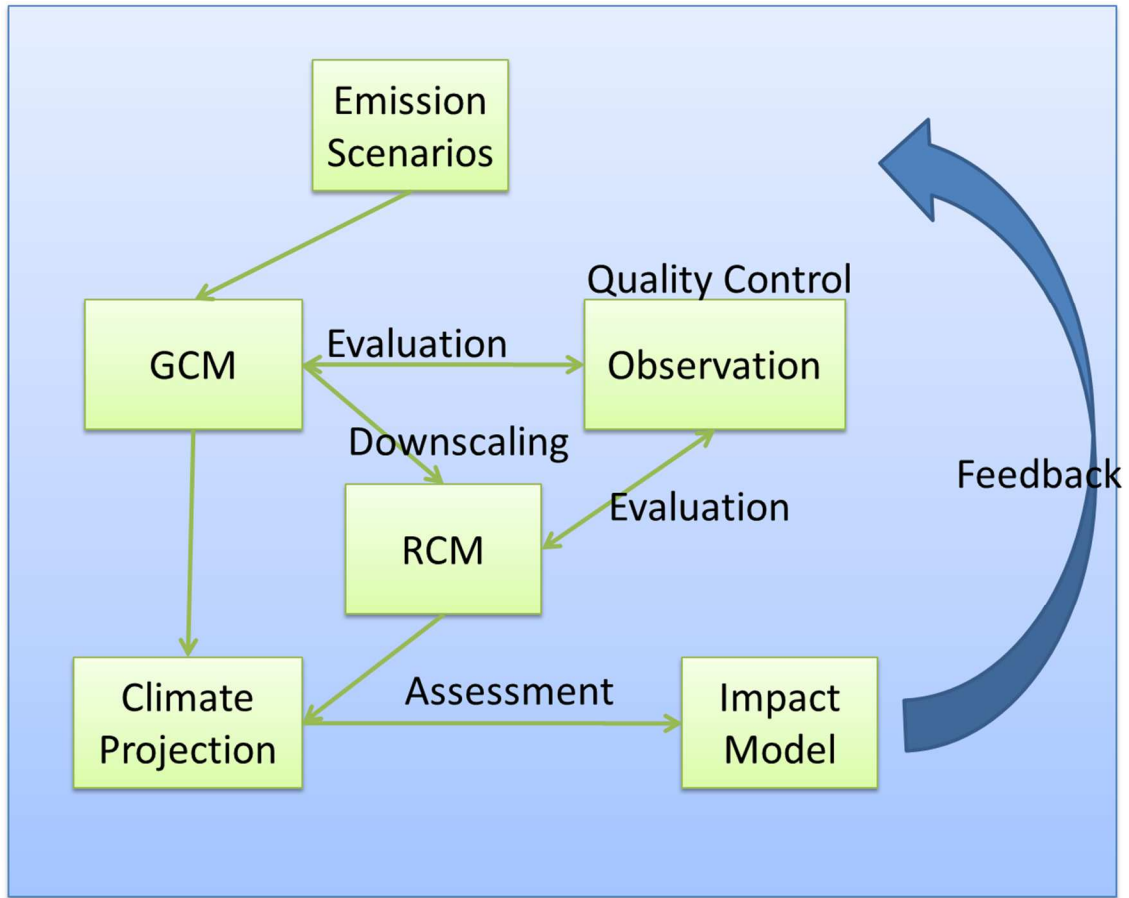


Figure 1-1. Framework for top-down climate change impact assessment study

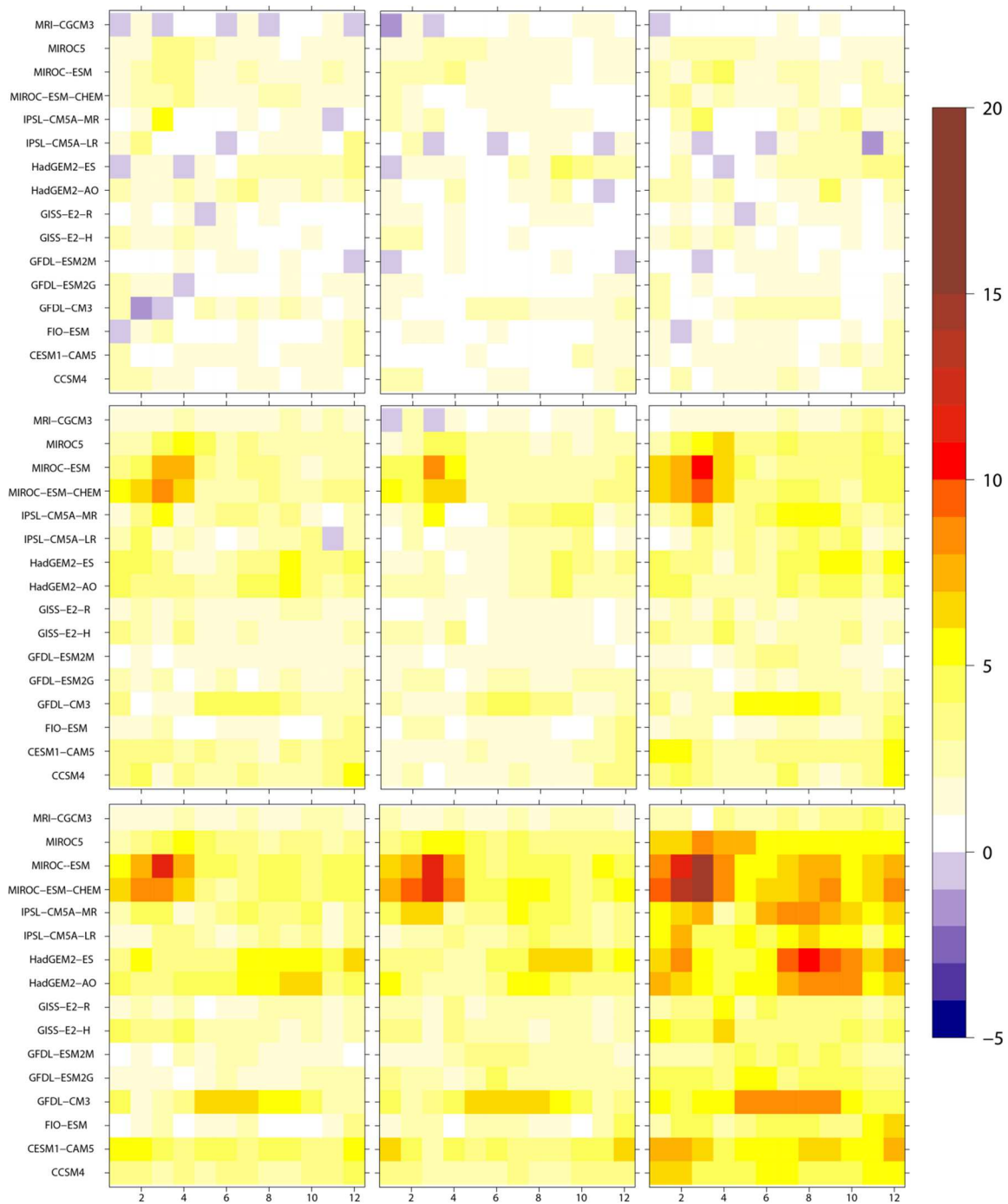


Figure 2-1. Change of monthly average of daily maximum temperature compared to baseline period (1980-2000) for CMIP5 models. The columns are the RCP 4.5, RCP 6.0, RCP 8.5, respectively. The rows are time slices of 2010-2030, 2040-2060, and 2070-2090, respectively. The unit is Celsius.

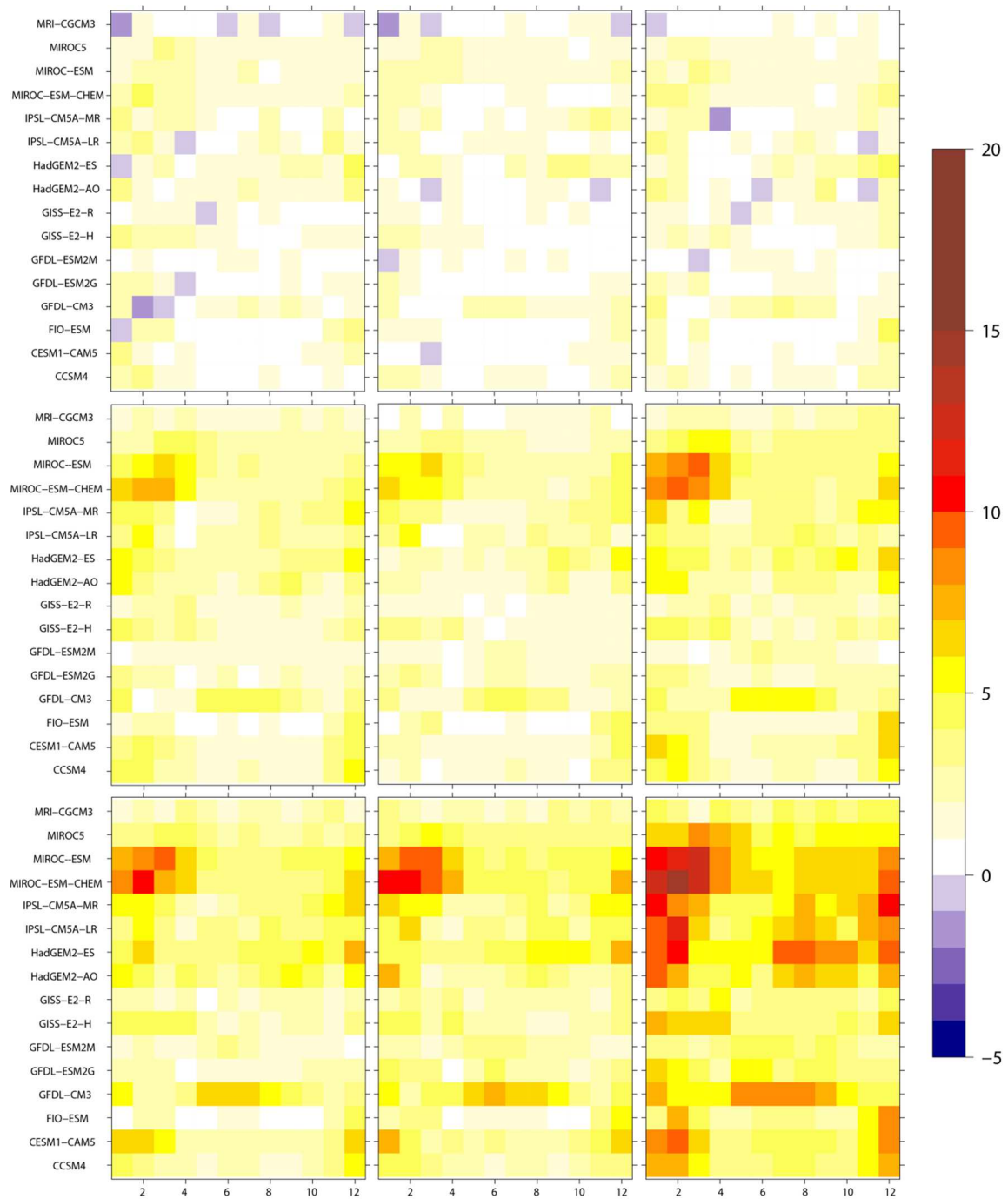


Figure 2-2. Same as Figure 2-1, but for daily minimum temperature.

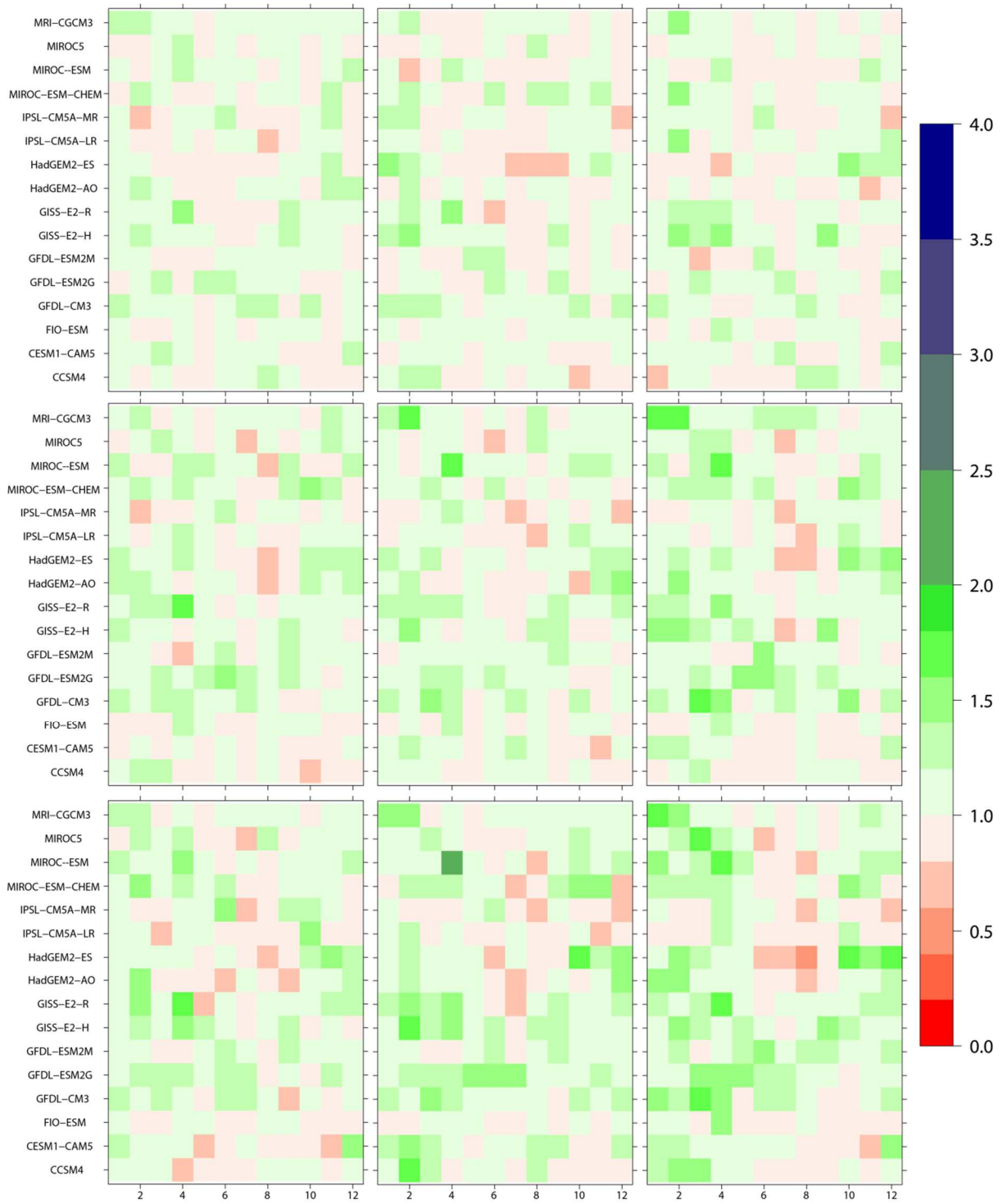


Figure 2-3. Same as Figure 2-1, but for daily precipitation. The change factor for precipitation is a ratio and unitless.

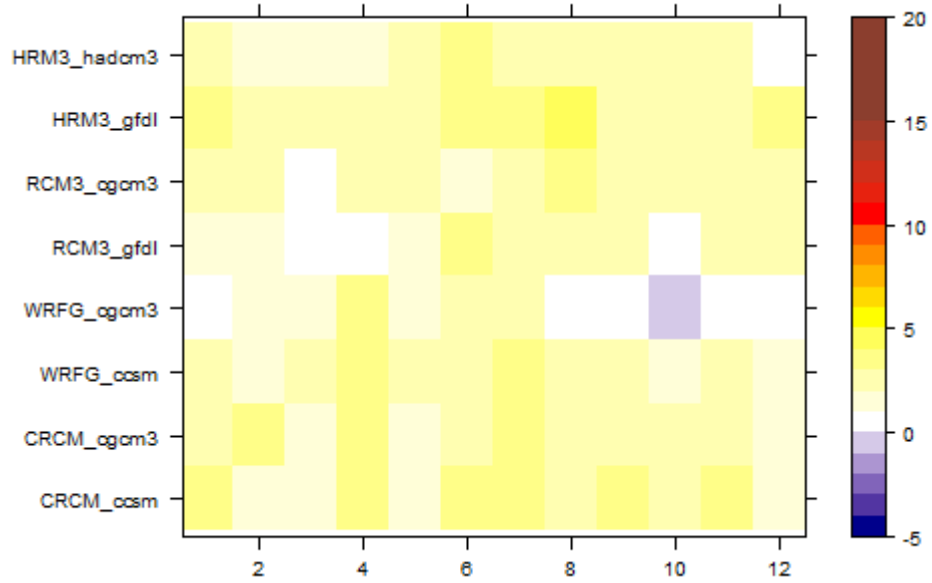


Figure 2-4. Change of monthly average of daily maximum temperature compared to baseline period (1978-1998) for NARCCAP models. The unit is Celsius.

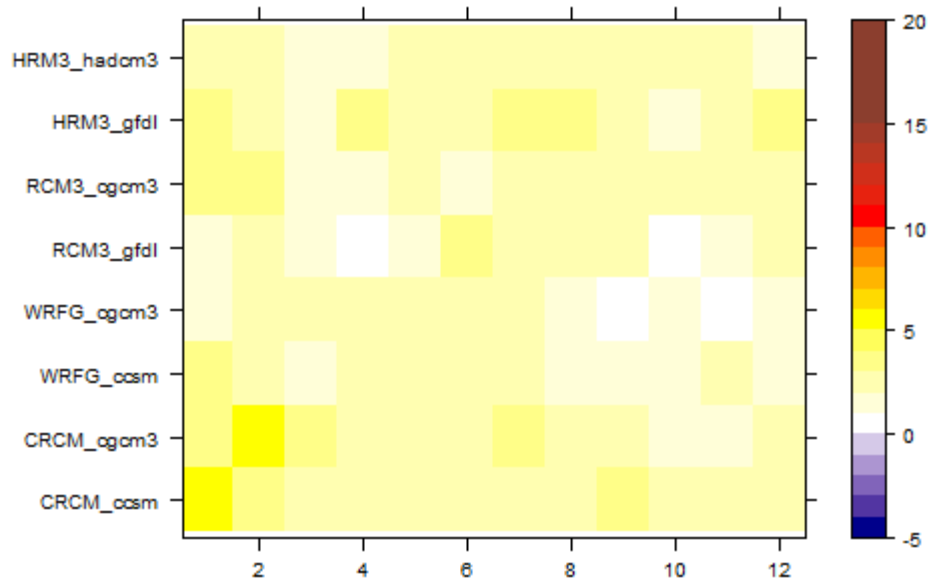


Figure 2-5. Same as Figure 2-4, but for daily minimum temperature.

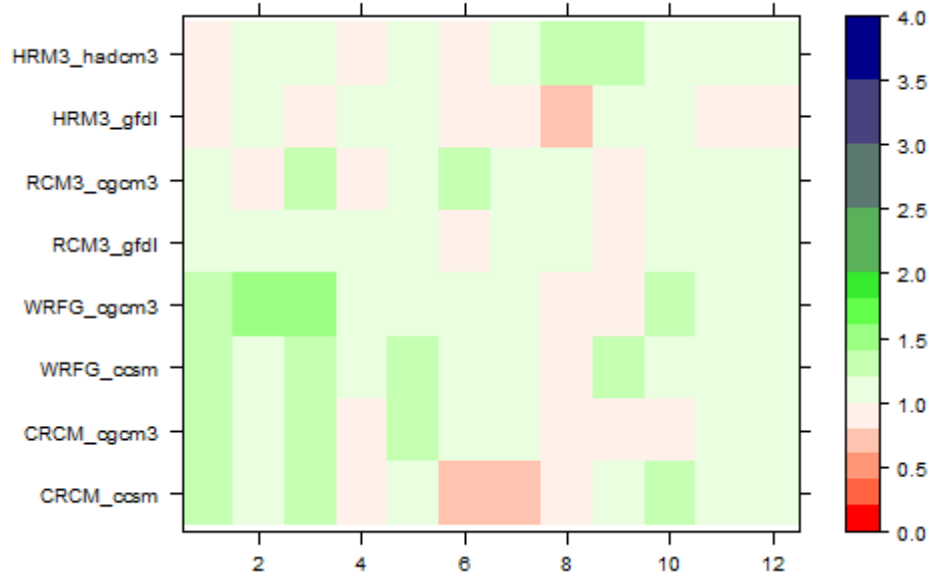


Figure 2-6. Same as Figure 2-4, but for daily precipitation. The change factor for precipitation is a ratio and unitless.

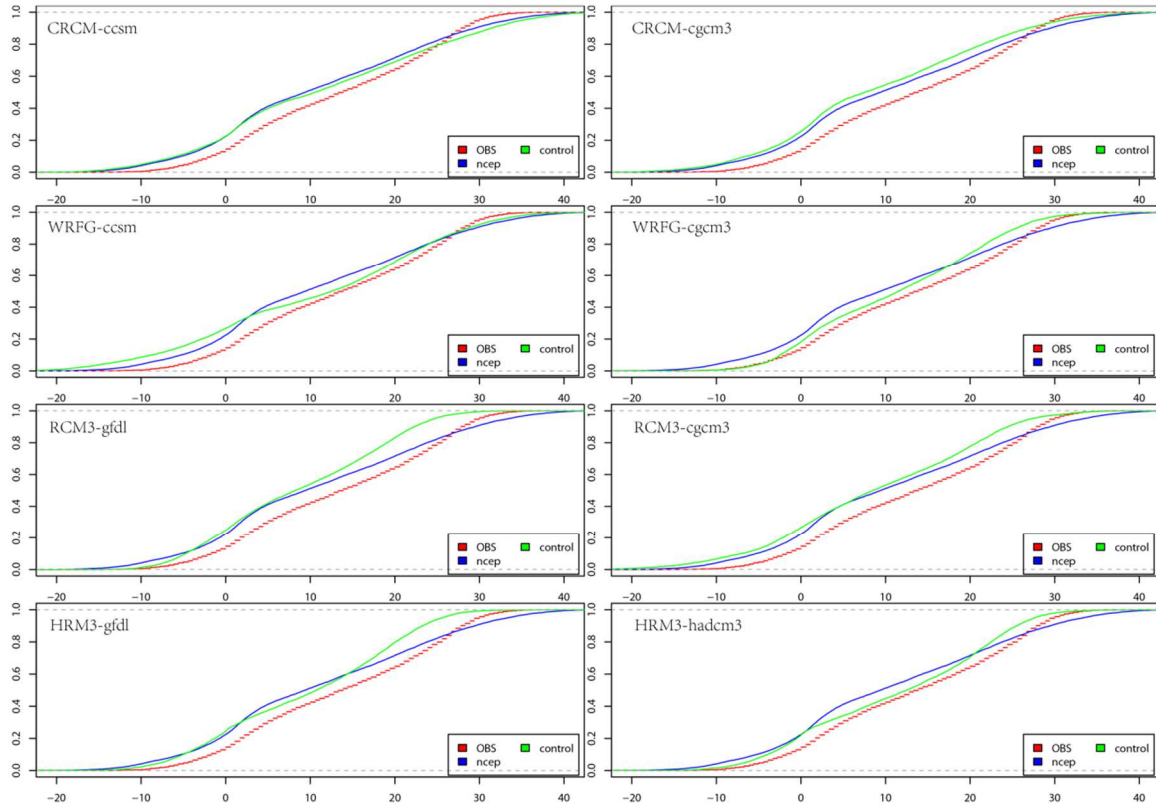


Figure 2-7. Empirical cumulative distribution function for daily maximum temperature for observation, NARCCAP NCEP run, and NARCCAP control run.

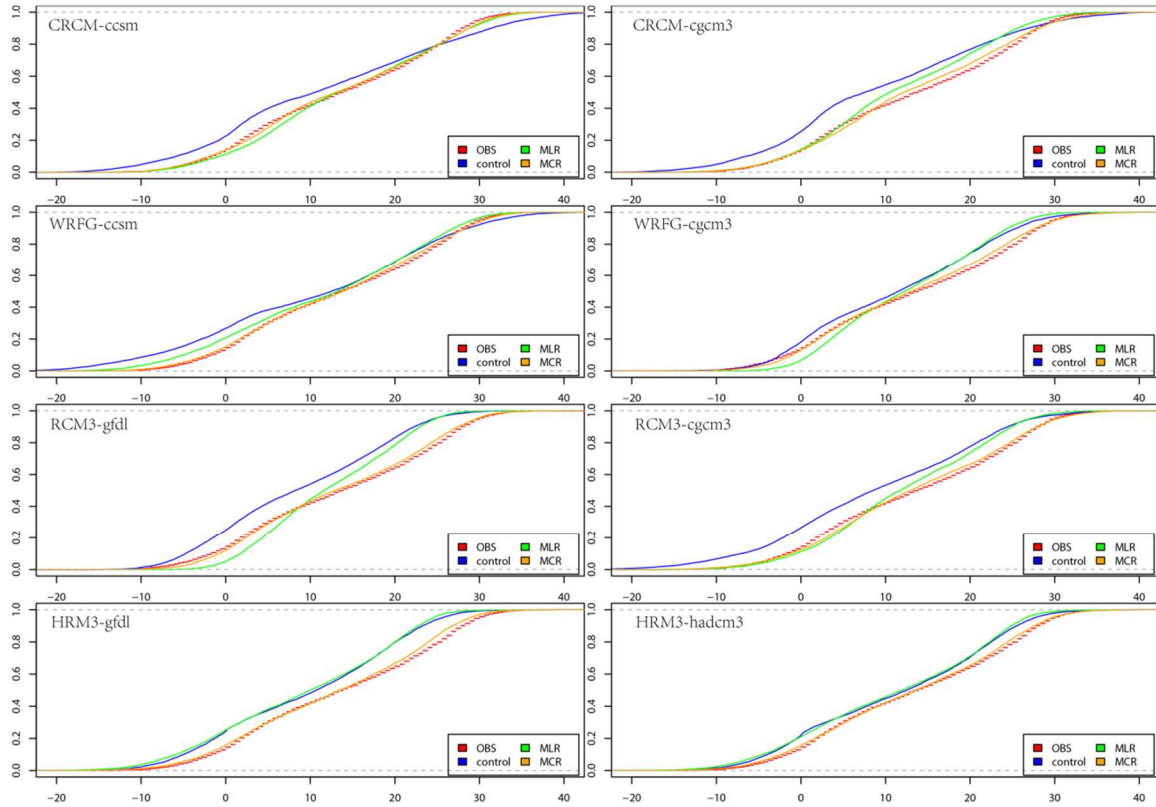


Figure 2-8. Empirical cumulative distribution function for daily maximum temperature for observation, NARCCAP control run, NARCCAP MLR projection, and NARCCAP MCR projection during current period.

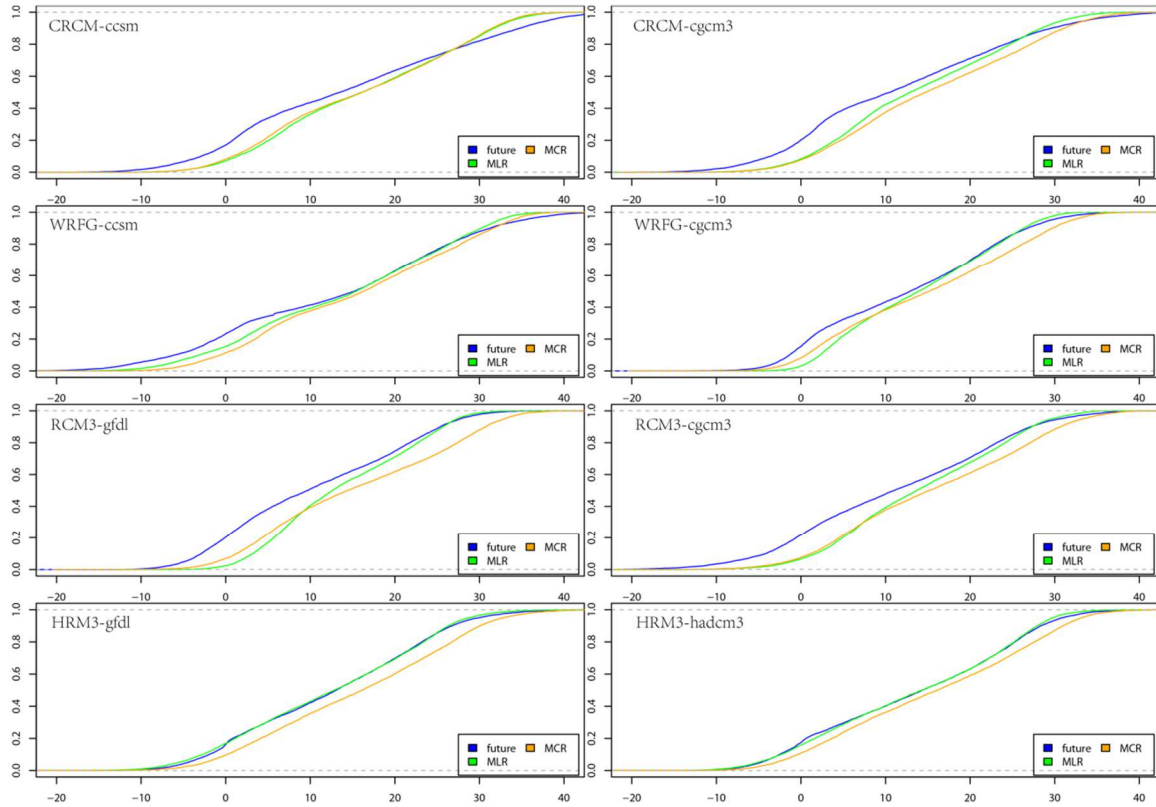


Figure 2-9. Empirical cumulative distribution function for daily maximum temperature for NARCCAP future run, NARCCAP MLR projection, and NARCCAP MCR projection during future period.

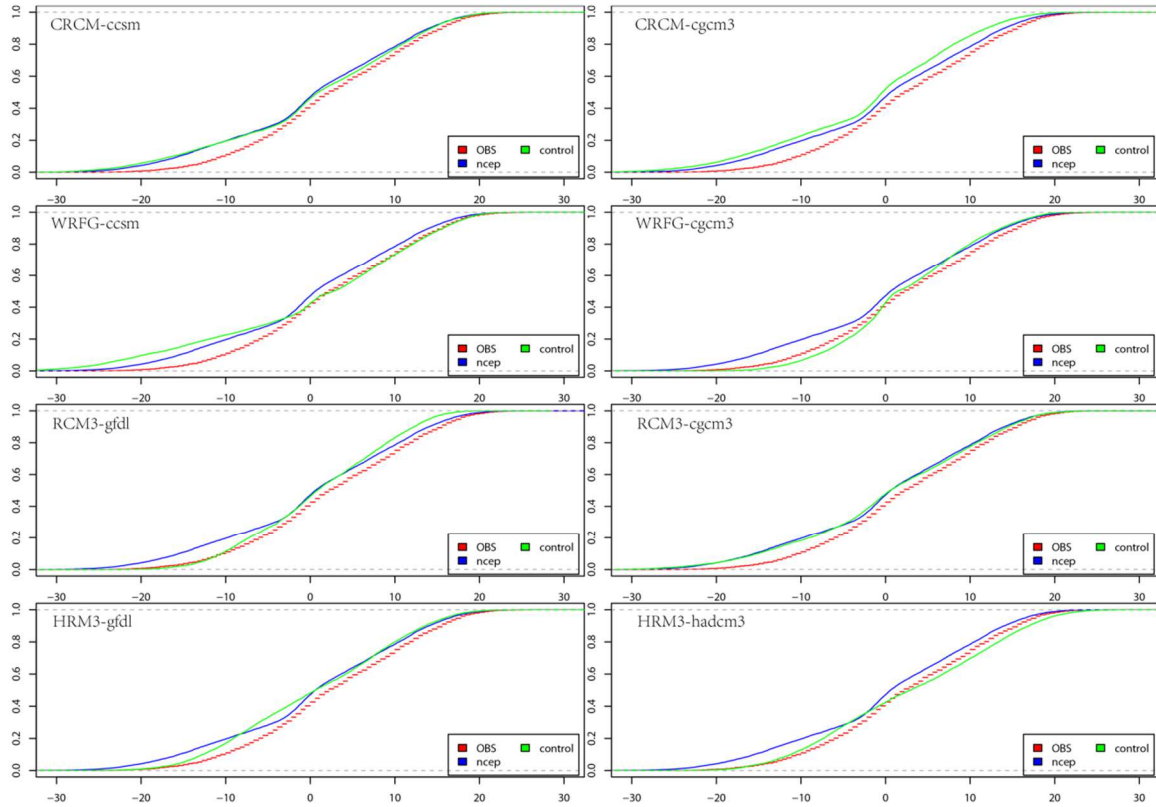


Figure 2-10. Same as Figure 2-7, but for daily minimum temperature.

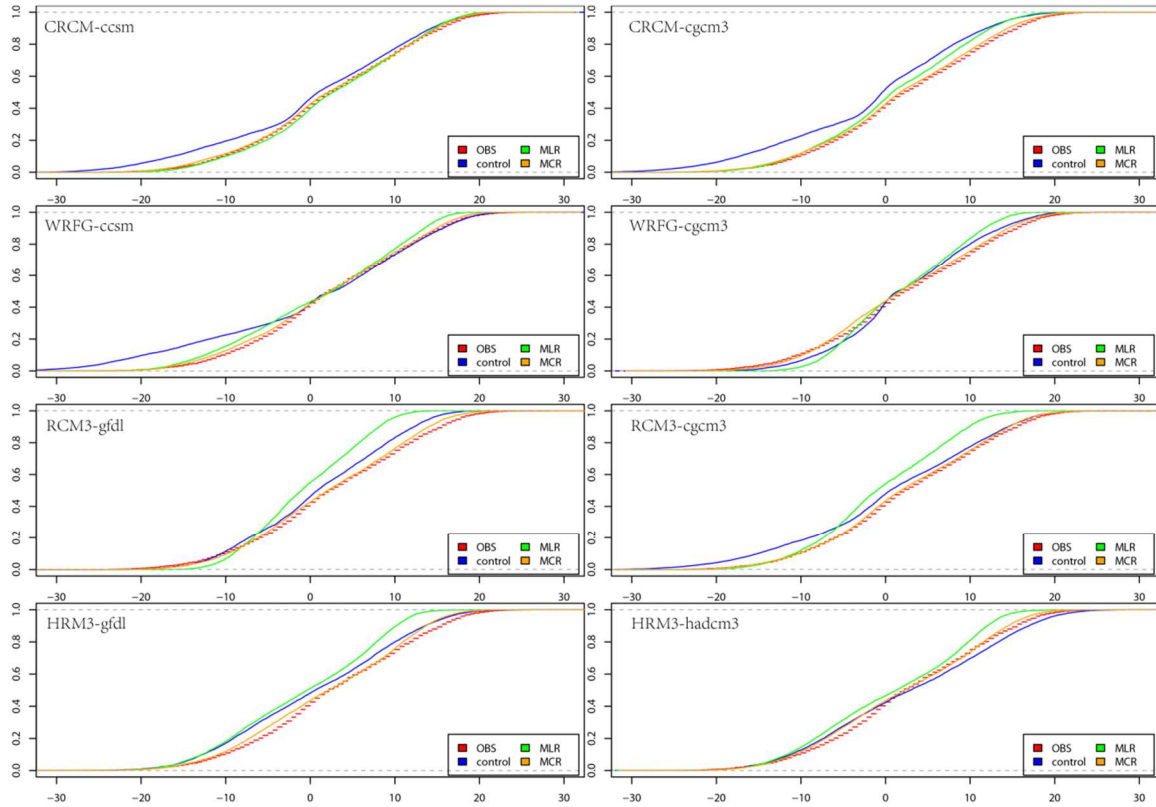


Figure 2-11. Same as Figure 2-8, but for daily minimum temperature.

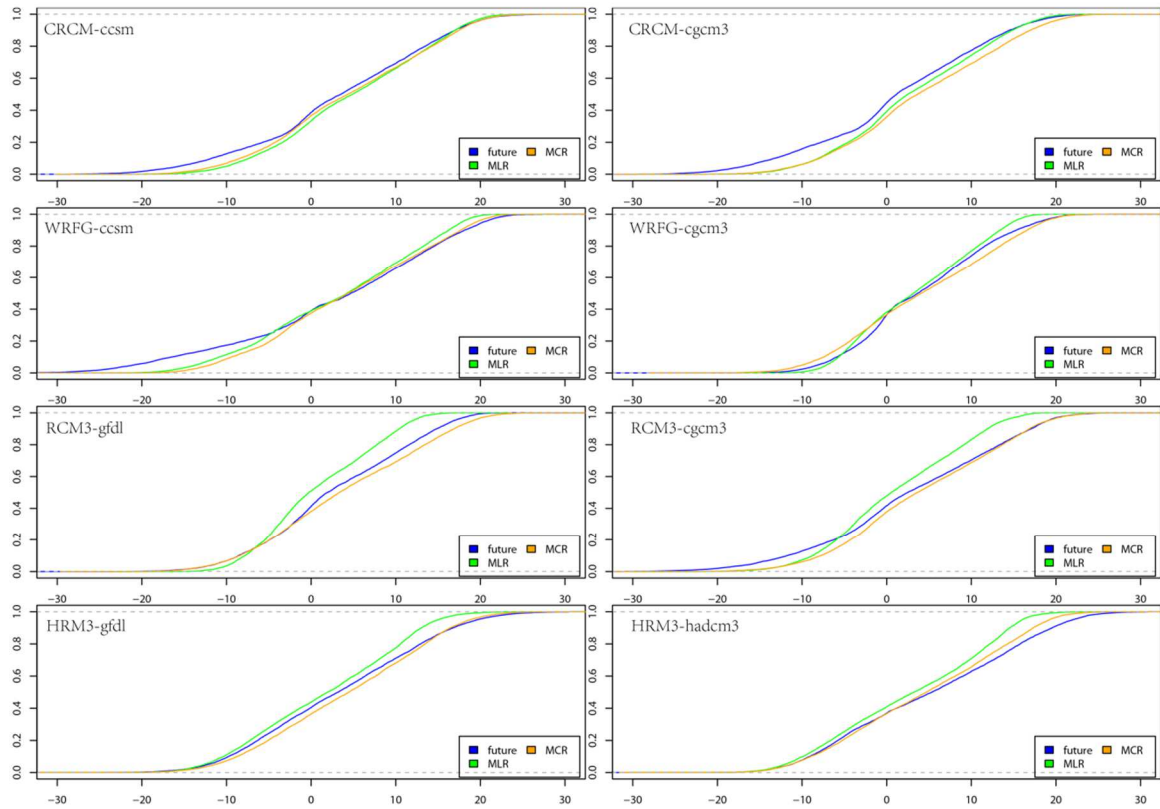


Figure 2-12. Same as Figure 2-9, but for daily minimum temperature.

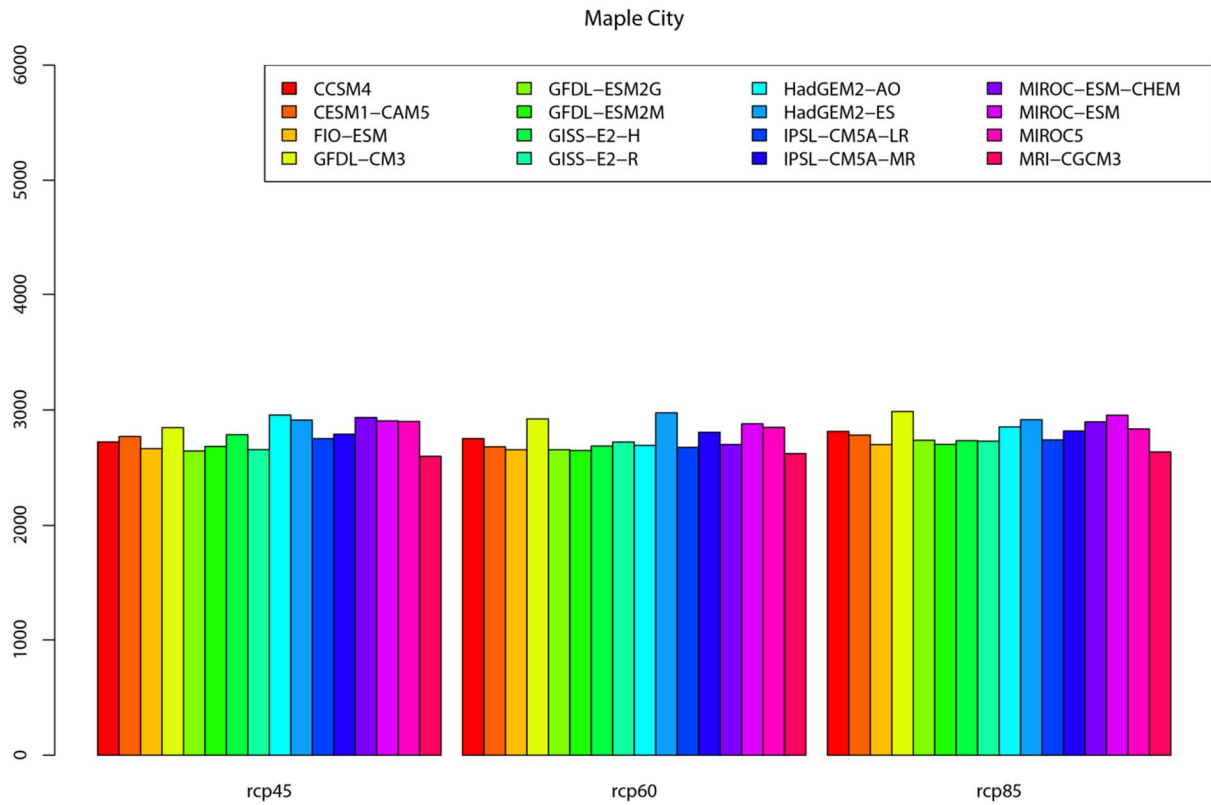


Figure 2-13. Median values of GDDs from CMIP5 delta projections for time slice 2010-2030.

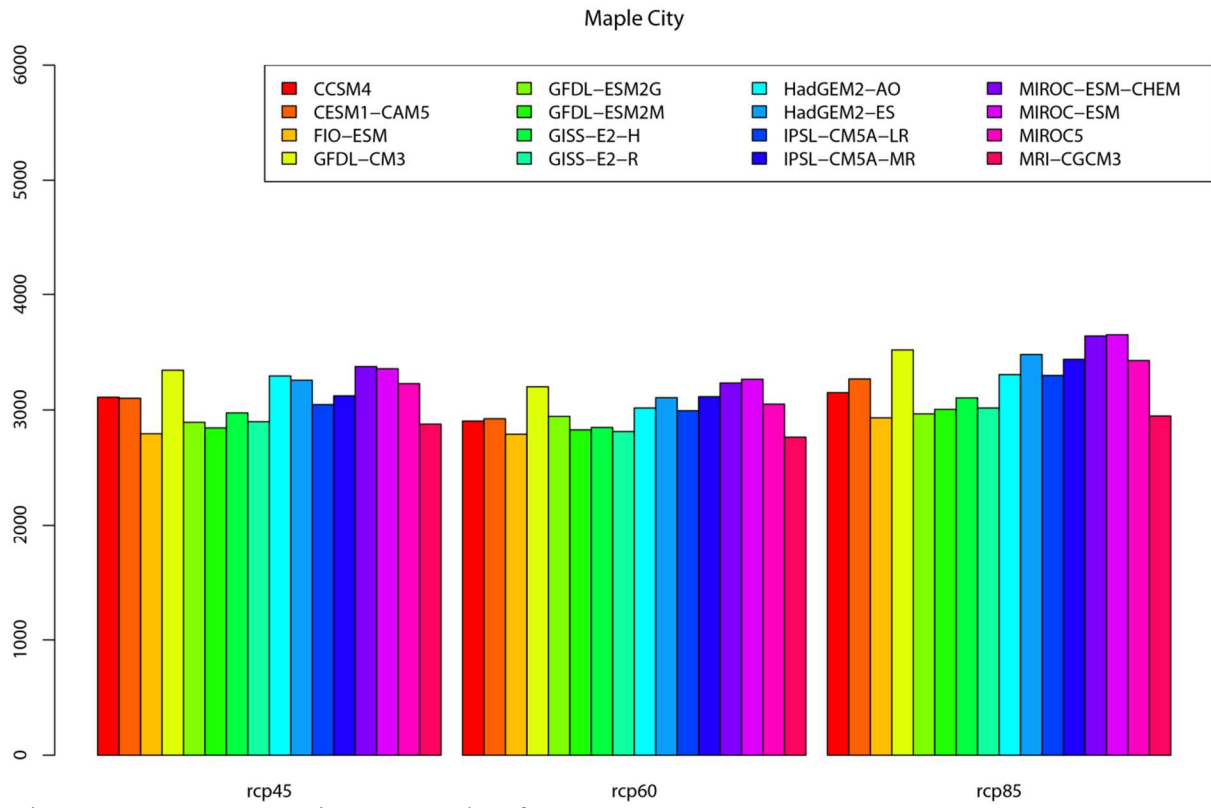


Figure 2-14. Same as Figure 2-13, but for 2040-2060.

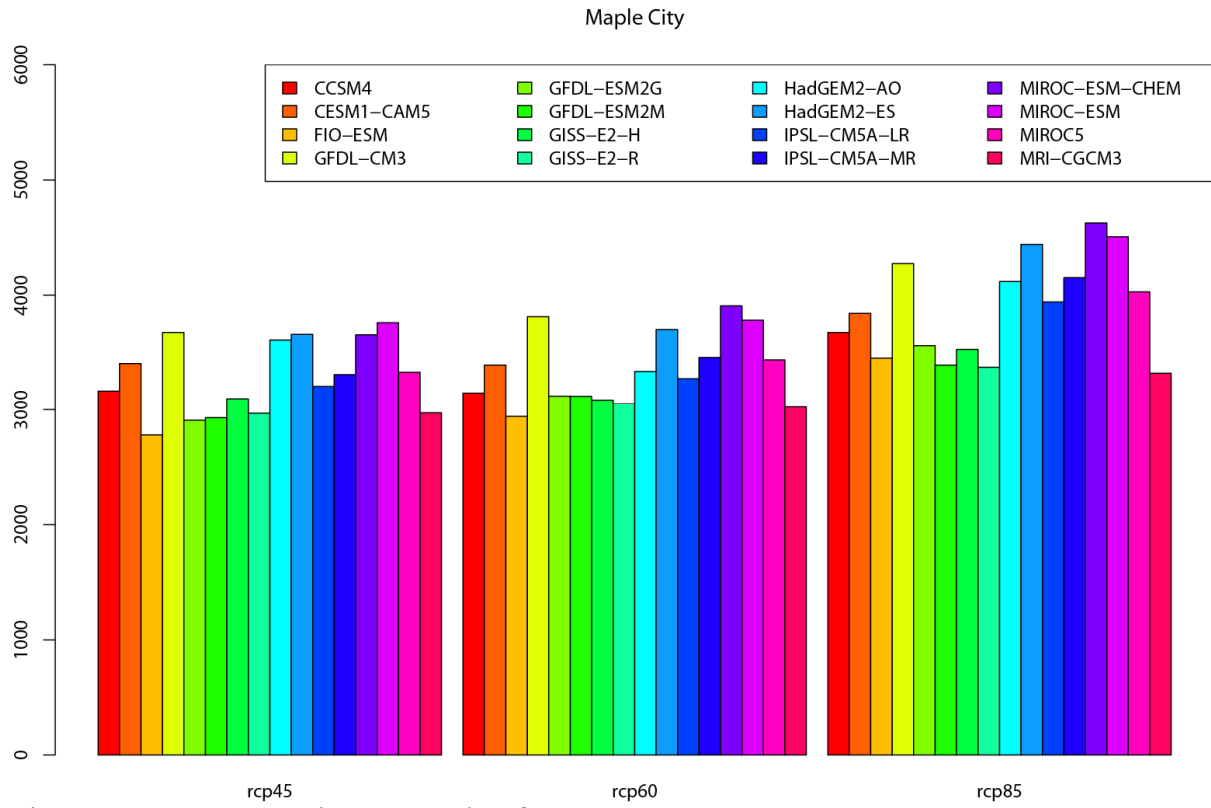


Figure 2-15. Same as Figure 2-14, but for 2070-2090.

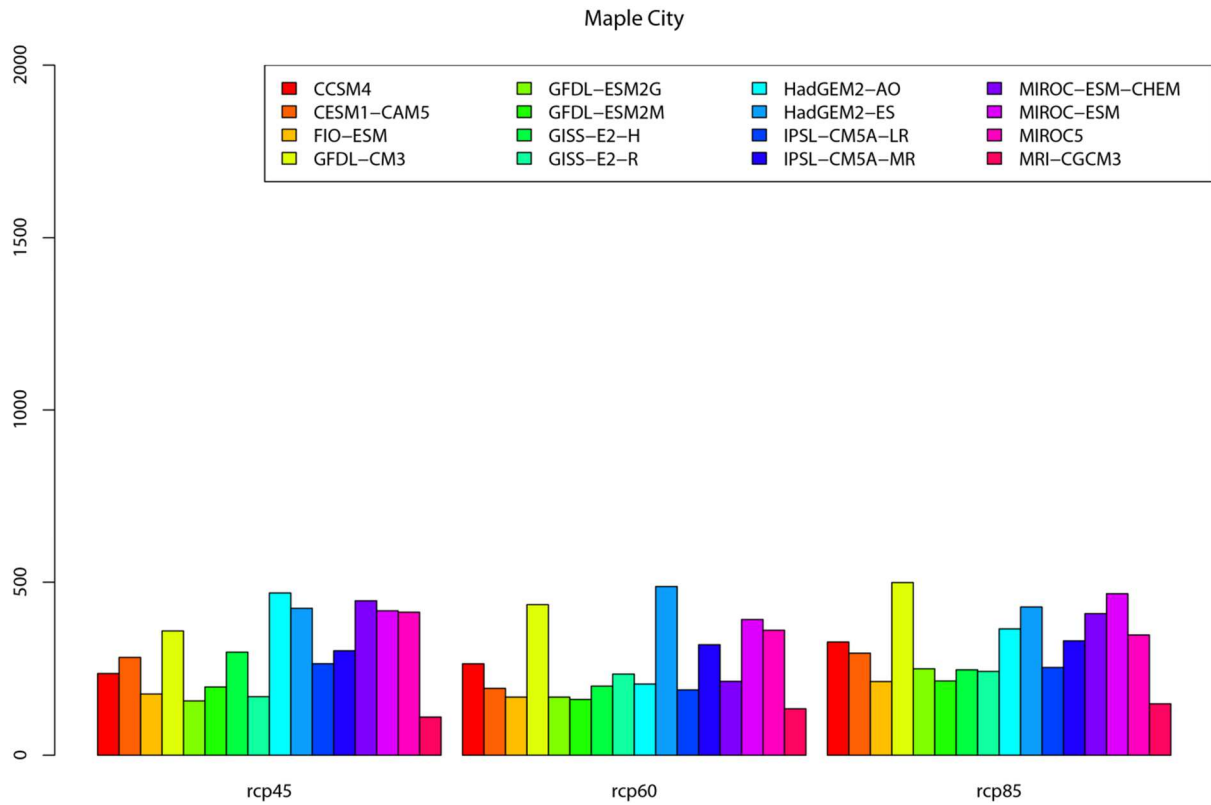


Figure 2-16. Differences of median GDDs from CMIP5 delta projections for time slice 2010-2030 and median observed GDDs for 1980-2000.

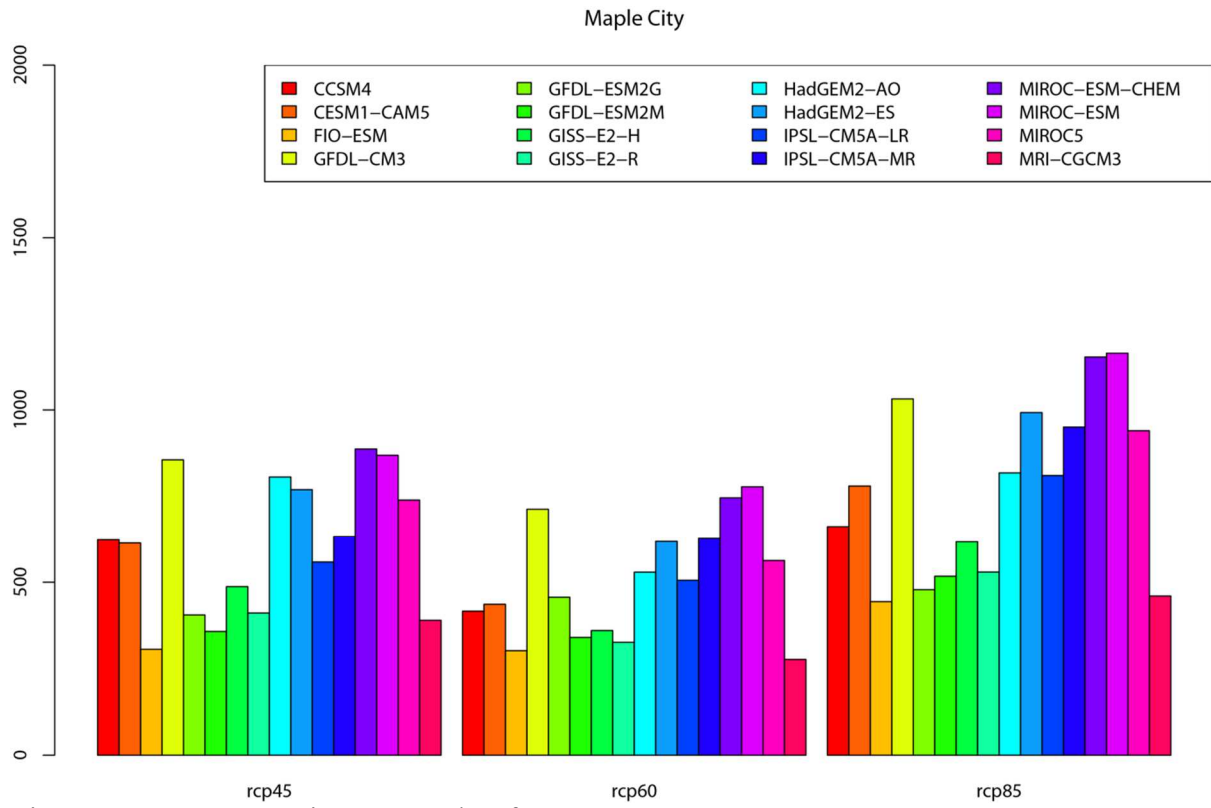


Figure 2-17. Same as Figure 2-16, but for 2040-2060.

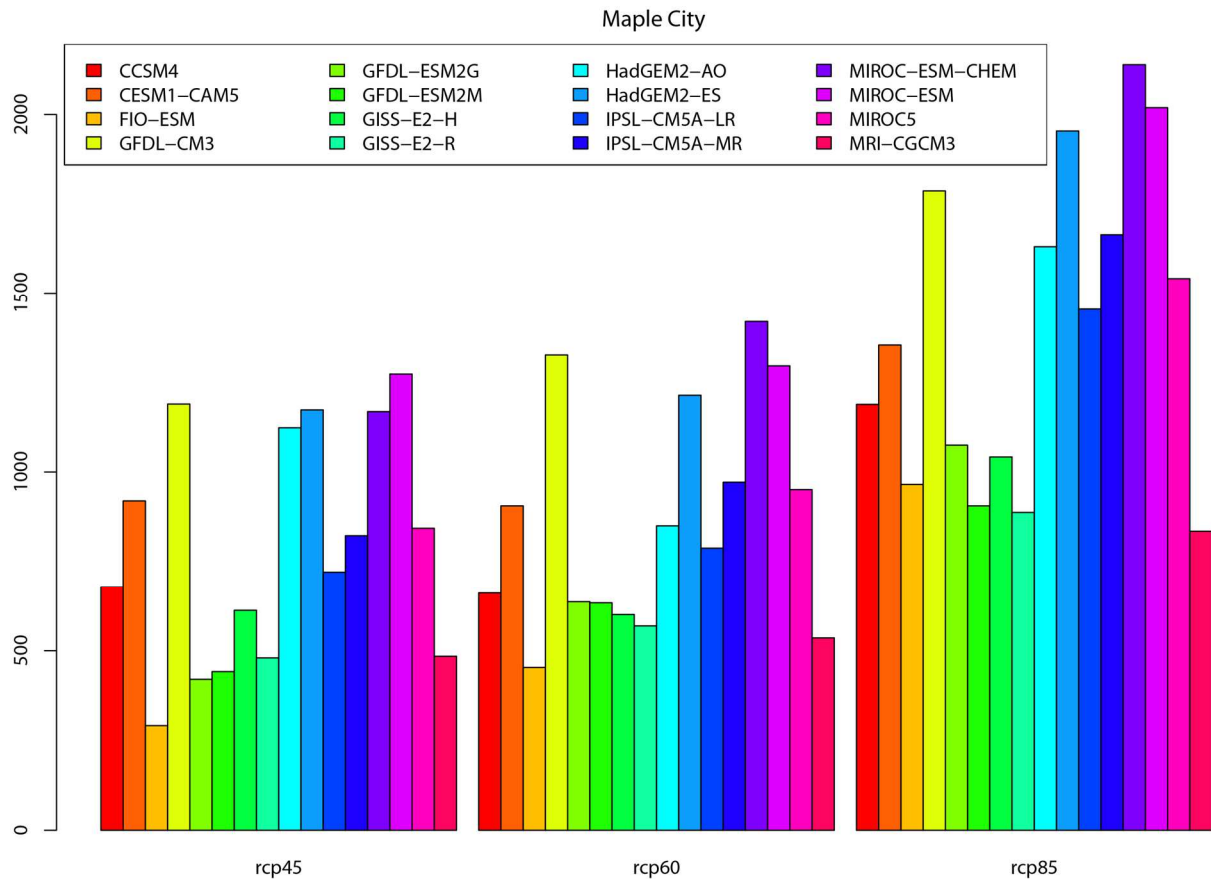


Figure 2-18. Same as Figure 2-16, but for 2070-2090.

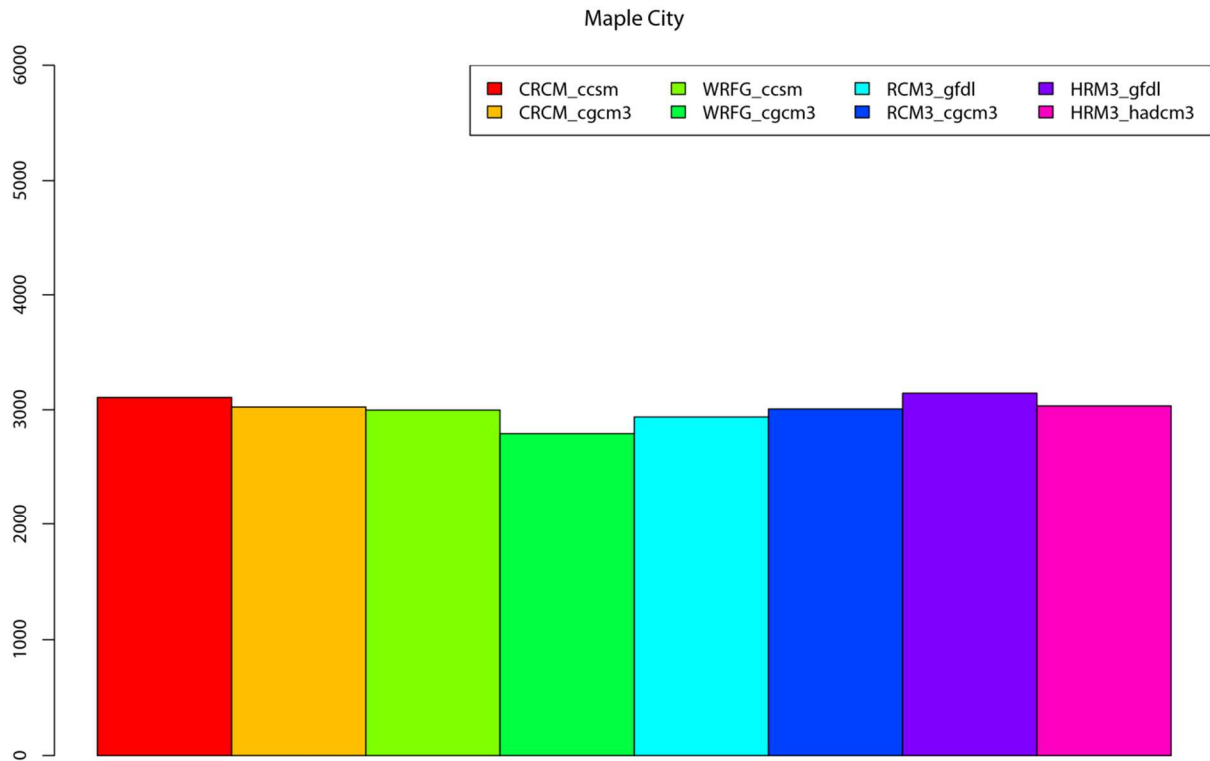


Figure 2-19. Median values of GDDs from NARCCAP delta projections for time slice 2040-2060.

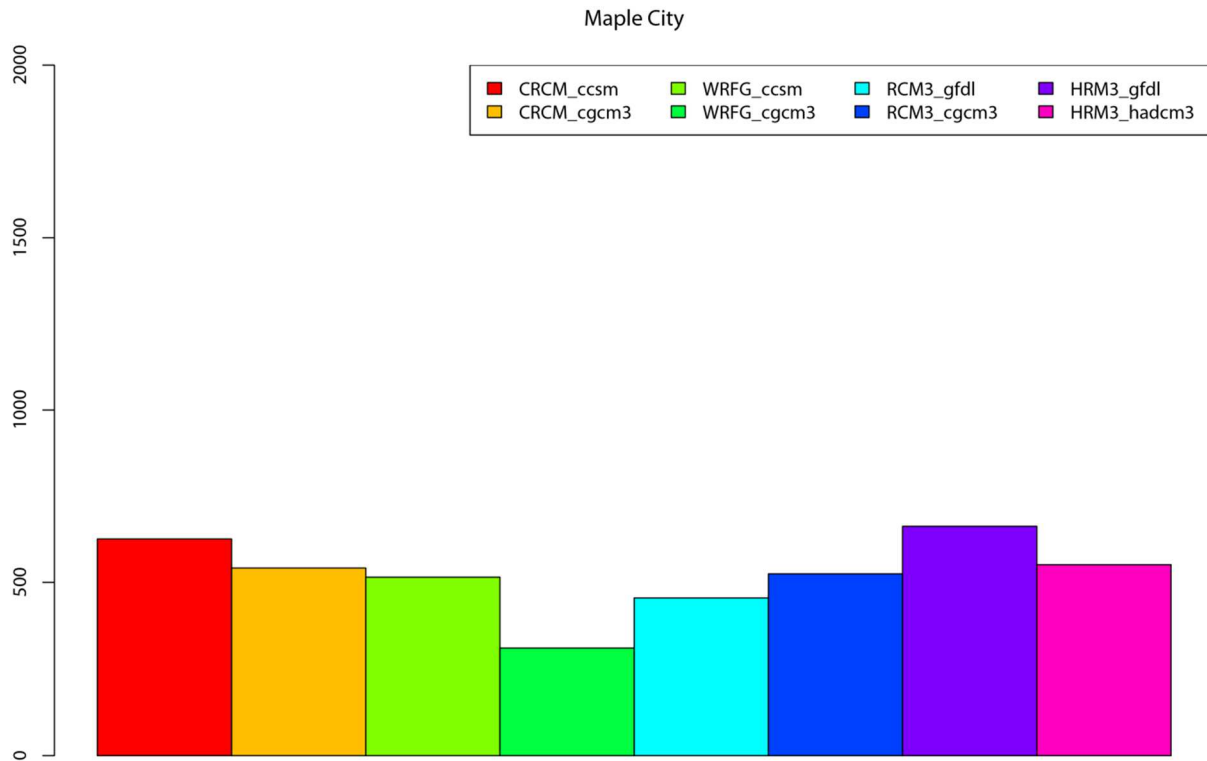


Figure 2-20. Differences of median values of GDDs from NARCCAP delta projections for time slice 2040-2060 and median observed GDDs for 1978-1998.



Figure 2-21. Median values of GDDs from NARCCAP NCEP simulations for time slice 1978-1998.

Maple City

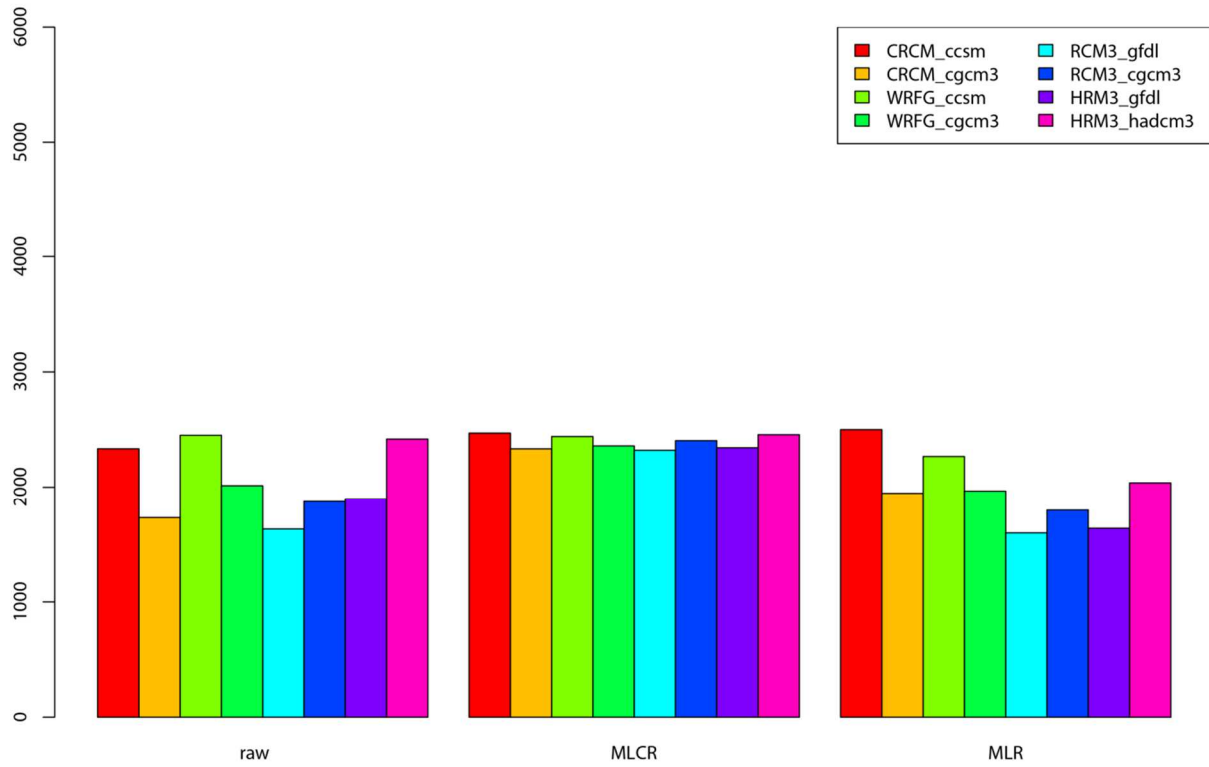


Figure 2-22. Median values of GDDs from NARCCAP raw control simulation, NARCCAP MCR projections, NARCCAP MLR projections for control period 1978-1998.

Maple City

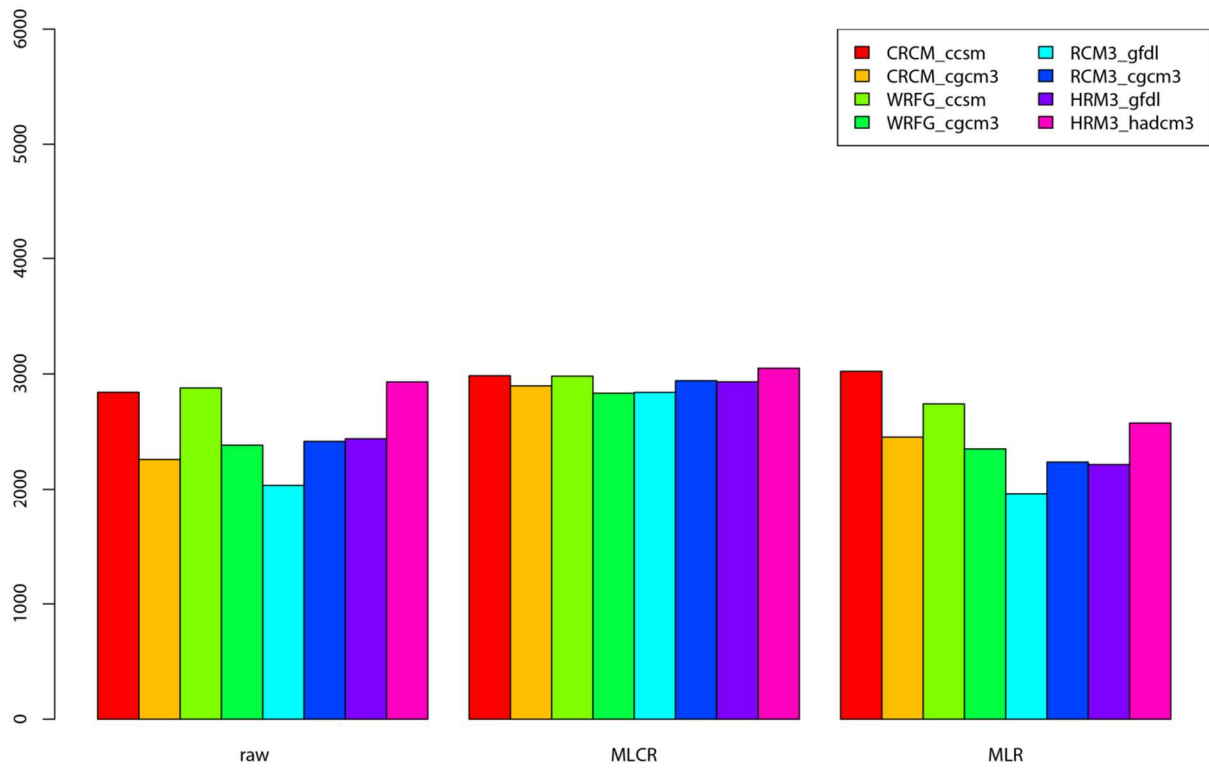


Figure 2-23. Same as Figure 2-22, but for future period of 2040-2060.

Maple City

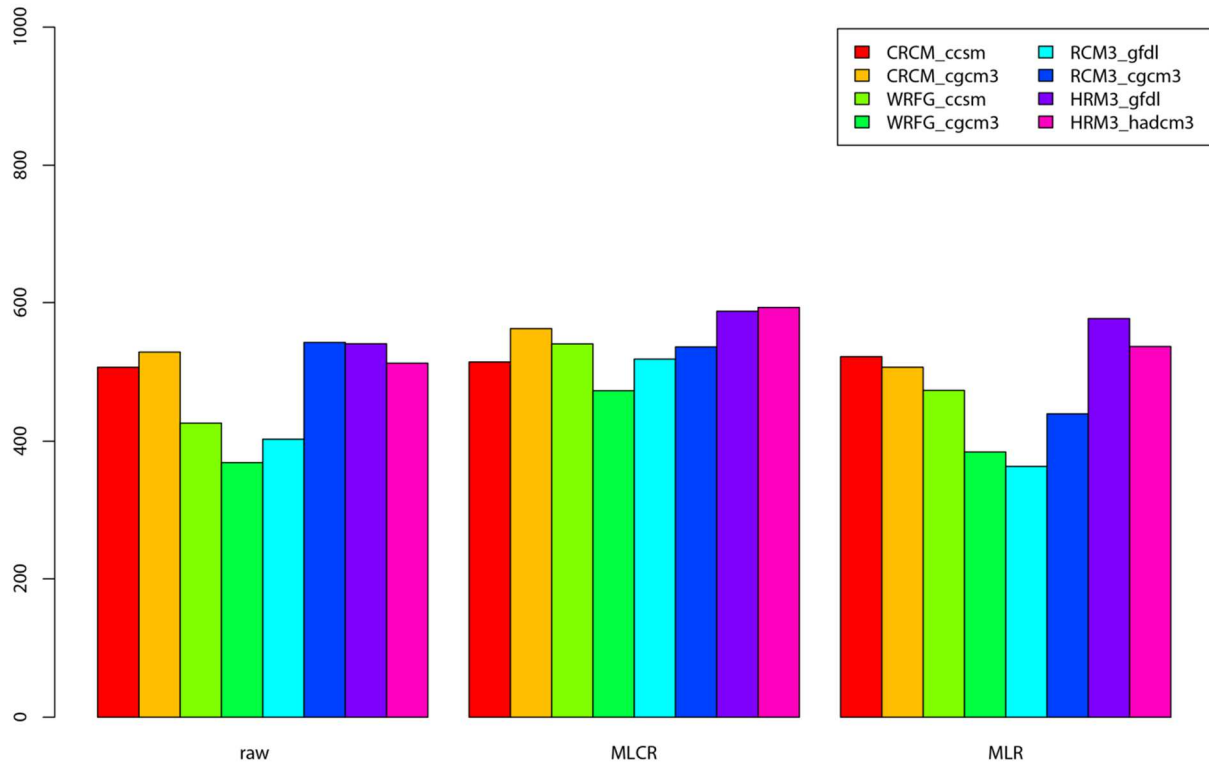


Figure 2-24. Differences of future and control period median values of GDDs from NARCCAP raw control simulation, NARCCAP MCR projections, NARCCAP MLR projections.

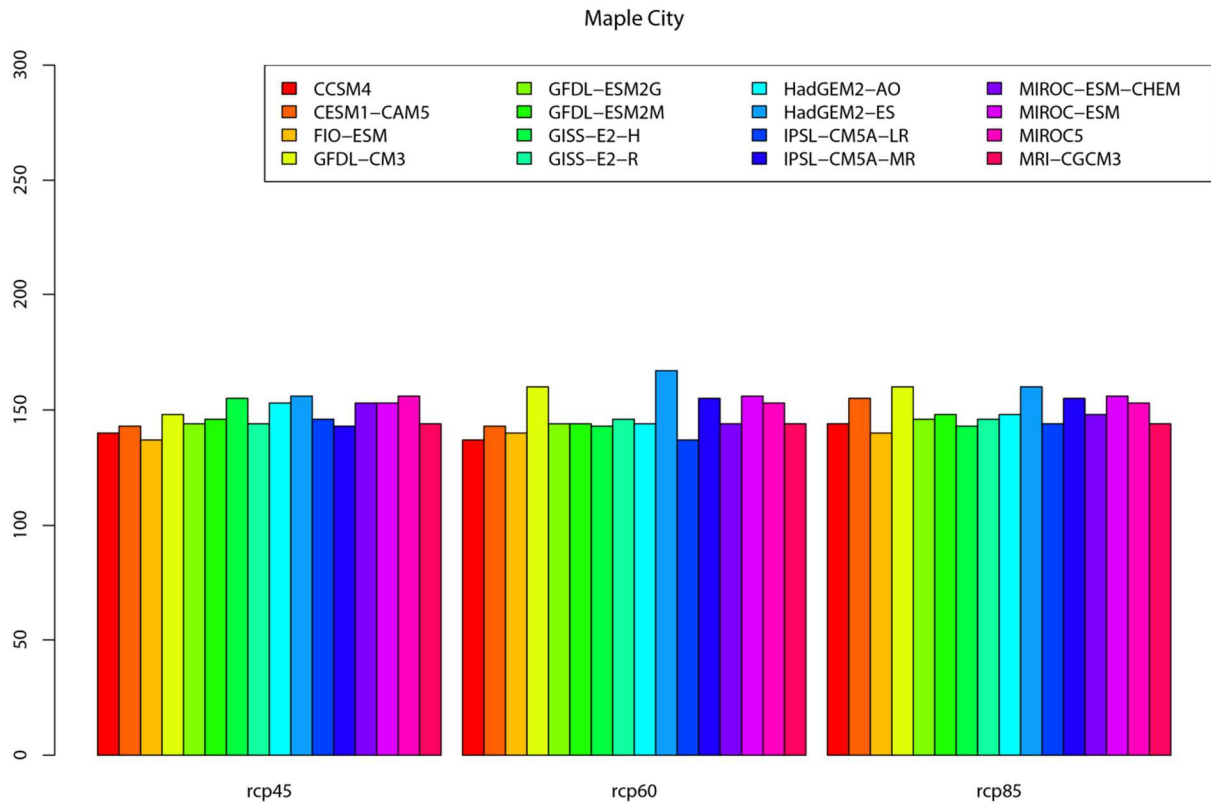


Figure 2-25. Median values of growing season length from CMIP5 delta projections for time slice 2010-2030.

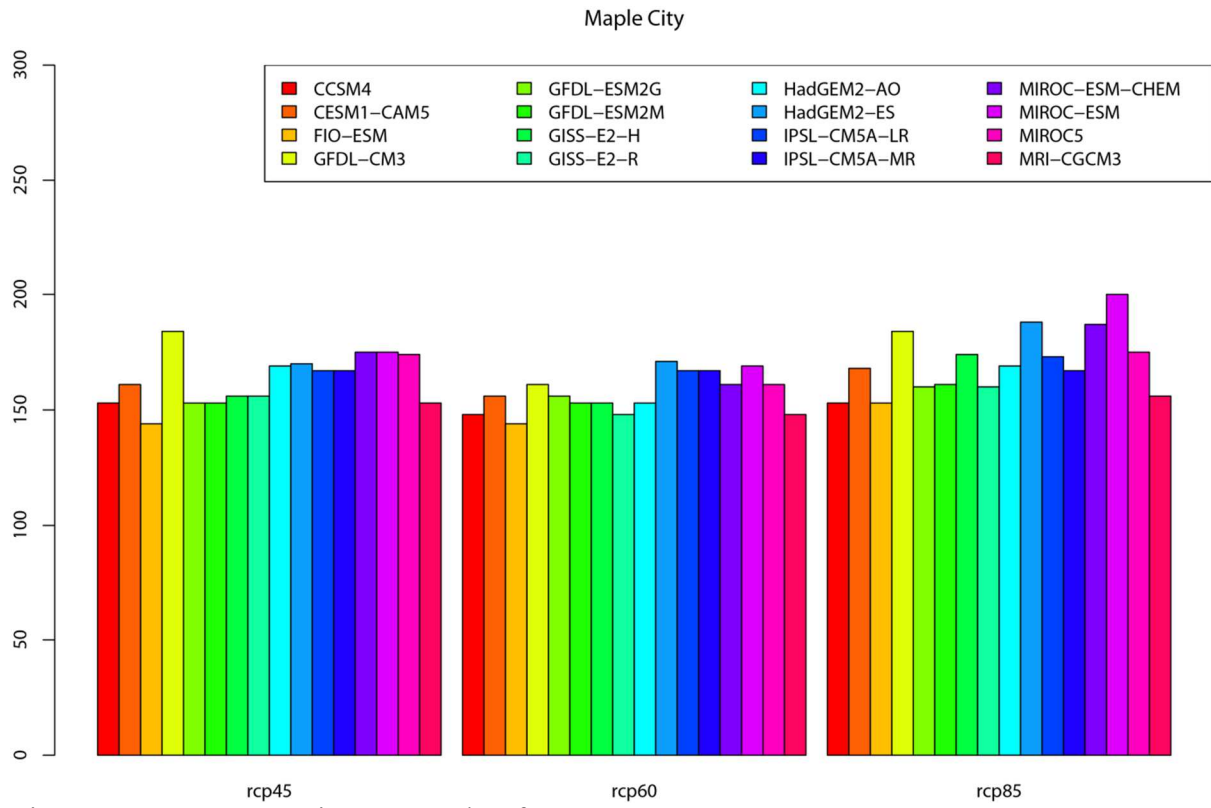


Figure 2-26. Same as Figure 2-25, but for 2040-2060.

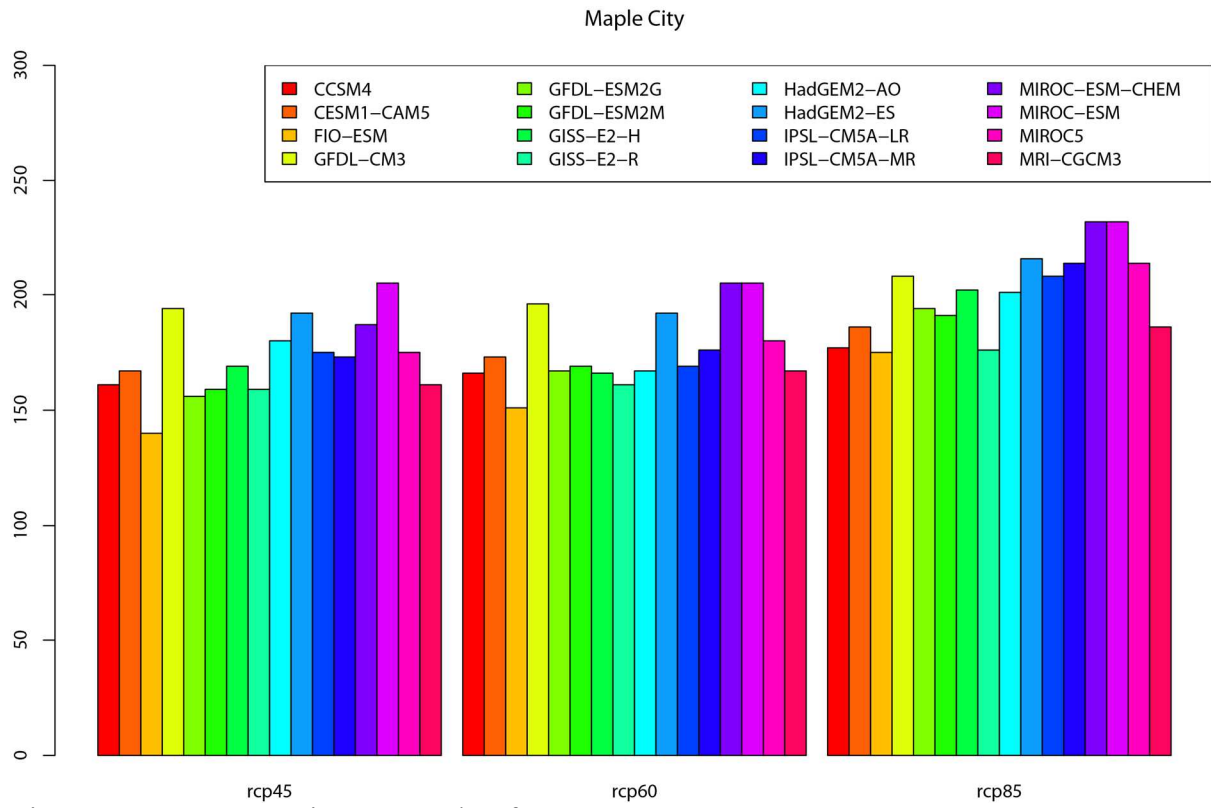


Figure 2-27. Same as Figure 2-25, but for 2070-2090.

Maple City

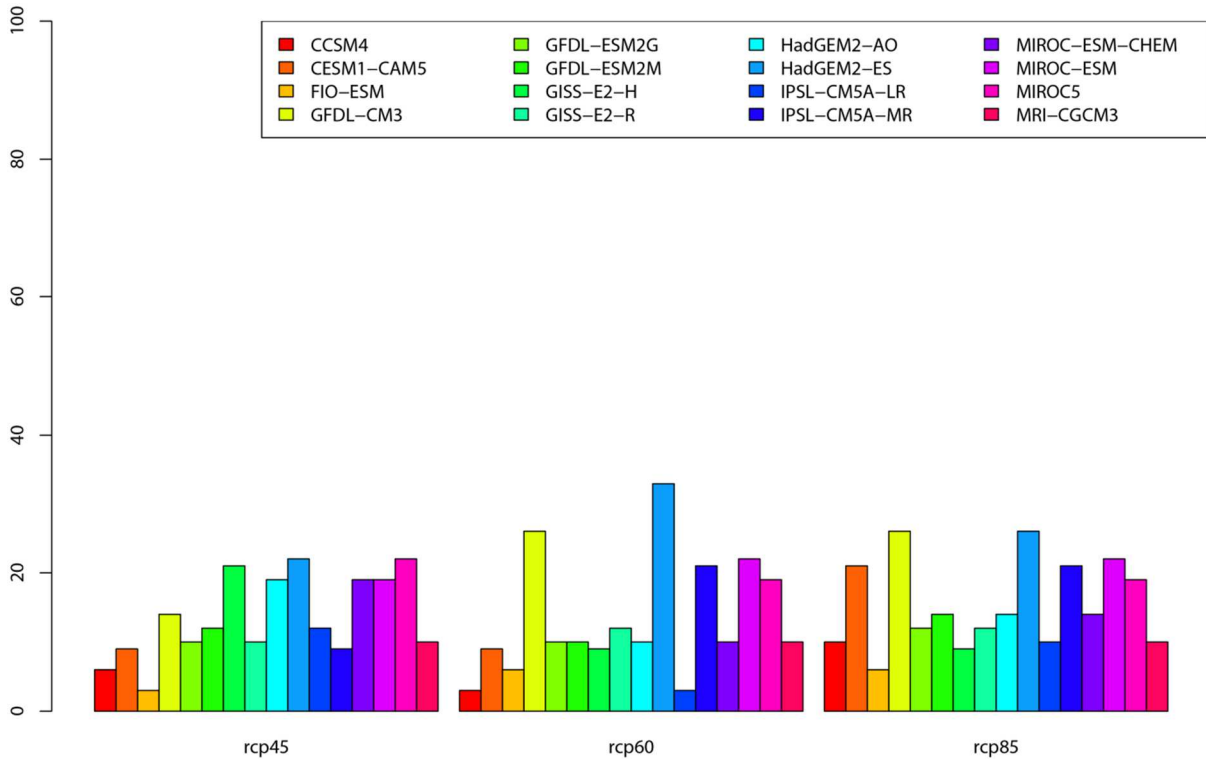


Figure 2-28. Differences of median values of growing season length from CMIP5 delta projections for time slice 2010-2030 and median observed growing season length for 1980-2000.

Maple City

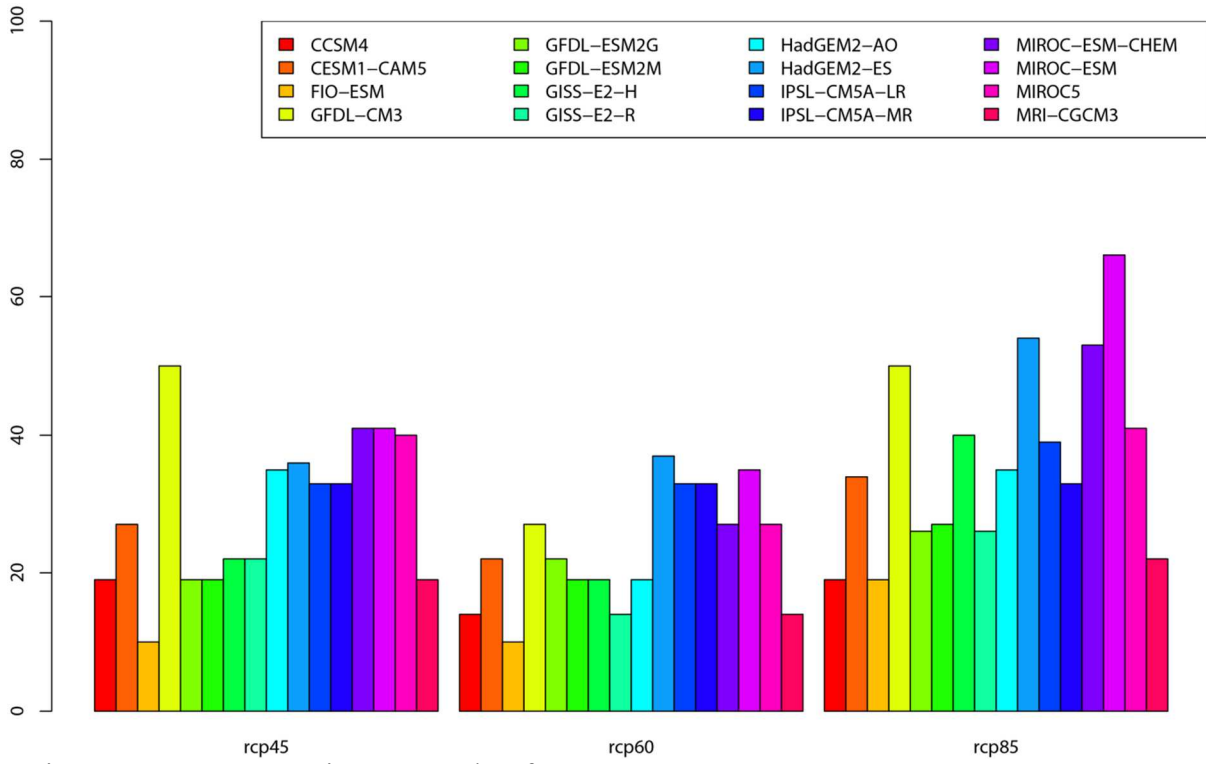


Figure 2-29. Same as Figure 2-28, but for 2040-2060.

Maple City

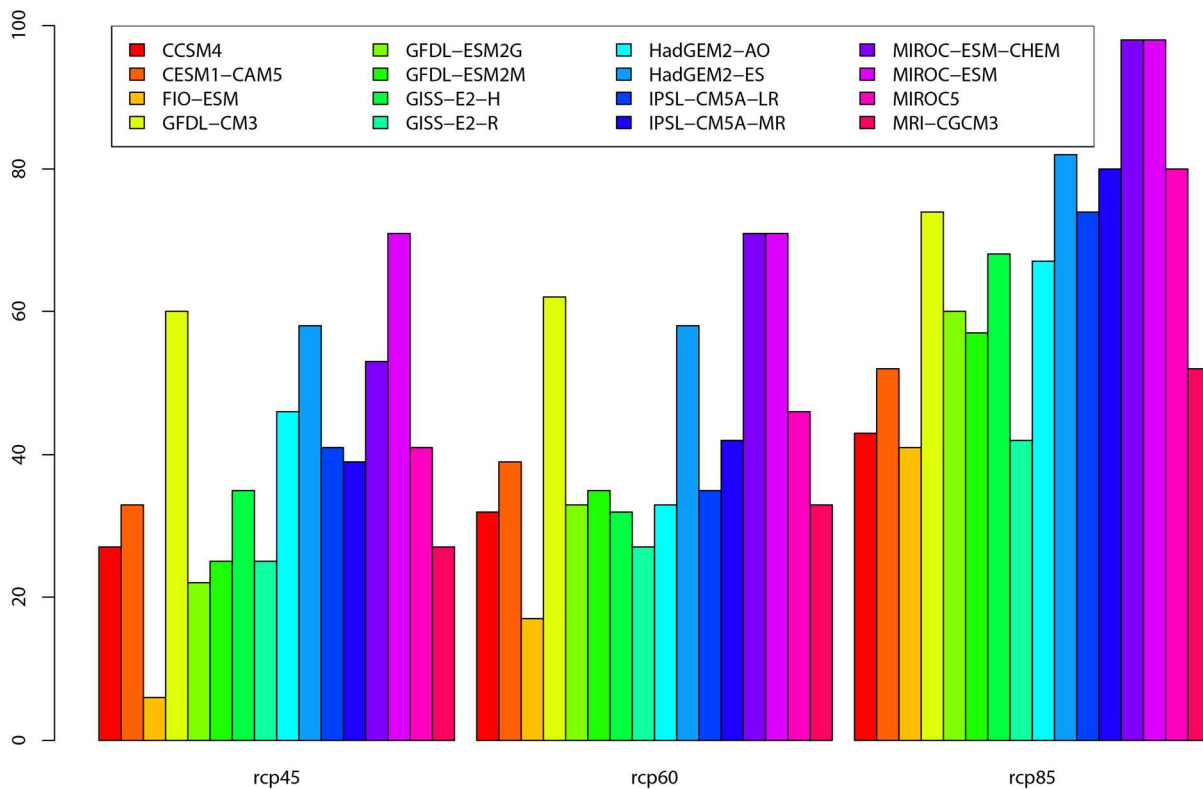


Figure 2-30. Same as Figure 2-28, but for 2070-2090.

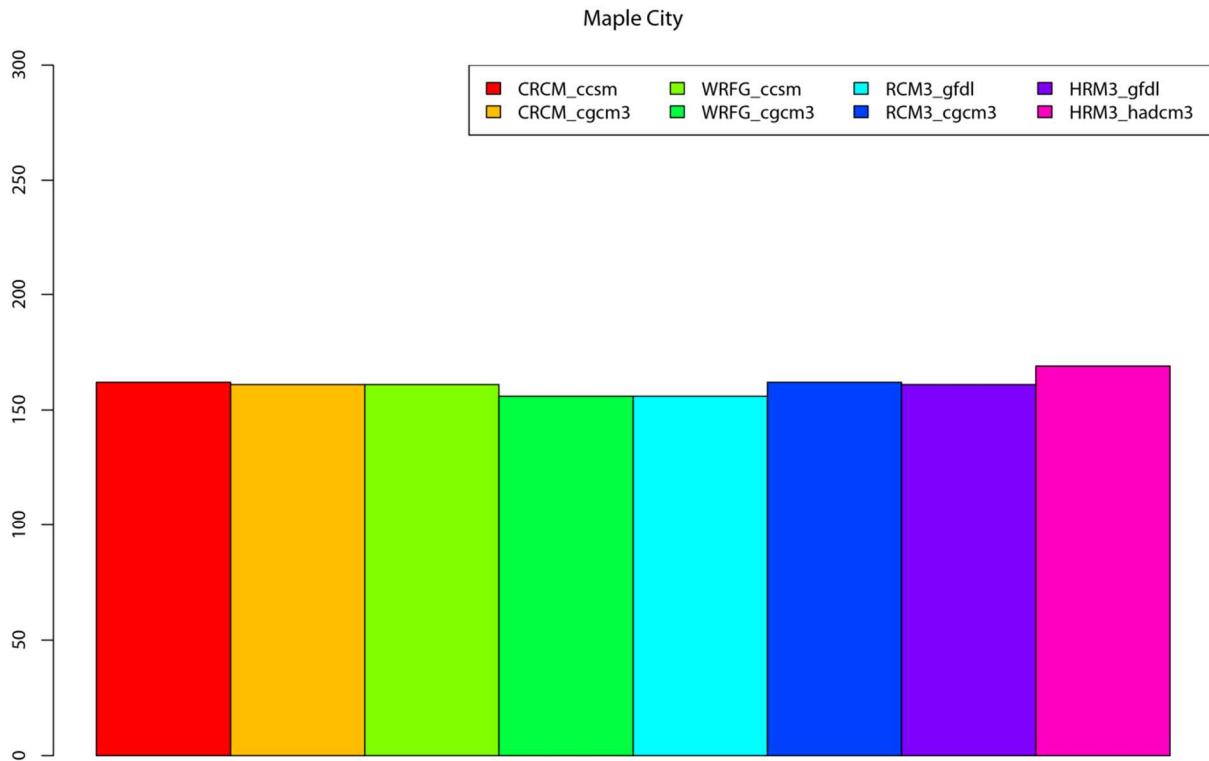


Figure 2-31. Median values of growing season length from NARCCAP delta projections for time slice 2040-2060.

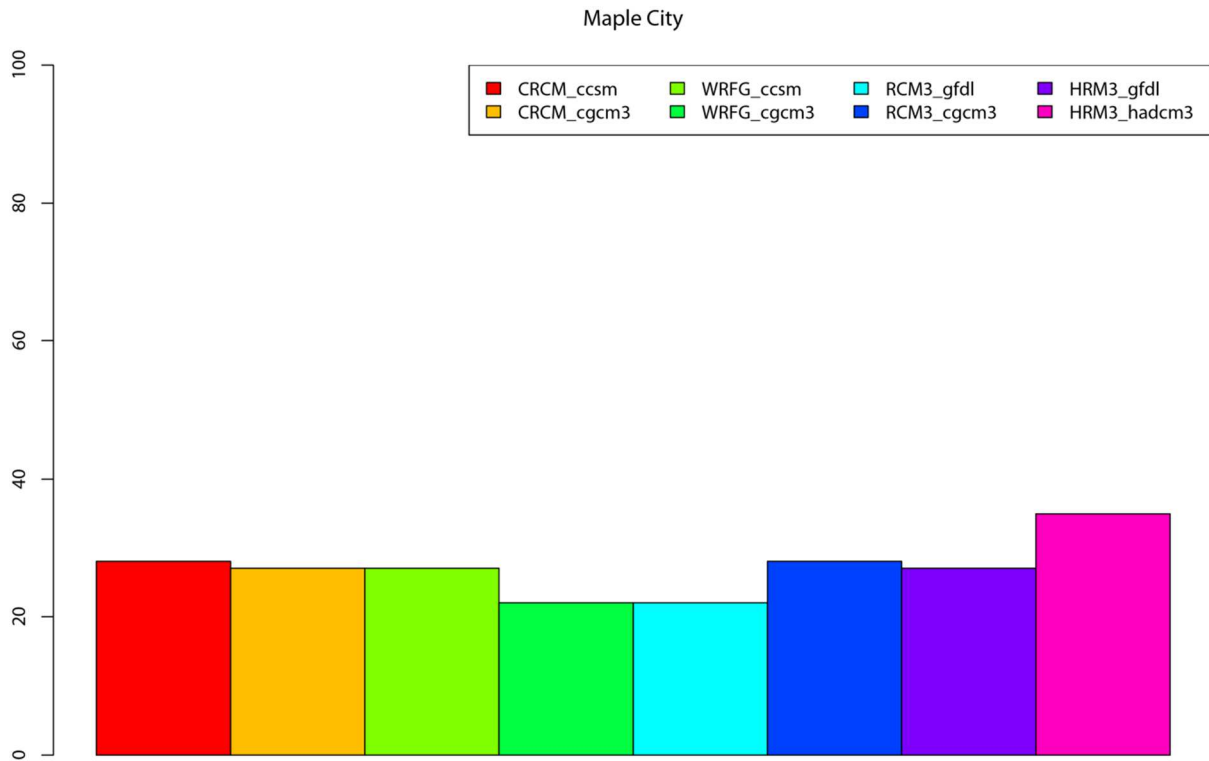


Figure 2-32. Differences of median values of growing season length from NARCCAP delta projections for time slice 2040-2060 and median observed growing season length for 1978-1998.

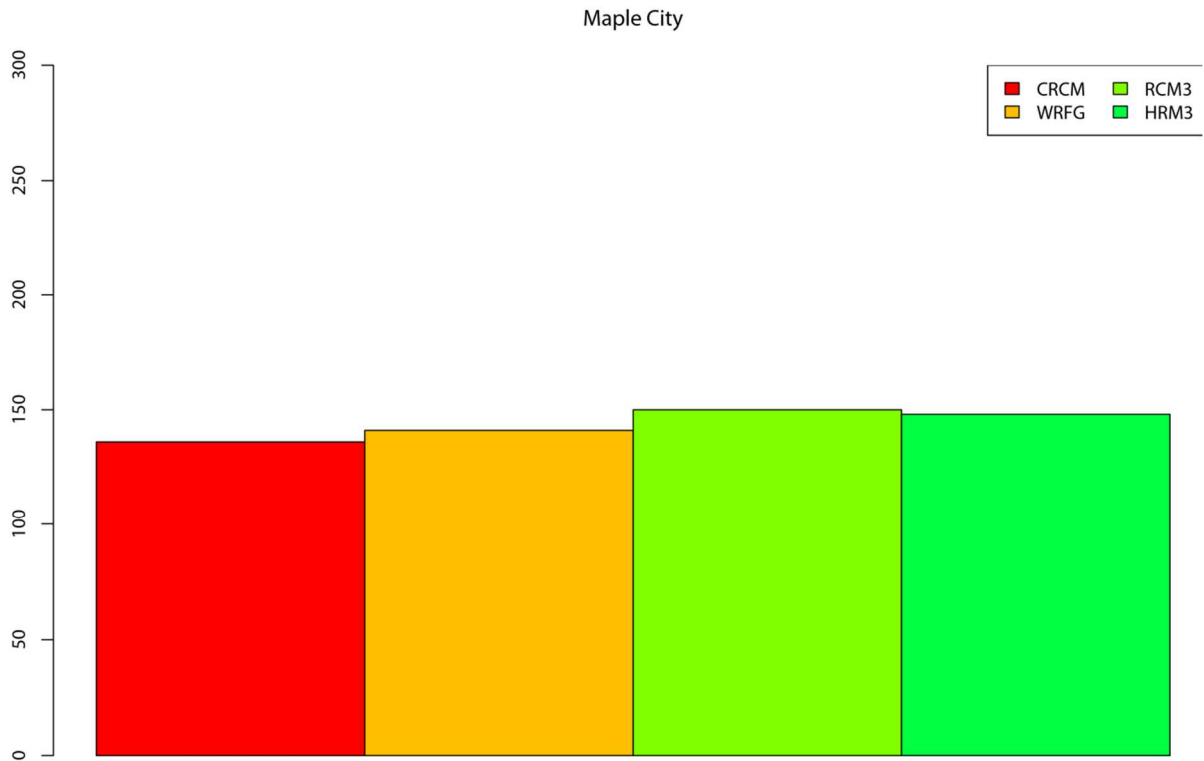


Figure 2-33. Median values of growing season length from NARCCAP NCEP simulations for time slice 1978-1998.

Maple City

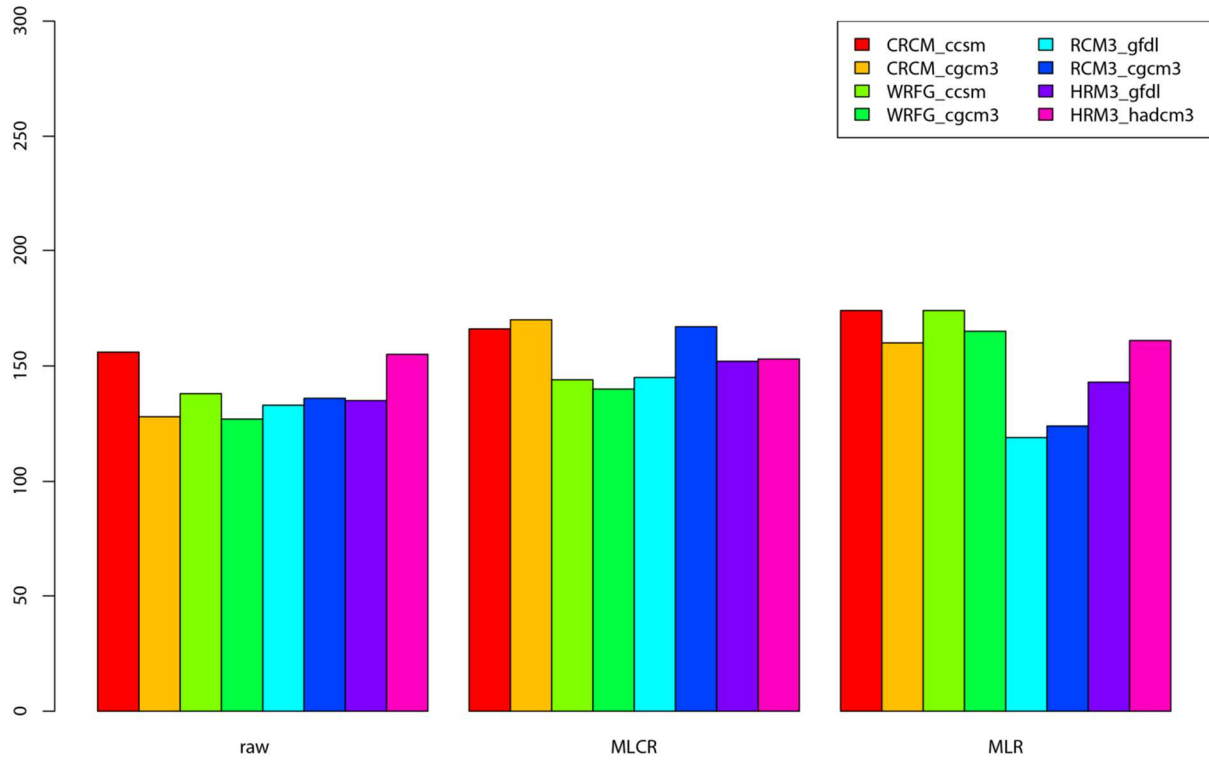


Figure 2-34. Median values of growing season length from NARCCAP raw control simulation, NARCCAP MCR projections, NARCCAP MLR projections for control period 1978-1998.

Maple City

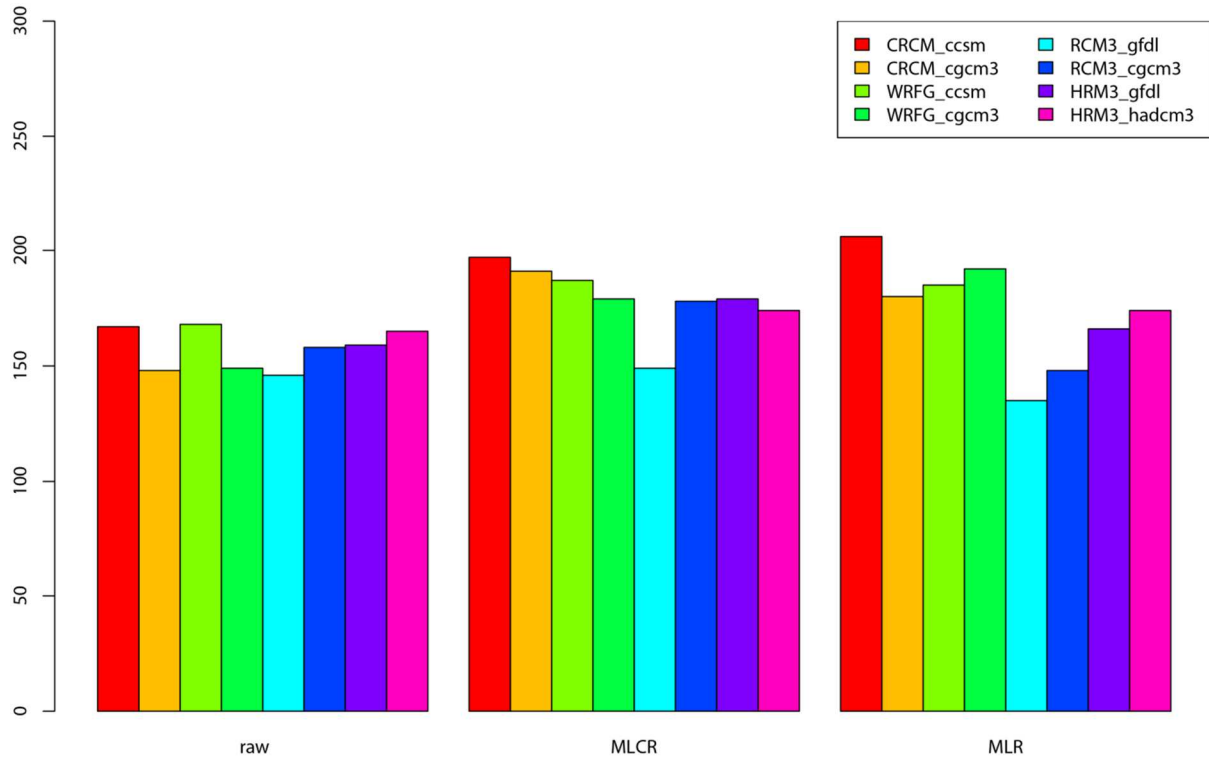


Figure 2-35. Same as Figure 2-31, but for future period of 2040-2060.

Maple City

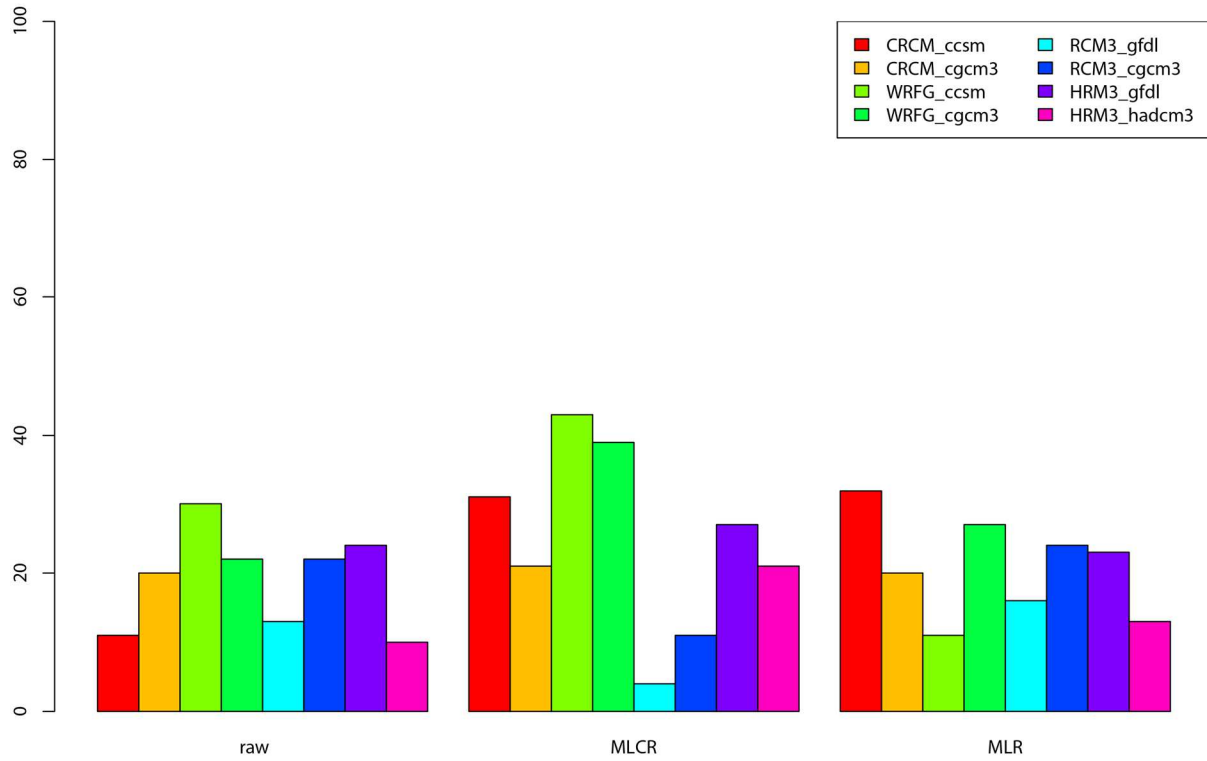


Figure 2-36. Differences of future and control period median values of growing season length from NARCCAP raw control simulation, NARCCAP MCR projections, NARCCAP MLR projections.

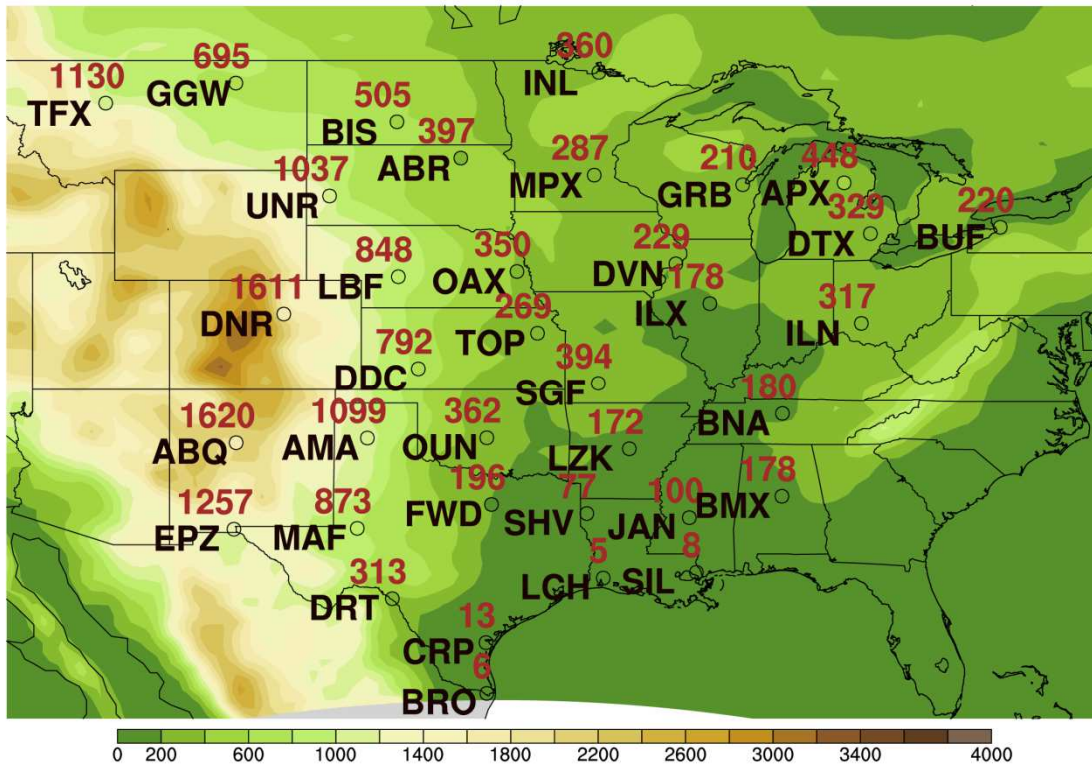


Figure 3-1. Study domain, the topography (shading) as resolved by the CRCM and the locations (circles) and evaluations (shading) of the 36 rawinsonde stations used in the study.

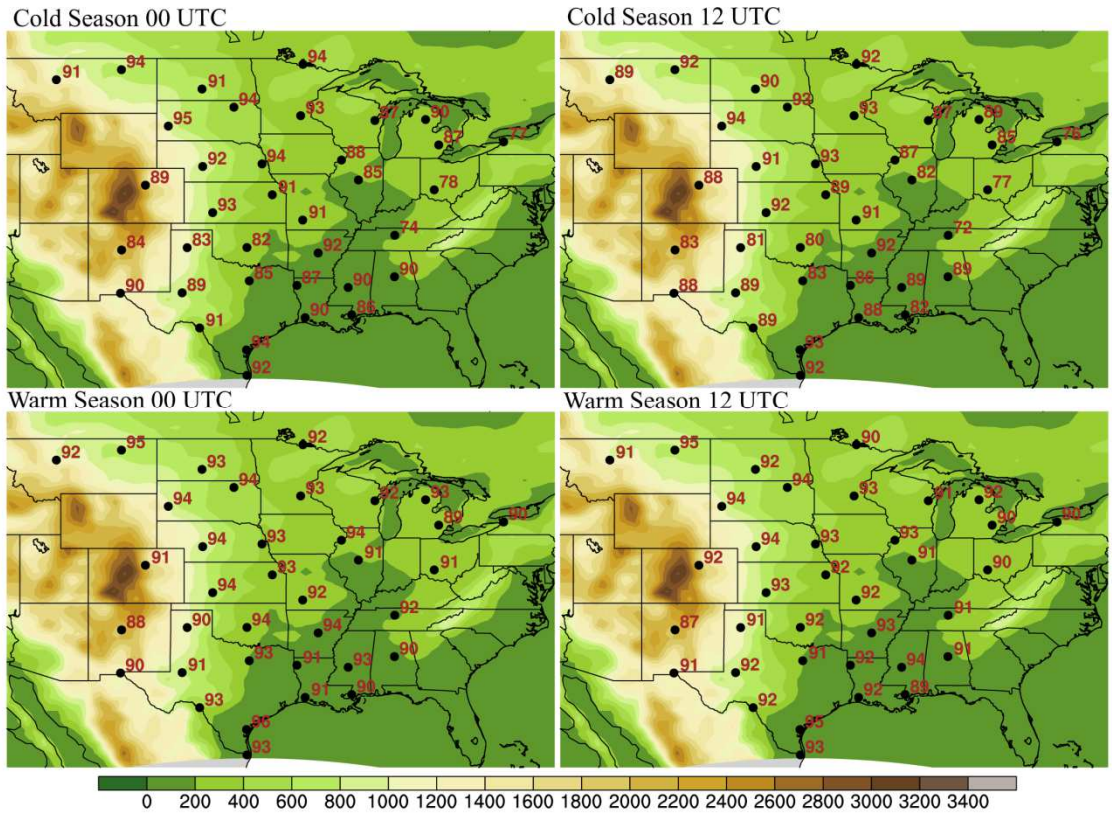


Figure 3-2. Percentage of useable soundings (numbers next to the stations) for the cold and warm seasons at 00 UTC and 12 UTC. The background shading is CRCM model elevation.

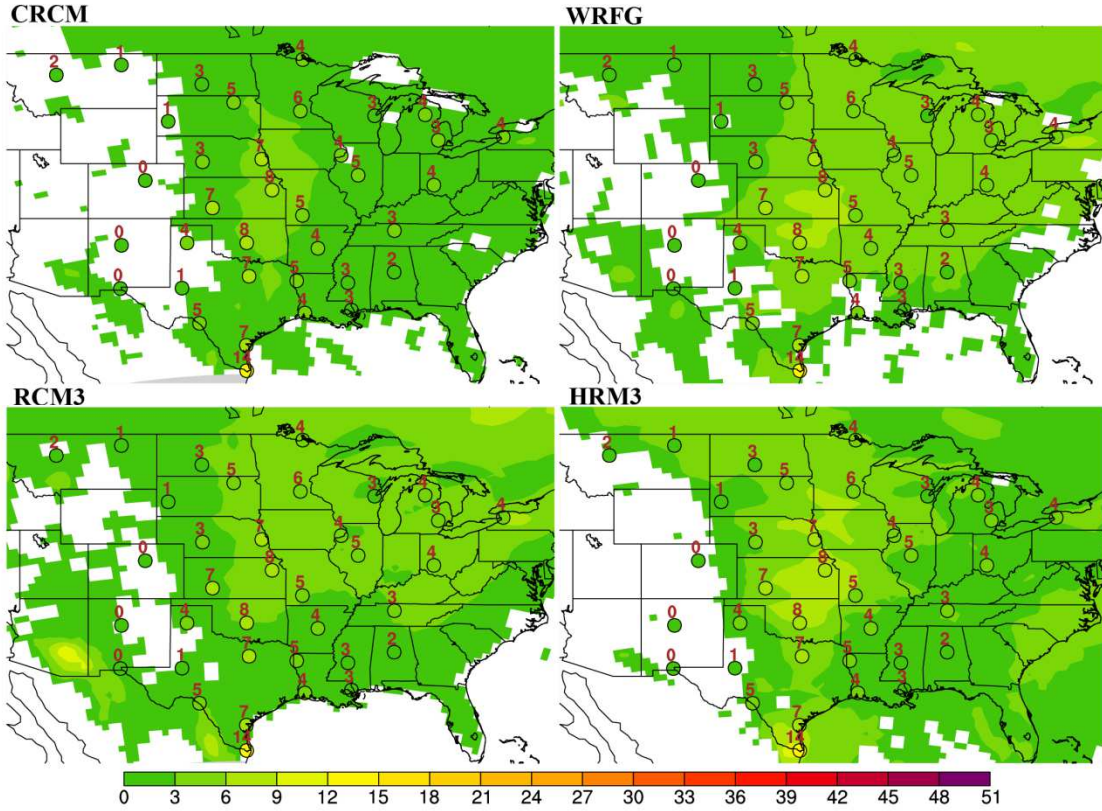


Figure 3-3. Cold-season 00 UTC RCM-simulated (shading) and rawinsonde observed (shading and number next to the station circle) jet frequency. The percentages are rounded. White regions represent places with no jet.

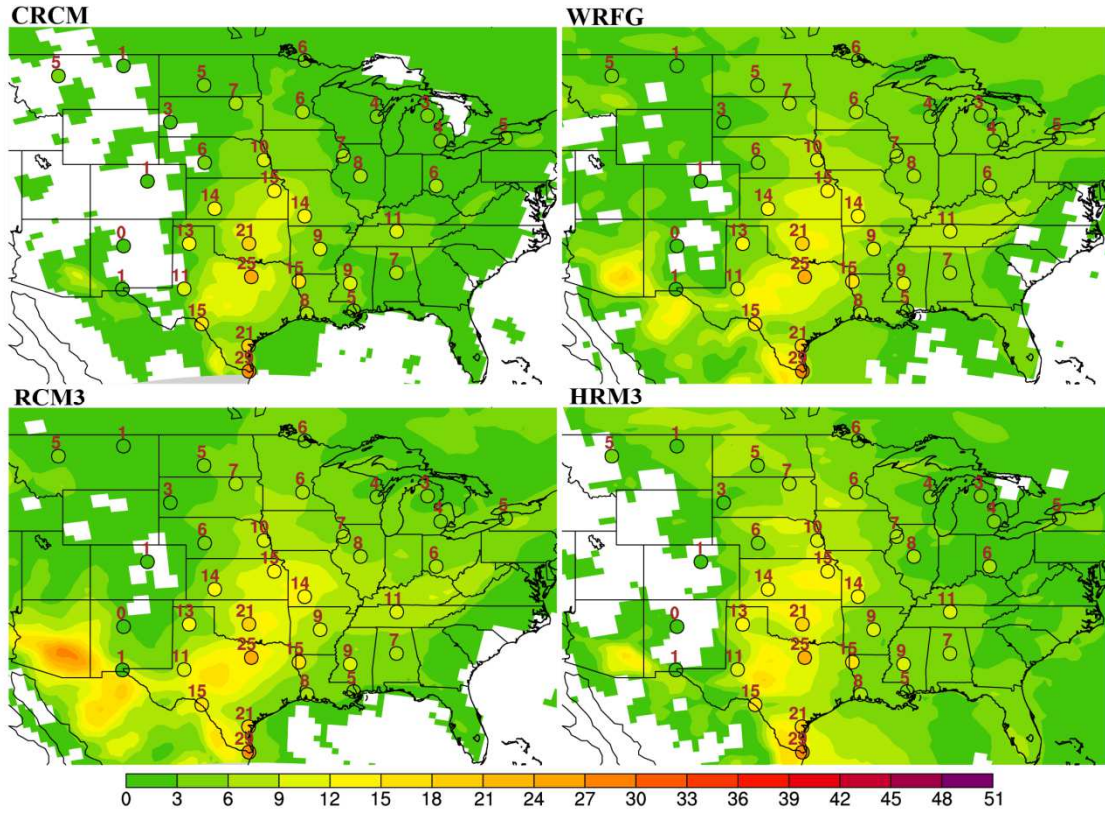


Figure 3-4. Same as Figure 3-3, but for 12 UTC

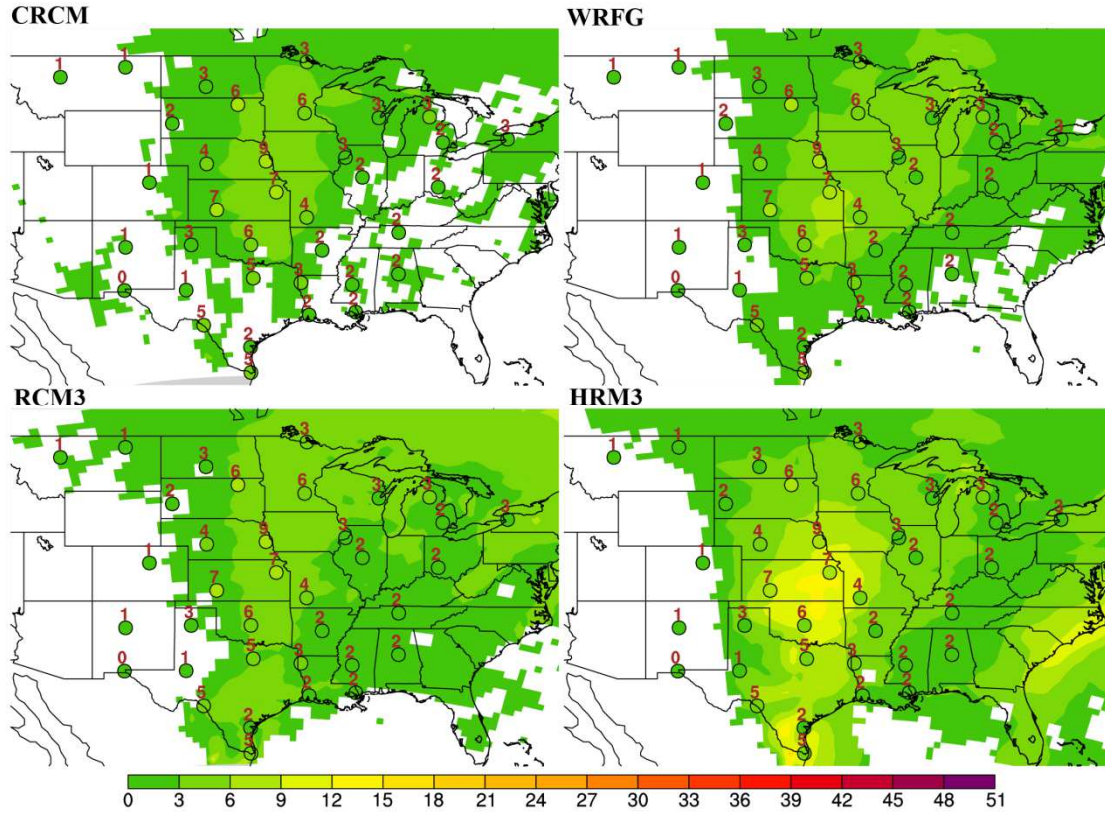


Figure 3-5. Same as Figure 3-3, but for warm season

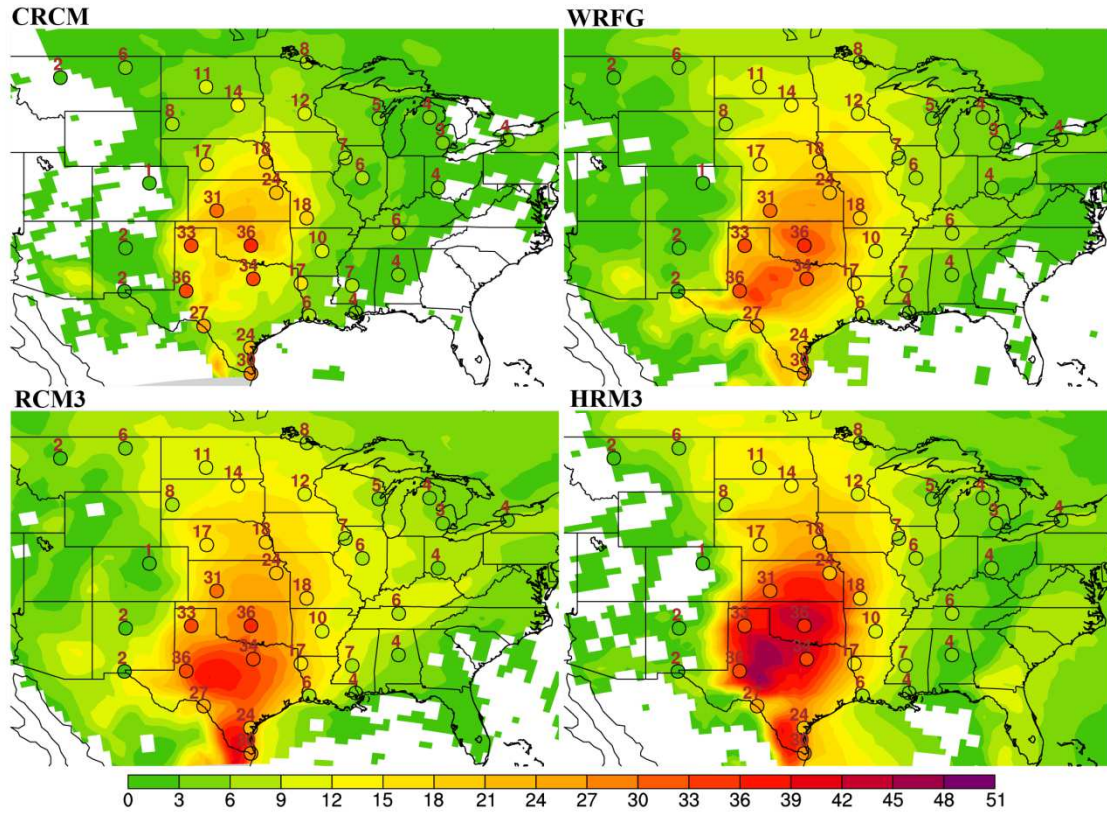


Figure 3-6. Same as Figure 3-5, but for 12 UTC

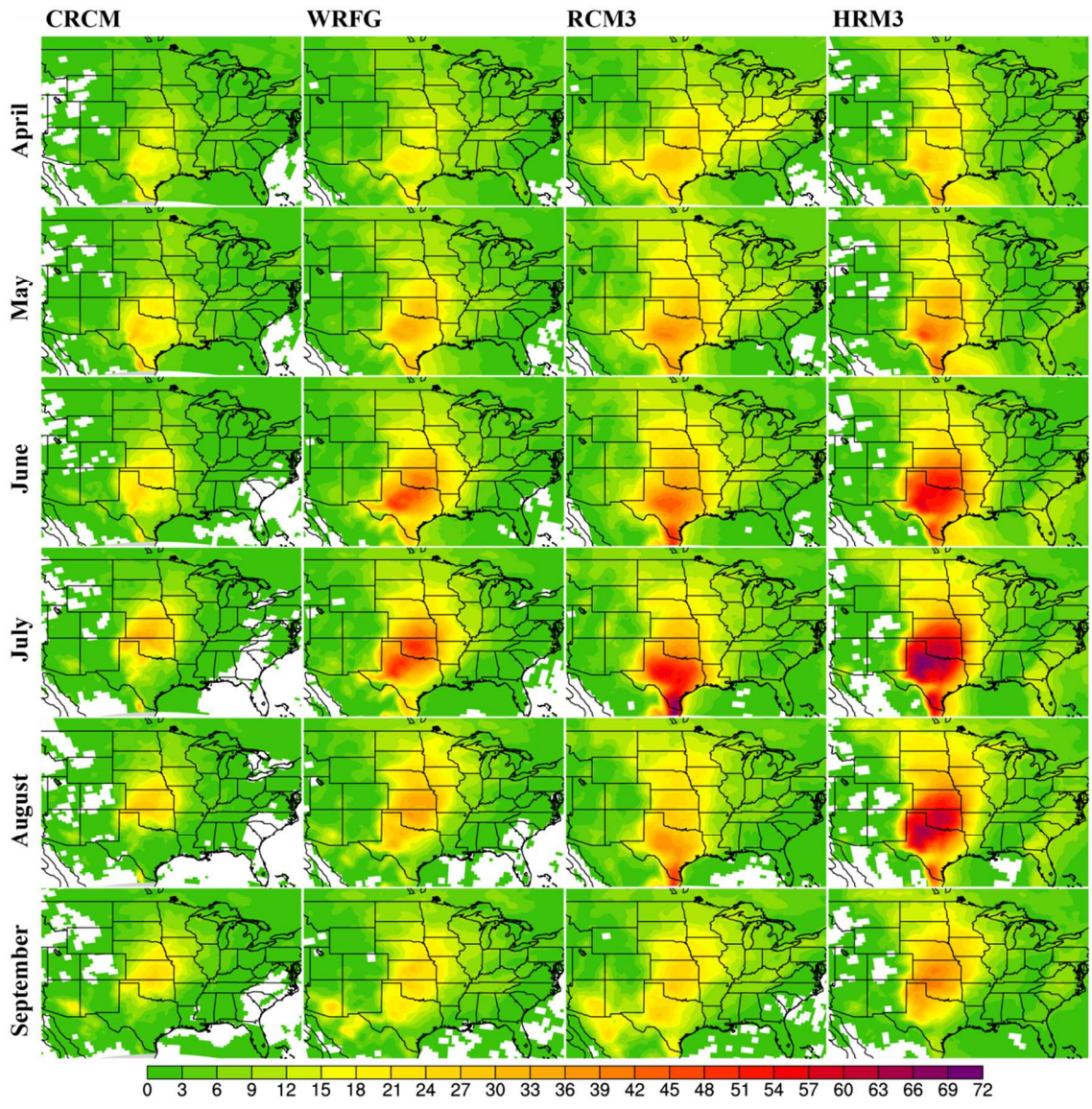


Figure 3-7. Jet frequency at 12 UTC during April to September for the four RCMs.

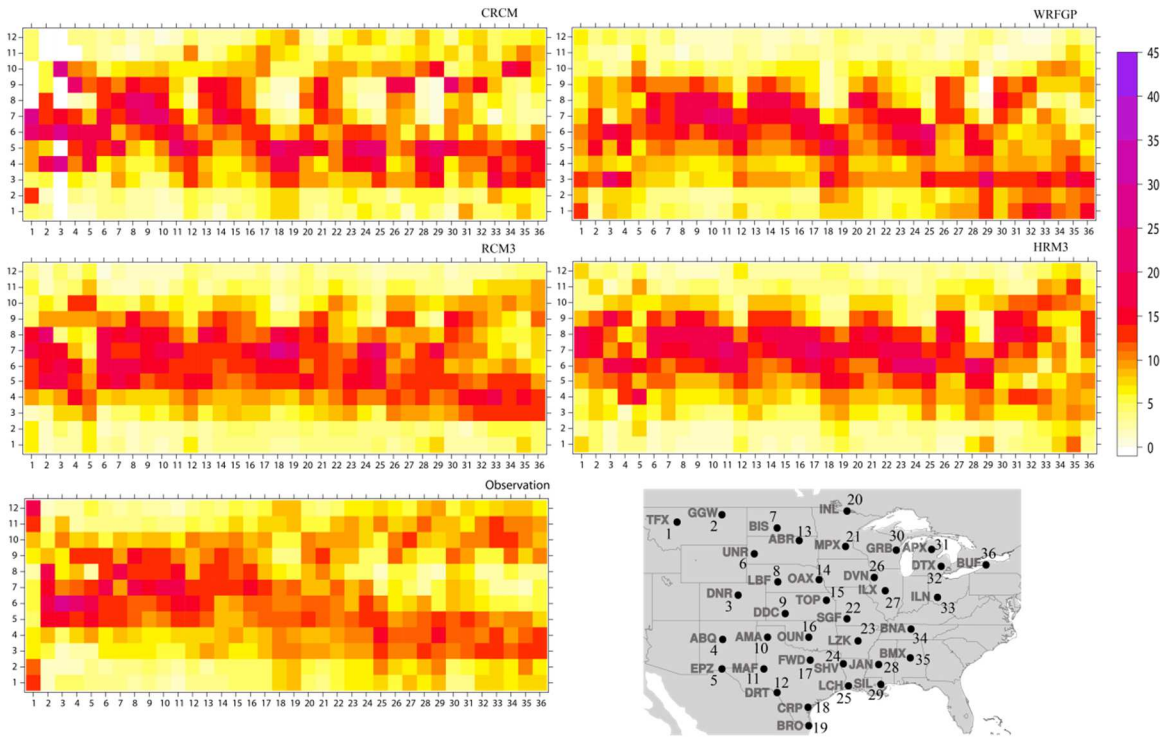


Figure 3-8. Percentage of jet number in each month of the year at each of the 36 stations. At each station, the percentages from all 12 months sum up to 100%.

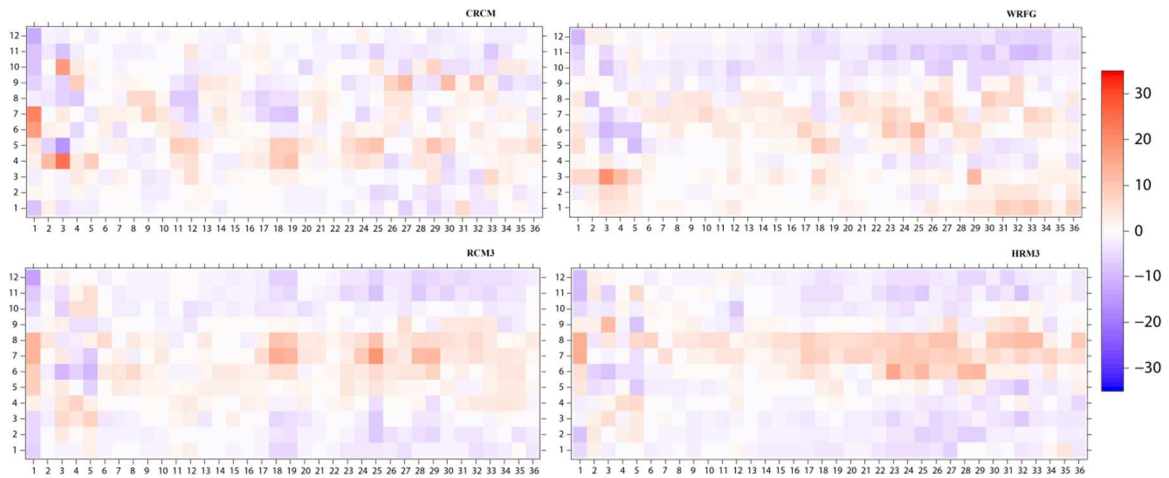


Figure 3-9. Difference of RCM simulated and observed percentage of jet number in each month of the year at each of the 36 stations.

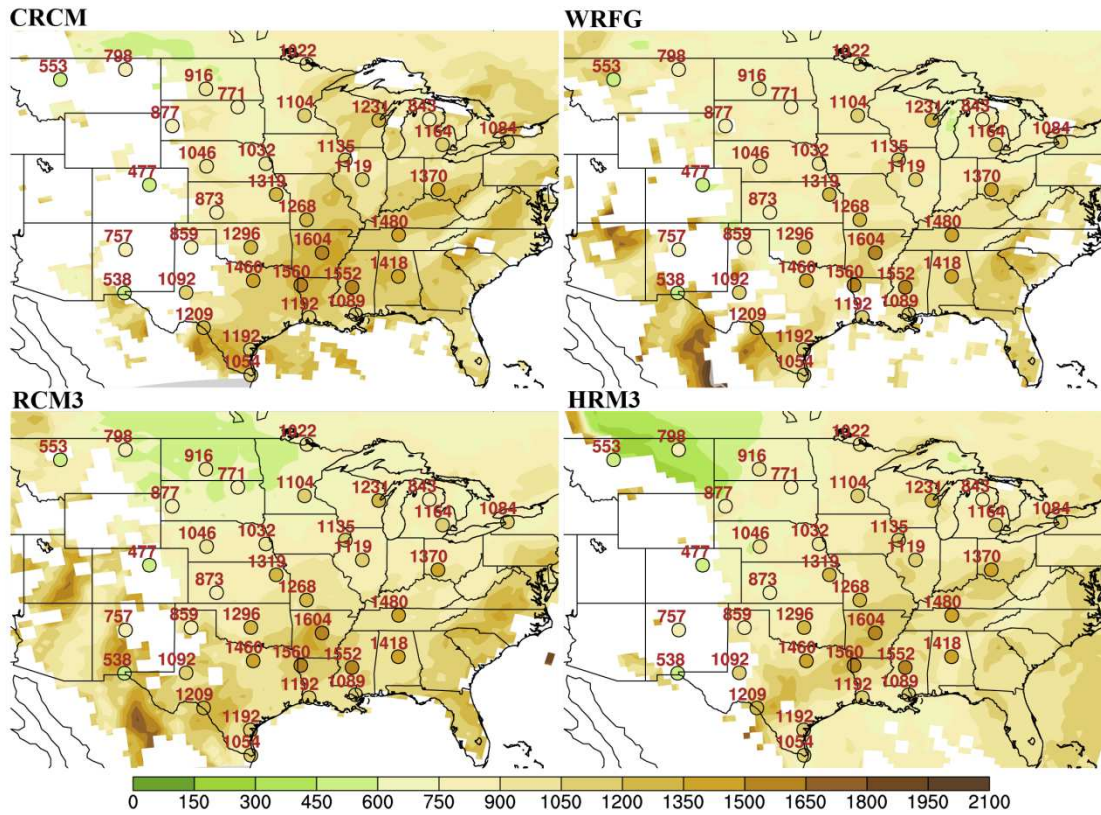


Figure 3-10. Cold-season 00 UTC RCM-simulated (shading) and rawinsonde observed (shading and number next to the station circle) jet height. Units in meters AGL.

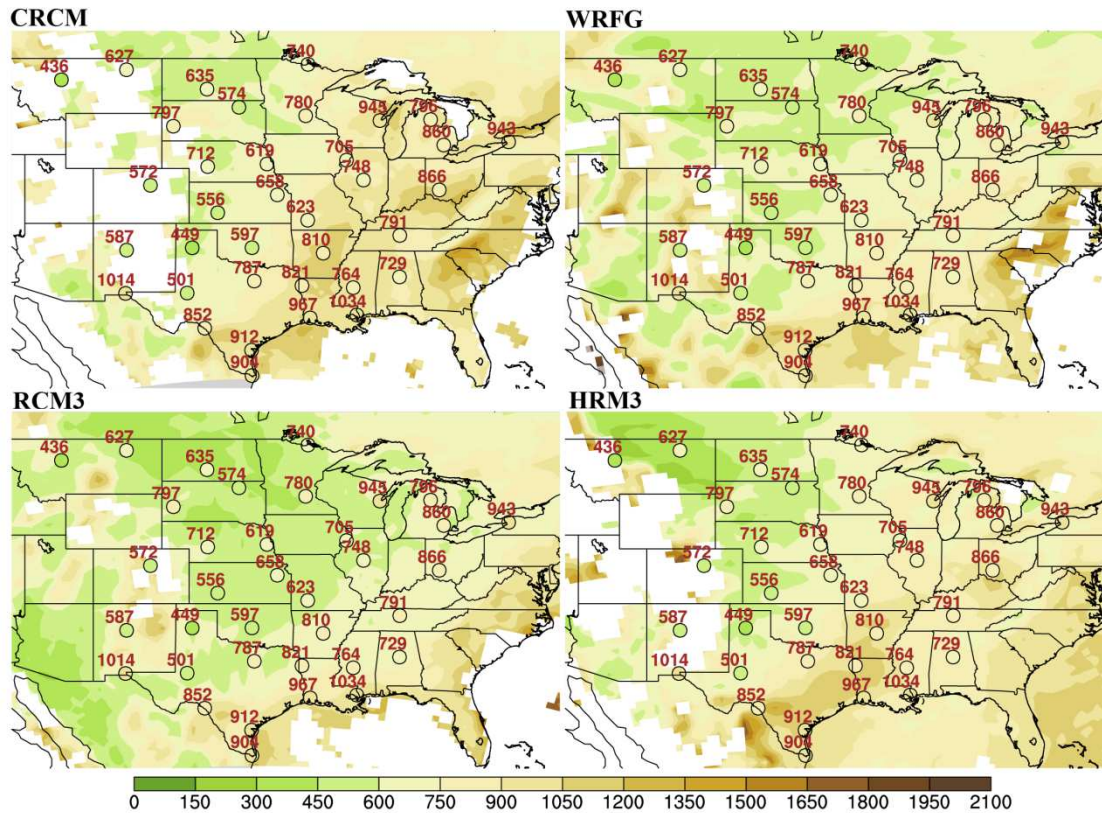


Figure 3-11. Same as Figure 3-10, but for 12 UTC

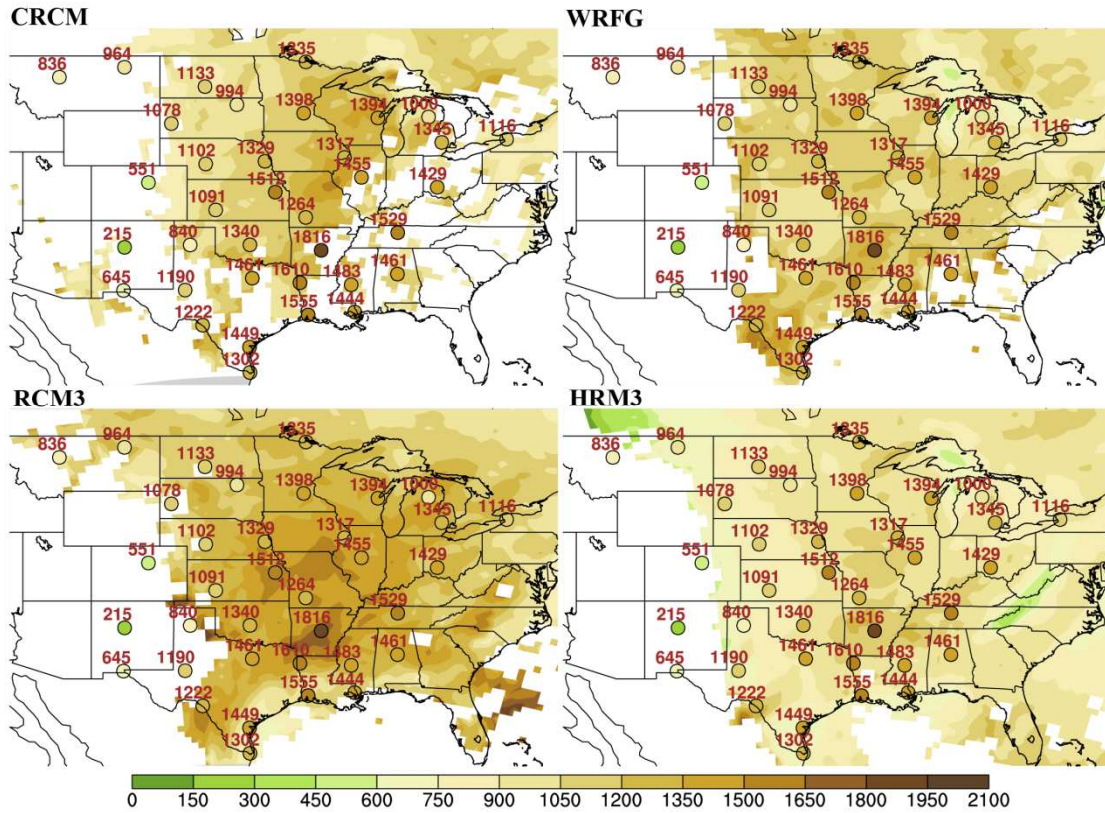


Figure 3-12. Same as Figure 3-10, but for warm season

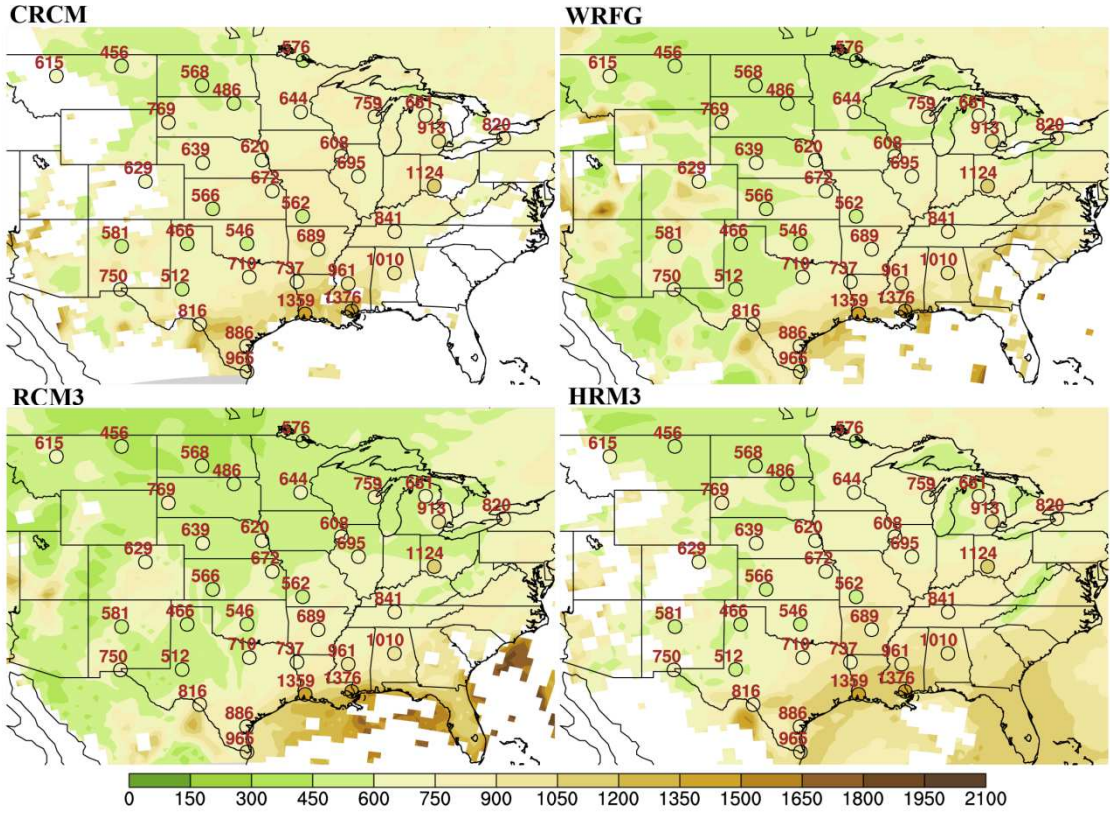


Figure 3-13. Same as Figure 3-12, but for 12 UTC

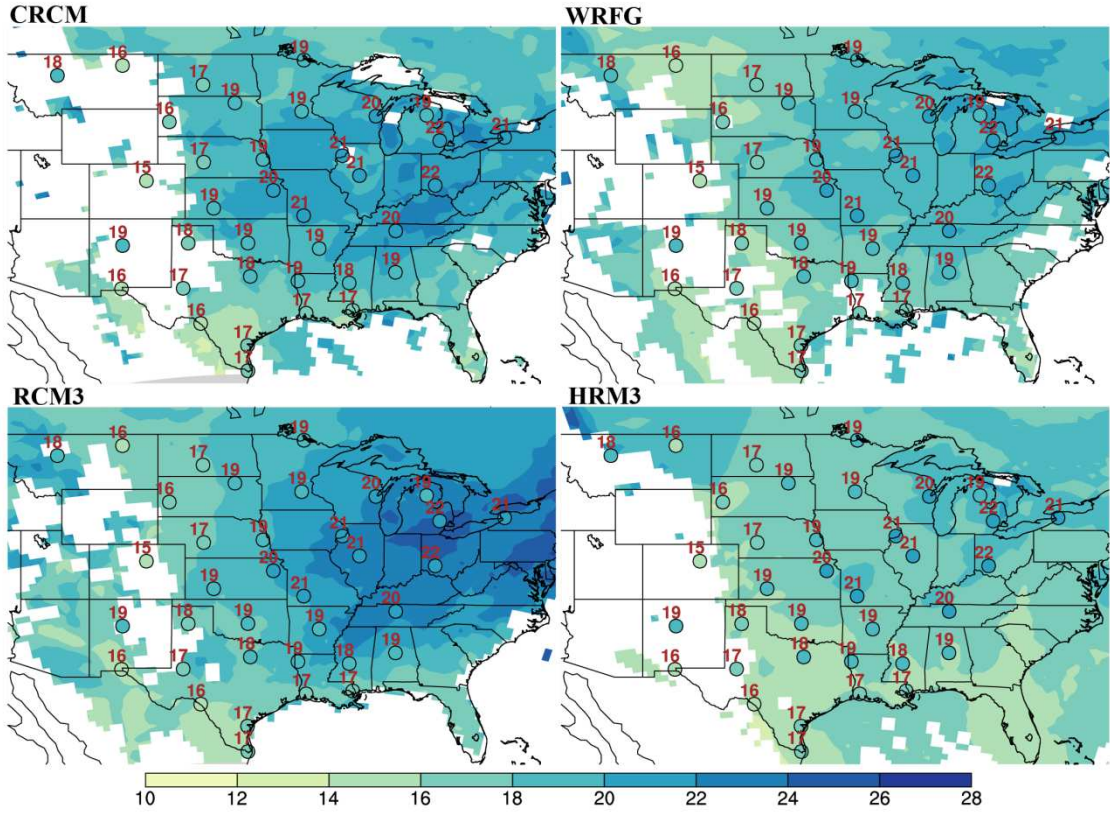


Figure 3-14. Cold-season 00 UTC RCM-simulated (shading) and rawinsonde observed (shading and number next to the station circle) jet speed. Units in ms^{-1} .

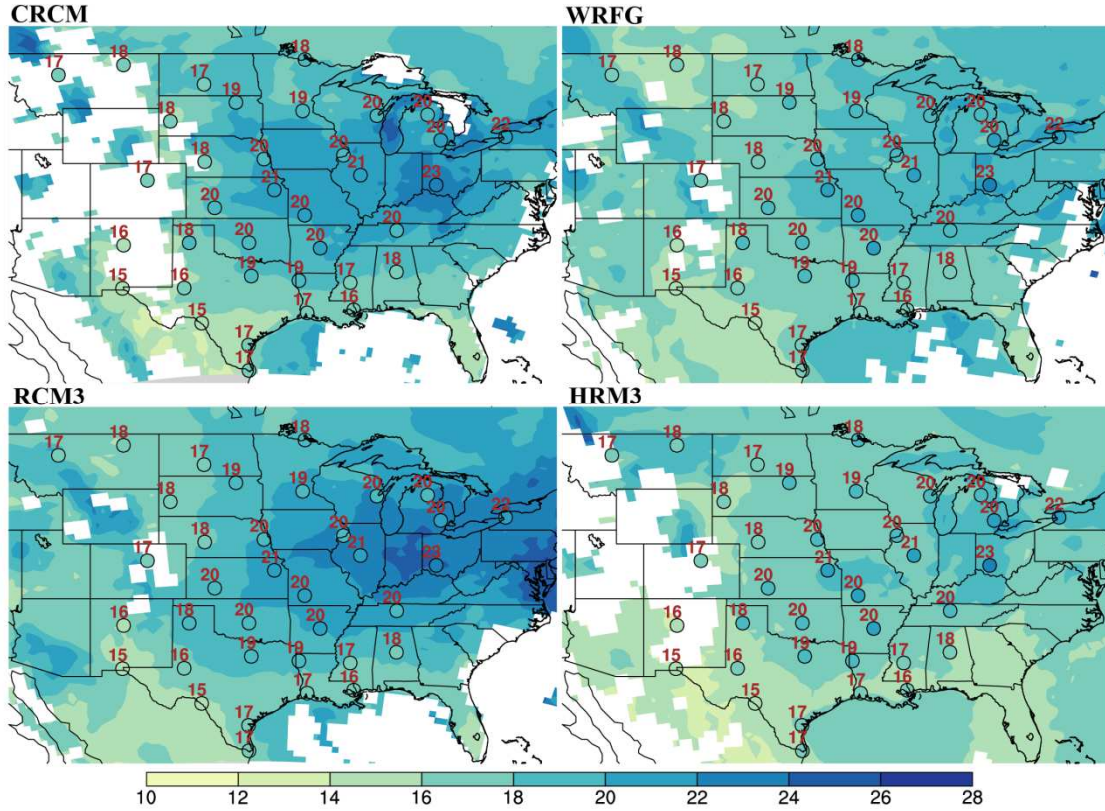


Figure 3-15. Same as Figure 3-14, but for 12 UTC

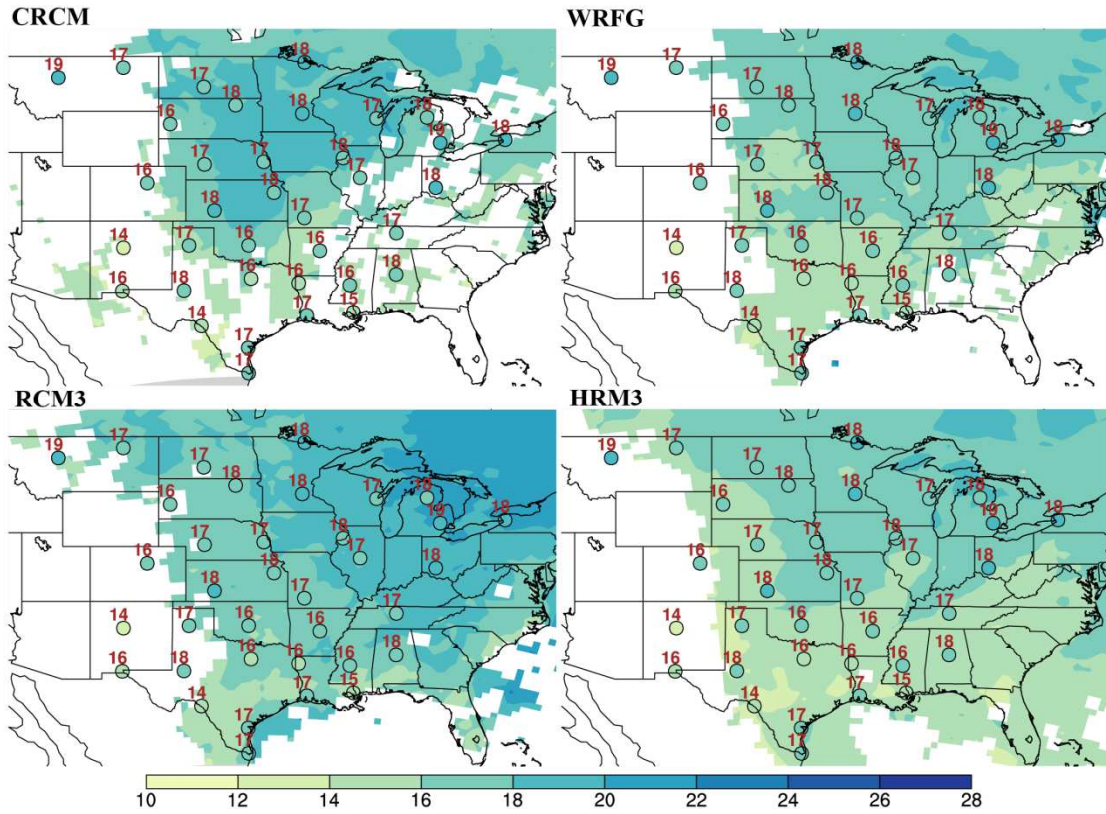


Figure 3-16. Same as Figure 3-14, but warm season

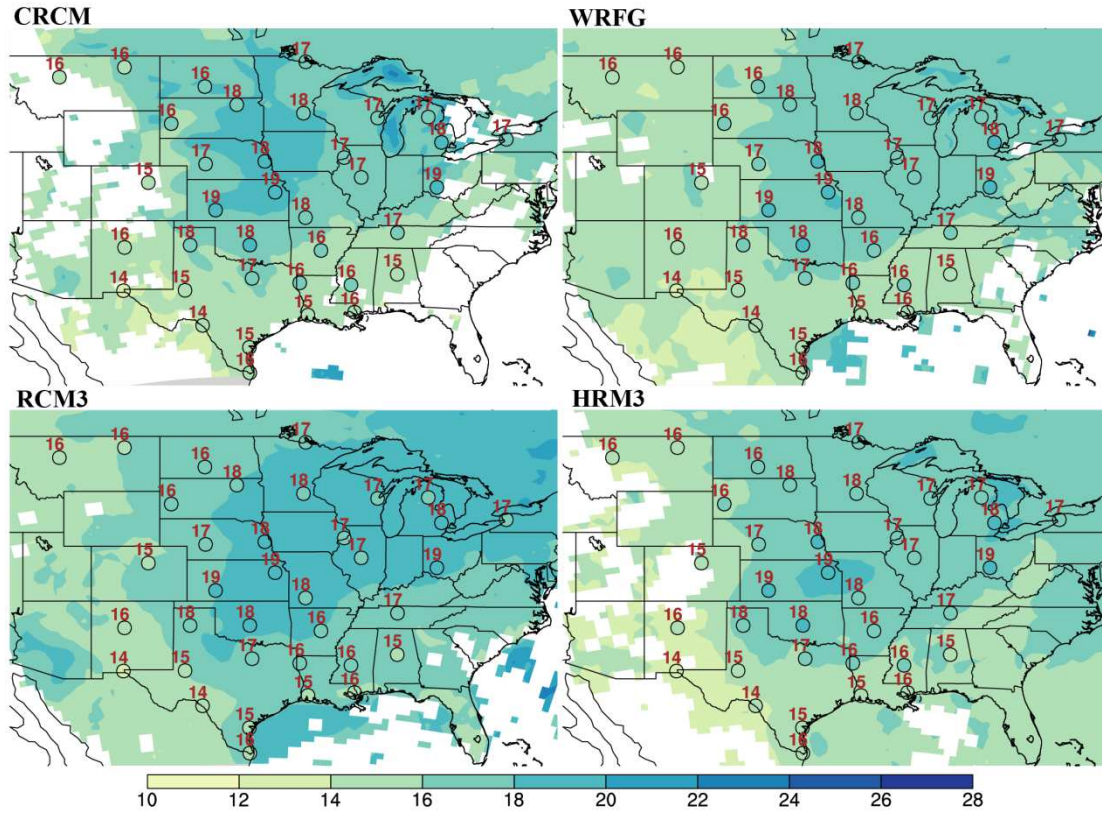


Figure 3-17. Same as Figure 3-16, but for 12 UTC

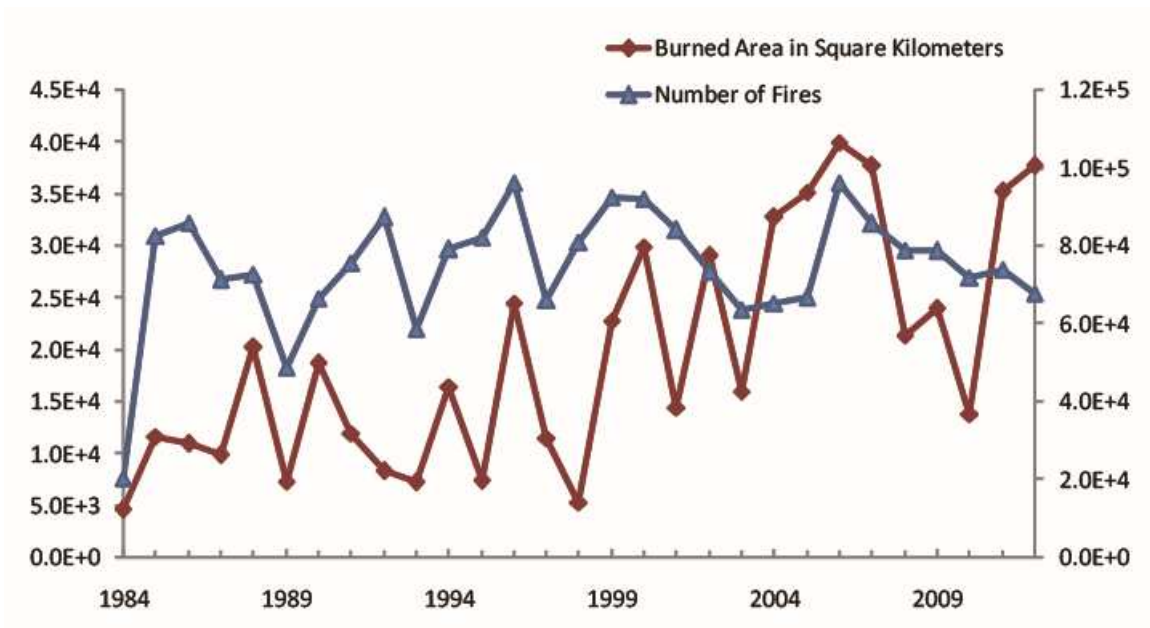


Figure 4-1. Burned area (left axis) and number of wildland fires (right axis) in United States from 1984 to 2012 (NIFC). The National Interagency Coordination Center at NIFC compiles annual wildland fire statistics for federal and state agencies. 2004 fires and acres do not include state lands for North Carolina.

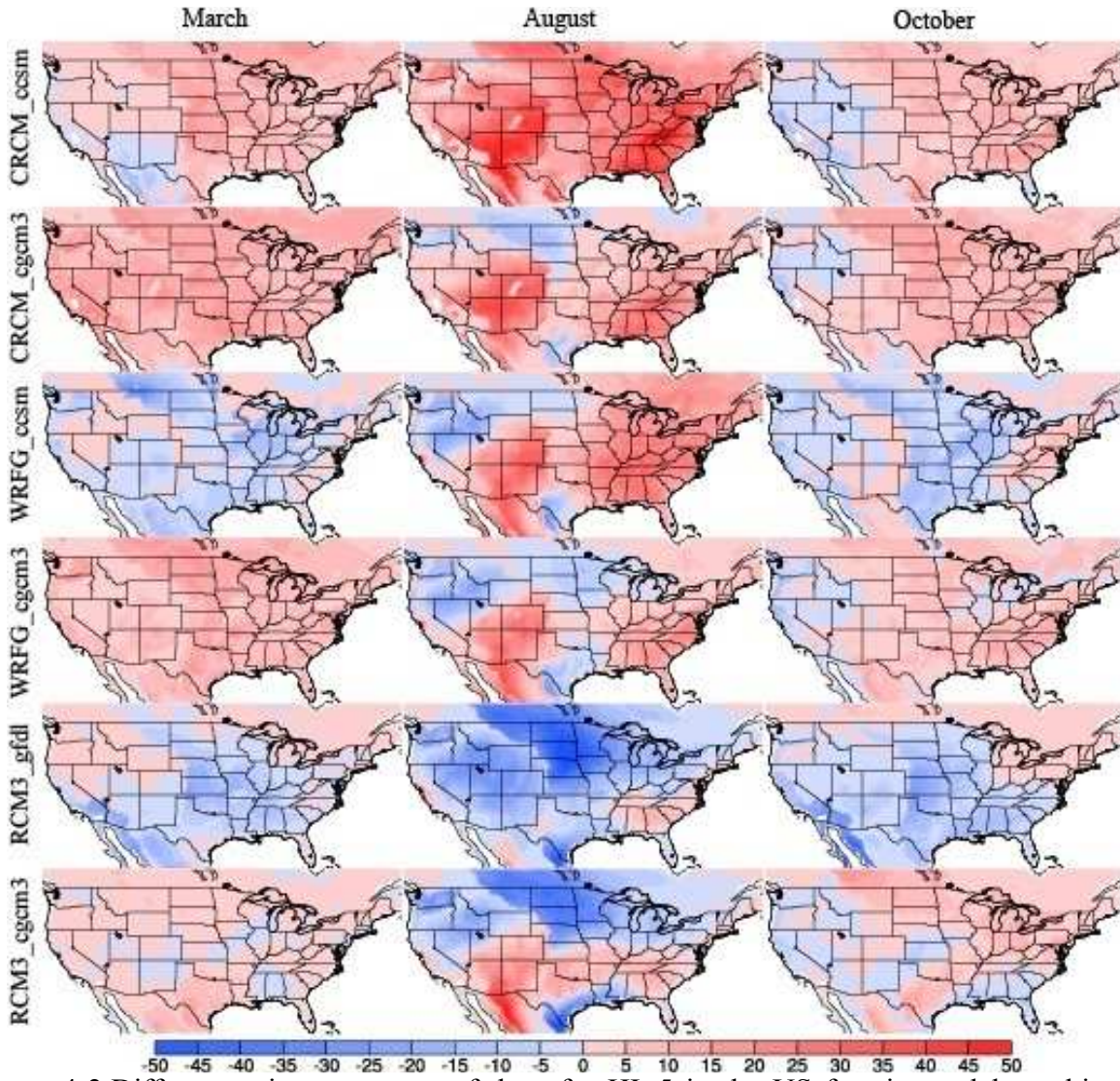


Figure 4-2. Differences in percentage of days for $HI \geq 5$ in the US for six model combinations between current and NCEP climate for March (left column), August (center column) and October (right column).

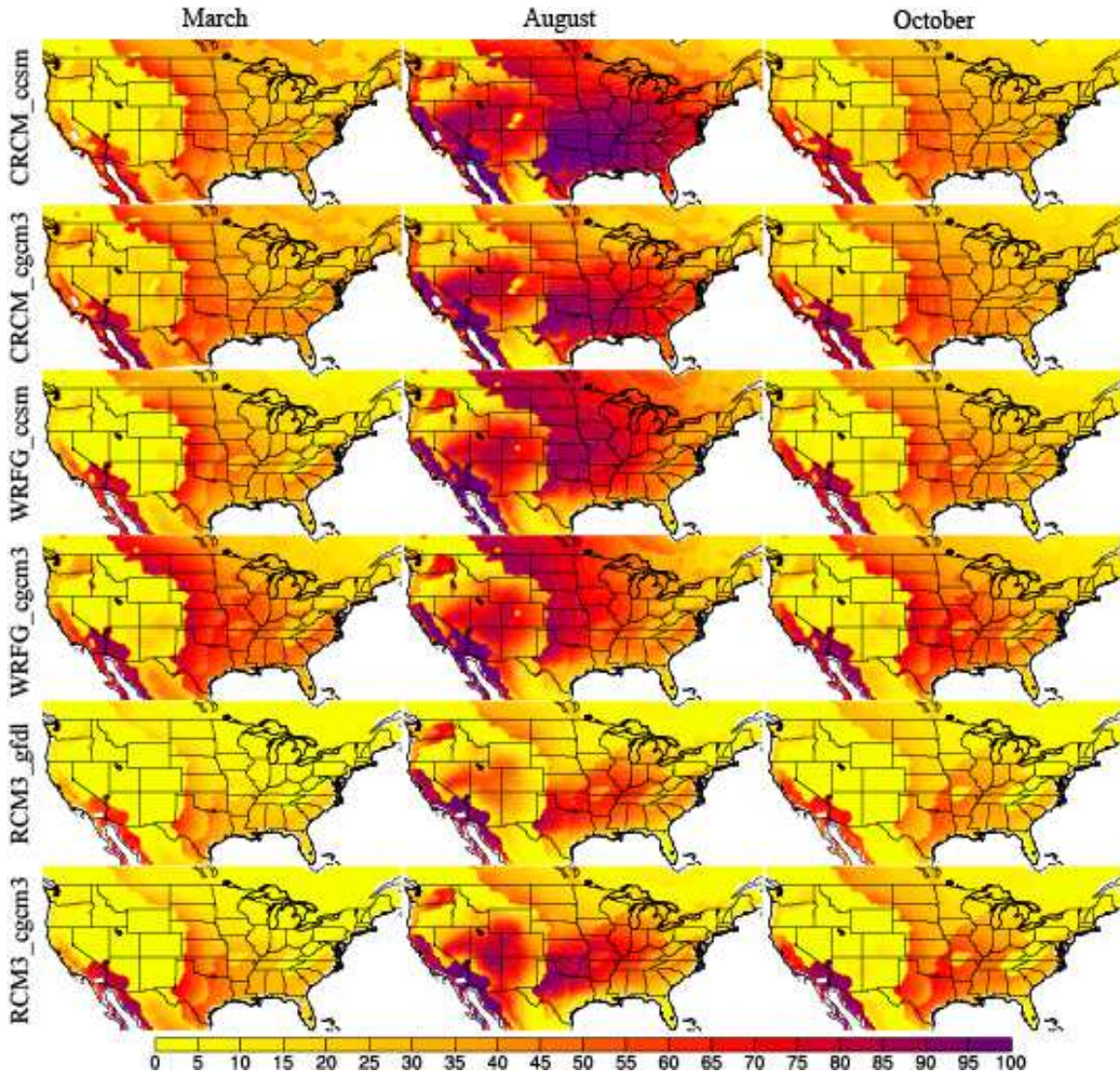


Figure 4-3. Percentage of days for $HI \geq 5$ in the US for six model combinations under current climate for March (left column), August (center column) and October (right column).

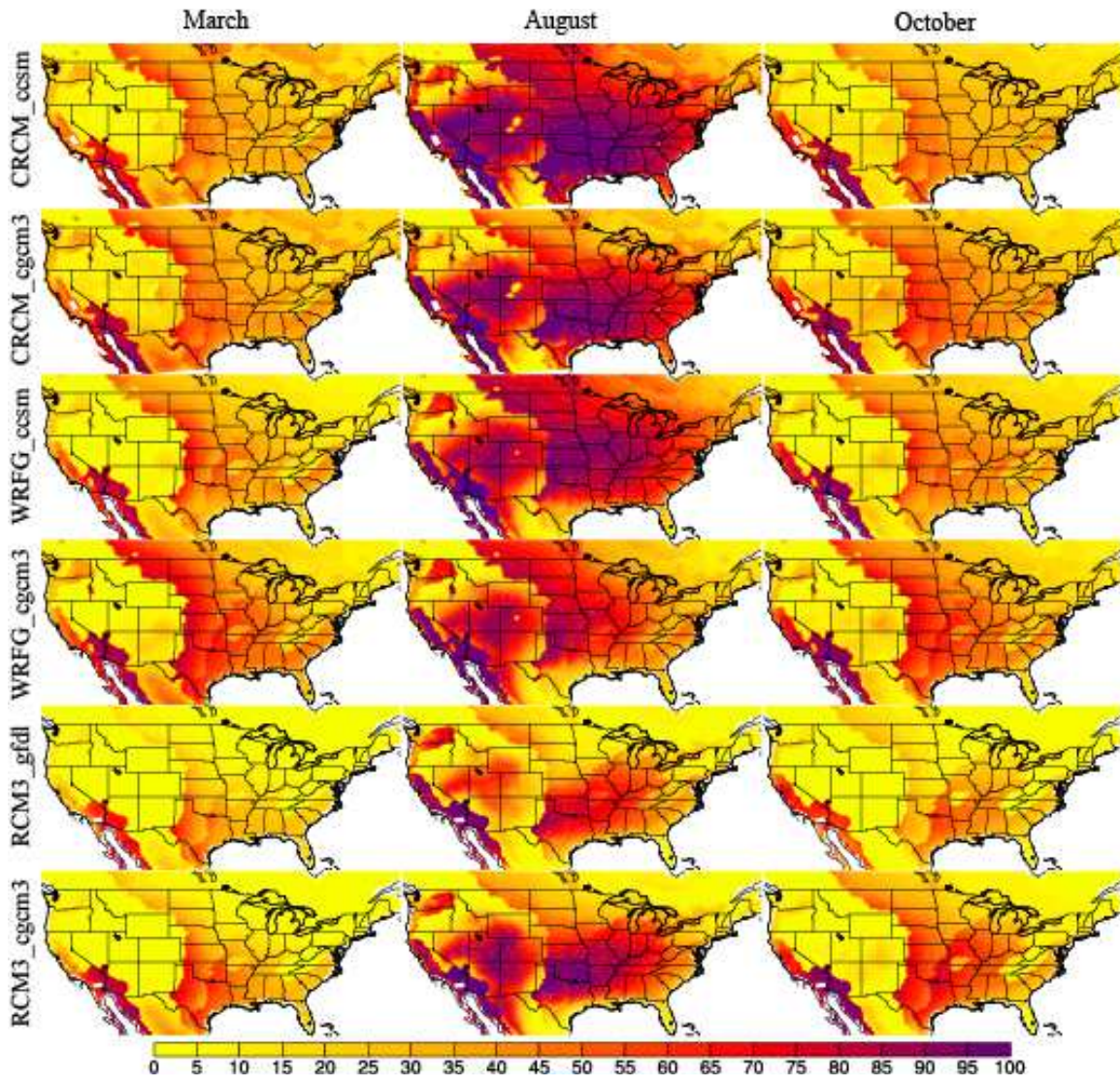


Figure 4-4. Percentage of days for $HI \geq 5$ in the US for six model combinations under future climate for March (left column), August (center column) and October (right column).

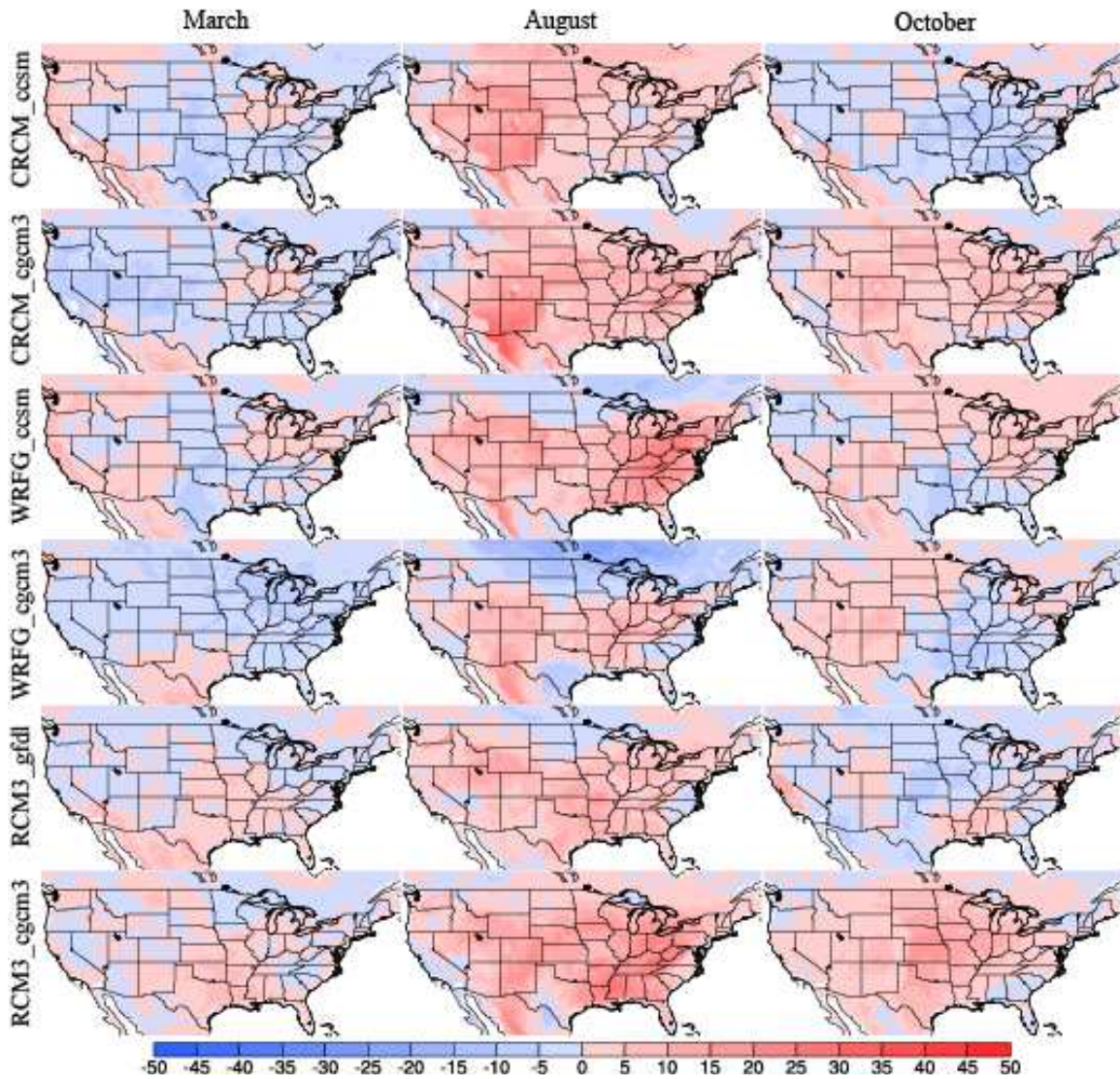


Figure 4-5. Change in percentage of days for $HI \geq 5$ in the US for six model combinations between current and future climate for March (left column), August (center column) and October (right column).

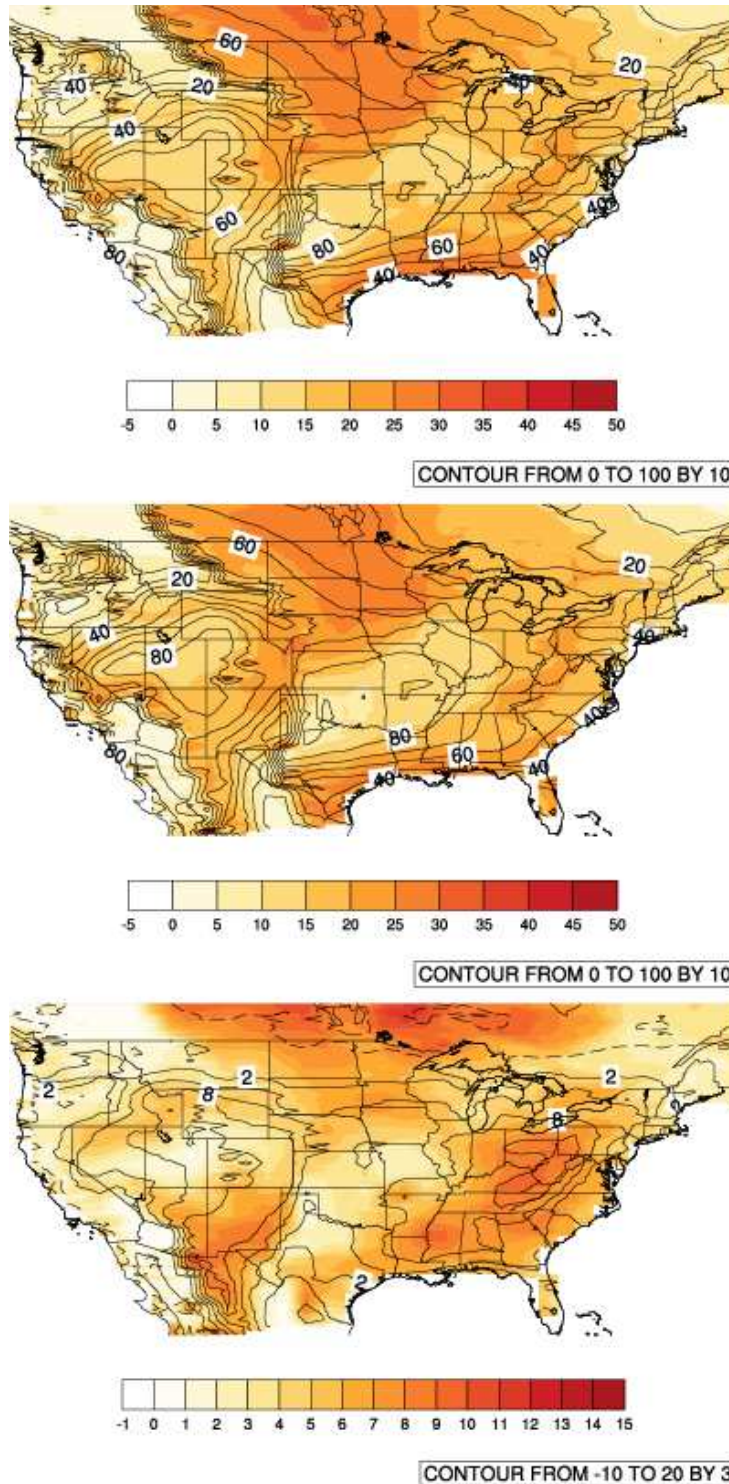


Figure 4-6. Mean (contour) and standard deviation (shading) of percentage of days for $HI \geq 5$ in the US for six model combinations for current climate (upper), future climate (center), and difference between current and future climate (lower) during August. The mean is contoured from 0 to 100 by 10 intervals for current (upper) and future (center) climate and from -10 to 20 by 3 intervals for the change between current and future climate (lower). The standard deviation is colored from -5 to 50 by 5 intervals for current (upper) and future (center) climate, and from -1

to 15 by 1 intervals for the change between current and future climate (lower).

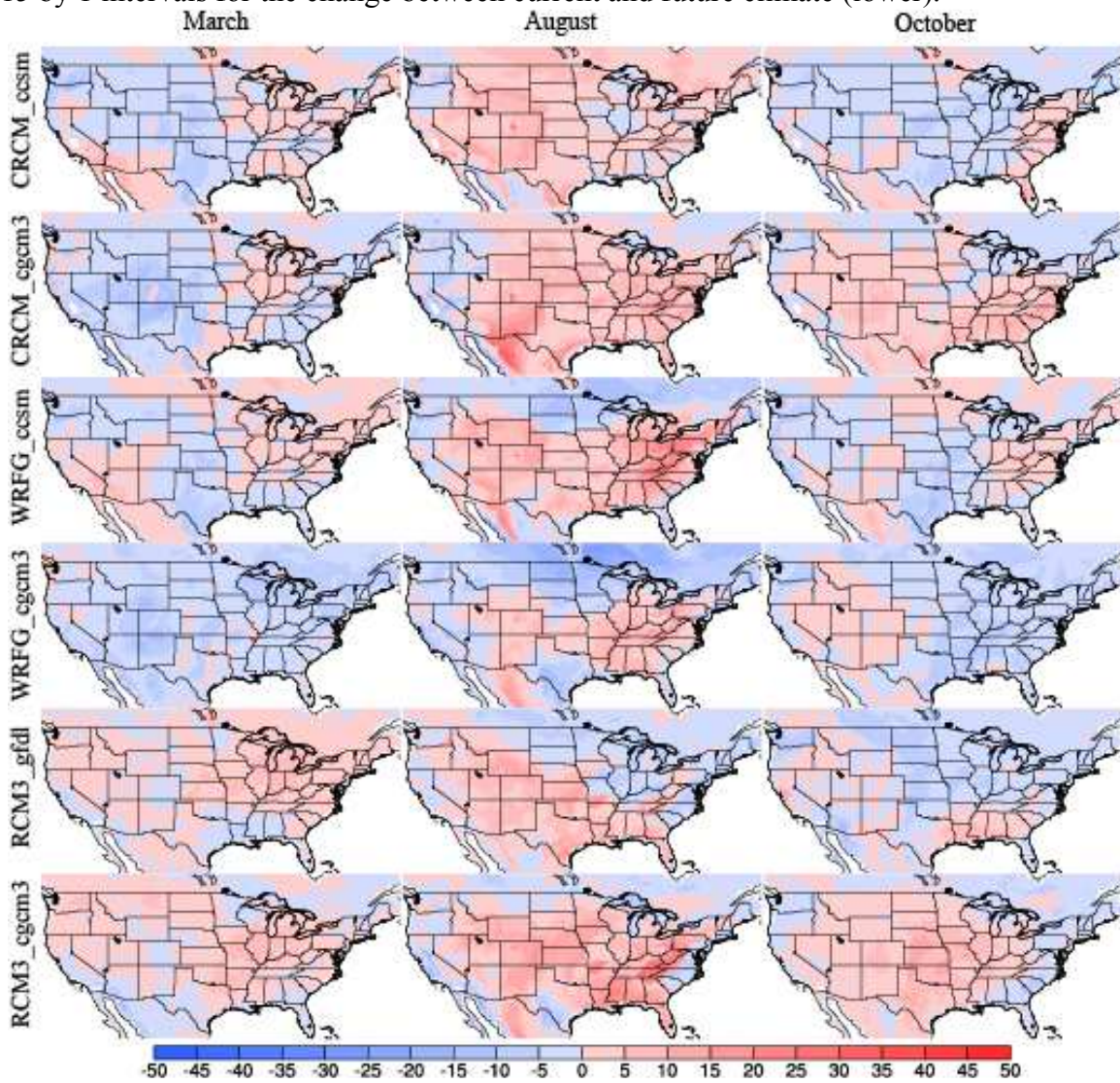


Figure 4-7. Change in percentage of days for A=3 in the US for six model combinations between current and future climate for March (left column), August (center column) and October (right column).

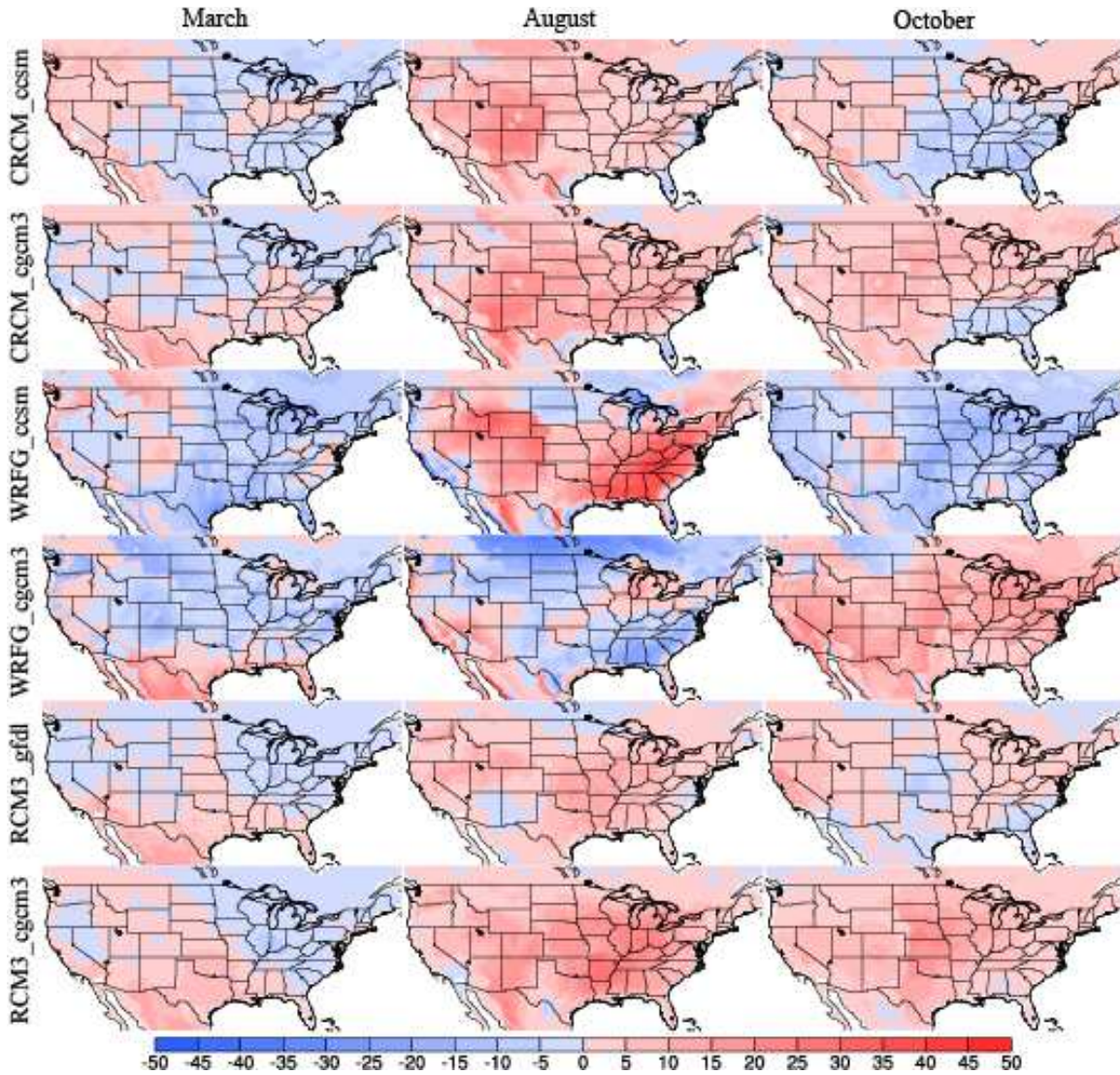


Figure 4-8. Change in percentage of days for B=3 in the US for six model combinations between current and future climate for March (left column), August (center column) and October (right column).

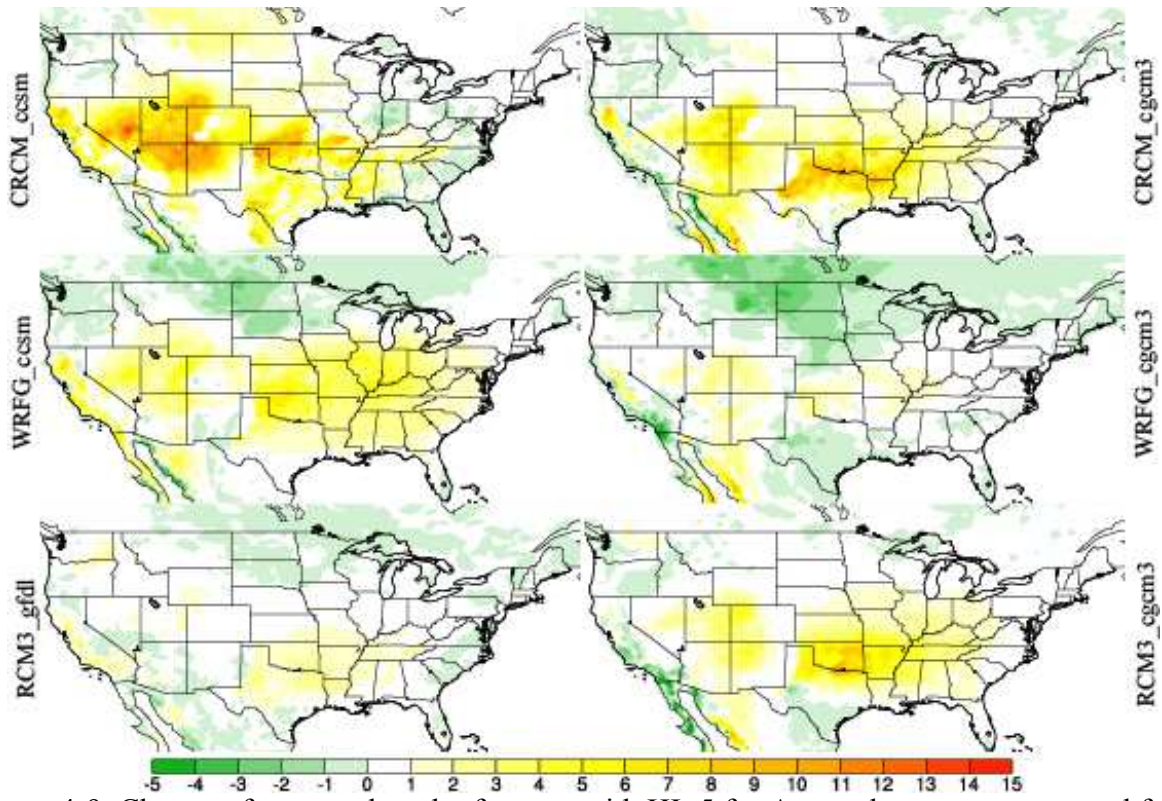
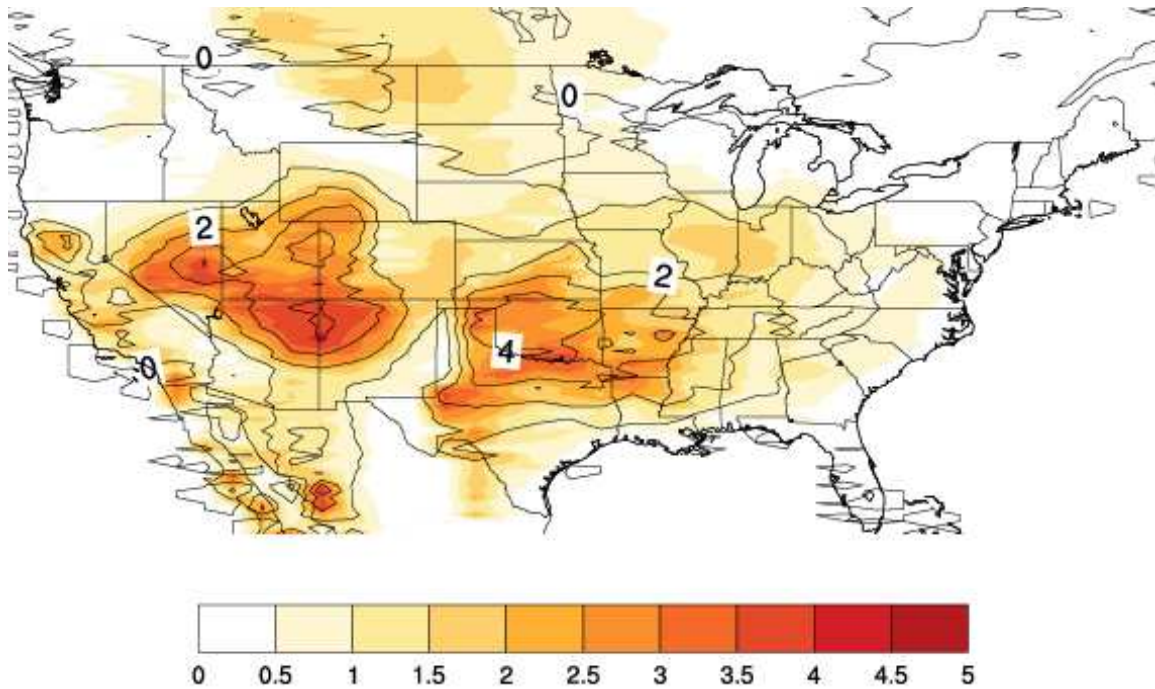


Figure 4-9. Change of average length of events with $HI \geq 5$ for August between current and future climate.



CONTOUR FROM -2 TO 5 BY 1

Figure 4-10. Mean (contour) and standard deviation (shading) of change of average length of events with $HI \geq 5$ for August between current and future climate for six model combinations. The mean is contoured from -2 to 5 by 1 intervals. The standard deviation is shaded from 0 to 5 by 0.5 intervals.

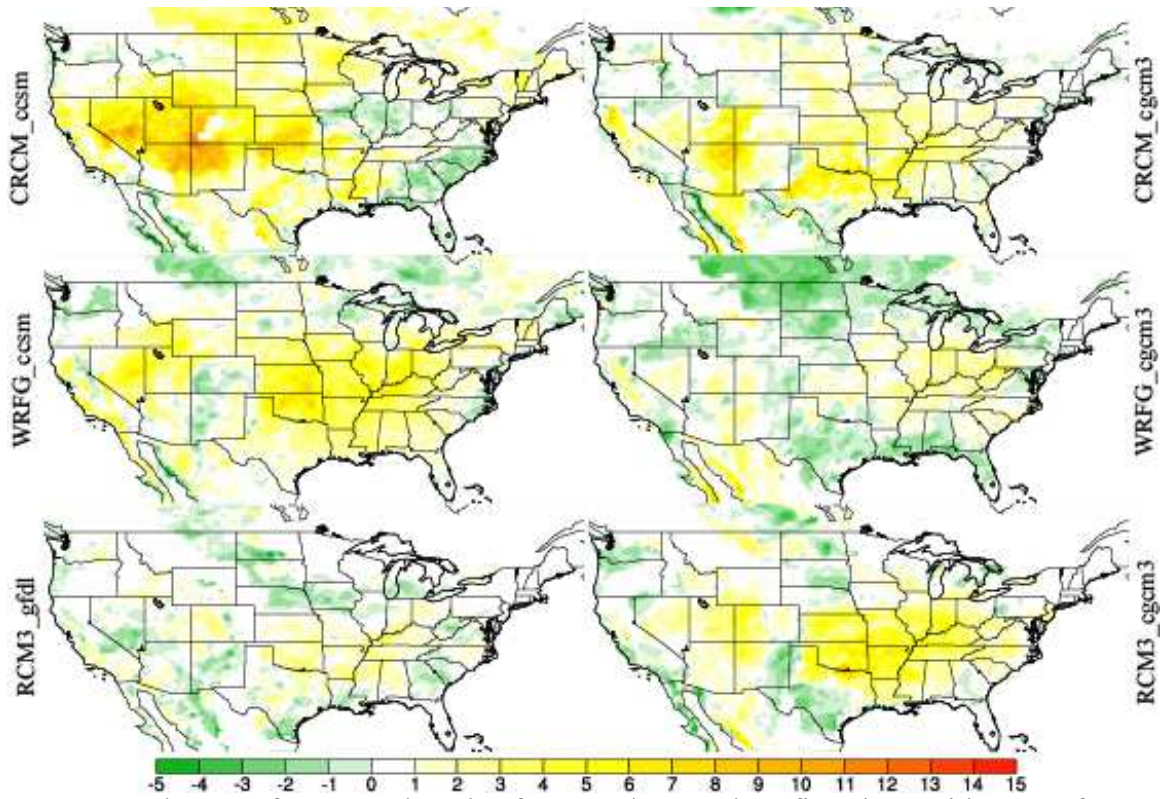


Figure 4-11. Change of average length of events longer than five days with $HI \geq 5$ for August between current and future climate.

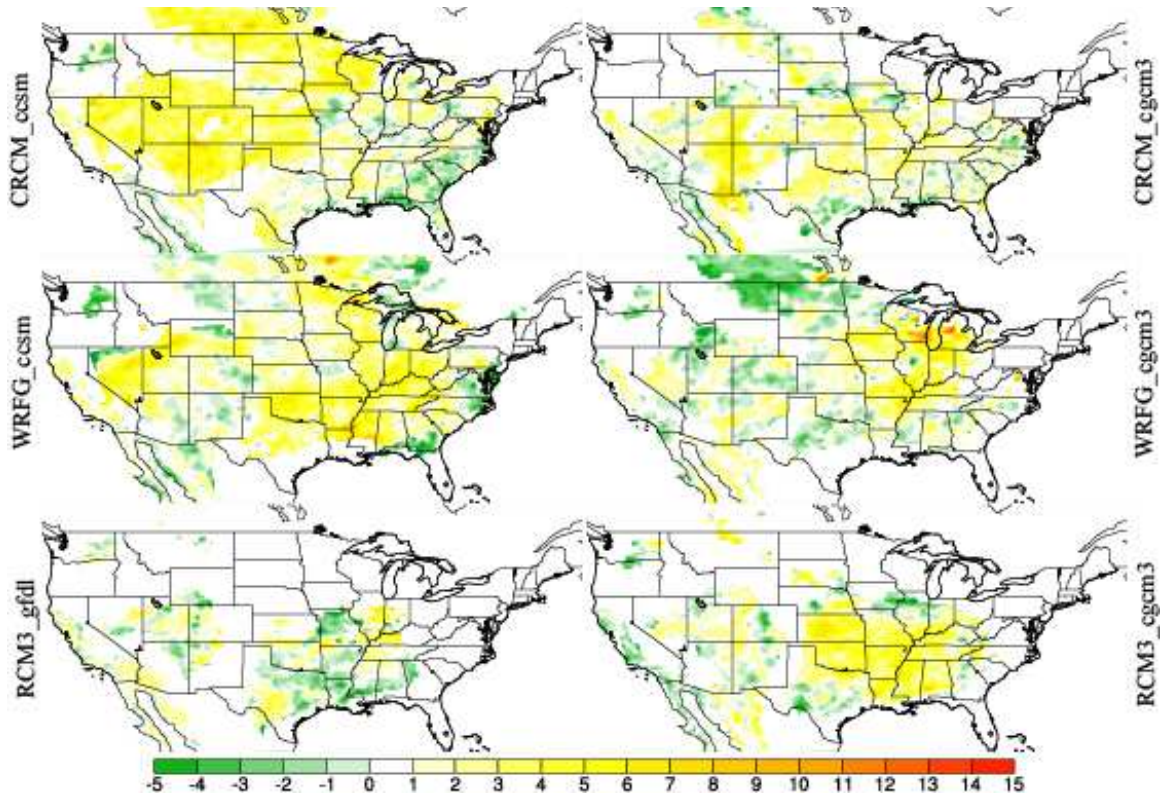


Figure 4-12. Change of average length of events longer than thirteen days with $HI \geq 5$ for August between current and future climate.

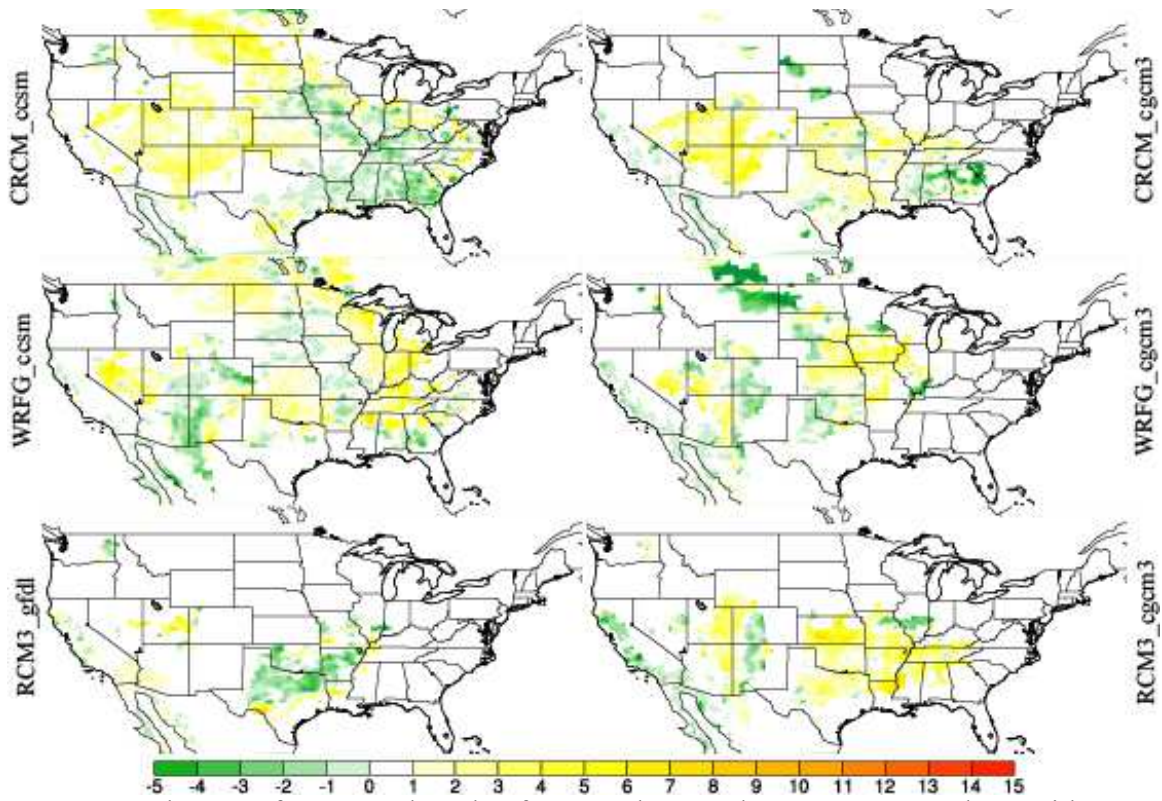


Figure 4-13. Change of average length of events longer than twenty-one days with $HI \geq 5$ for August between current and future climate.

REFERENCES

REFERENCES

- Abraham, Z., M. Liszewska, Perdinan, P.-N. Tan, J. A. Winkler, and S. Zhong. 2013. Distribution Regularized Regression Framework for Climate Modeling. *SDM*: 333-341.
- Anderson, C. J., and R. W. Arritt. 1998. Mesoscale convective complexes and persistent elongated convective systems over the United States during 1992 and 1993. *Monthly Weather Review* 126: 578–599.
- Arritt, R. W., T. D. Rink, M. Segal, and D. P. Todey. 1997. The Great Plains low-level jet during the warm season of 1993. *Monthly Weather Review* 125: 2176-2193.
- Asseng S., F. Ewert, C. Rosenzweig, et al. 2013. Uncertainty in simulating wheat yields under climate change. *Nature Climate Change* 3: 827-832.
- Banta R. M., R. K. Newsom, J. K. Lundquist, Y. L. Pichugina, R. L. Coulter, and L. Mahrt. 2002. Nocturnal low-level jet characteristics over Kansas during CASES-99. *Boundary-Layer Meteorology* 105: 221-252. doi: 10.1023/A:1019992330866.
- Baskerville, G. L. and P. Emin. 1969. Rapid estimation of heat unit accumulation from maximum and minimum temperatures. *Ecology* 50:514-517.
- Blackadar A. K.. 1957. Boundary layer wind maxima and their significance for the growth of nocturnal inversions. *Bulletin of the American Meteorological Society* 38: 283-290.
- Bonner, W. D. 1966. Case study of thunderstorm activity in relation to the low-level jet. *Monthly Weather Review* 94: 167–78.
- Bonner, W. D. 1968. Climatology of the low-level jet. *Monthly Weather Review* 96: 833–50.
- Bradshaw, L. S., J. E. Deeming, R. E. Burgan, and J. D. Cohen. 1984. The 1978 National Fire Danger Rating system: technical documentation. USDA Forest Service General Technical Report INT-169, U.S. Department of Agriculture, Forest Service, Intermountain Forest and Range Experiment Station, Ogden, UT.
- Brown, T., B. Hall, and A. Westerling. 2004. The impact of twenty-first century climate change on wildland fire danger in the western United States: an applications perspective. *Climatic Change* 62: 365–388.
- Bukovsky M. S., D. J. Gochis, and L.O. Mearns. 2013. Toward assessing NARCCAP regional climate model credibility for the North American Monsoon: Current Climate simulations. *Journal of Climate* 26: 8802-8826.
- Bukovsky M.S. 2012. Temperature trends in the NARCCAP regional climate models. *Journal of*

Climate 25: 3985-3991.

Carr F. H., and J. P. Millard. 1985. A composite study of comma clouds and their association with severe weather over the Great Plains. *Monthly weather review* 113: 370-387.

Carter, T. R., E. L. La Rovere, R. N. Jones, R. Leemans, L. O. Mearns, N. Nakicenovic, ... & J. Skea. 2001. Developing and applying scenarios. In: McCarthy, J. J., O. F. Canziani, N. A. Leary, D. J. Dokken, and K. S. White ed. *Climate change 2001: impacts, adaptation, and vulnerability. Contribution of Working Group II to the Third Assessment Report of the Intergovernmental Panel on Climate Change*. Cambridge: Cambridge University Press: 145–190.

Castro, C. L., R. A. Pielke, and G. Leoncini. 2005. Dynamical downscaling: Assessment of value retained and added using the Regional Atmospheric Modeling System (RAMS). *Journal of Geophysical Research: Atmospheres* (1984–2012) 110.D5.

Caya, D., and R. Laprise. 1999. A semi-implicit semi-Lagrangian regional climate model: The Canadian RCM. *Monthly Weather Review* 127: 341–362.

Cerezo-Mota, R., M. Allen, and R. Jones. 2011. Mechanisms controlling precipitation in the northern portion of the North American monsoon. *Journal of Climate* 24: 2771-2783. doi: <http://dx.doi.org/10.1175/2011JCLI3846.1>.

Challinor, A. J. and T. R. Wheeler. 2008. Crop yield reduction in the tropics under climate change: processes and uncertainties. *Agricultural and Forest Meteorology* 148: 343 - 356.

Charney J. J., X. Bian, B. E. Potter, and W. E. Heilman. 2003. Low level jet impacts on fire evolution in the Mack Lake and other severe wildfires. *Proceedings, 5th Symposium on fire and forest meteorology*. American Meteorological Society: Boston, USA.

Chavas, D. R., R. C. Izaurralde, A. M. Thomson, and X. Gao. 2009. Long-term climate change impacts on agricultural productivity in eastern China. *Agricultural and Forest Meteorology* 149: 1118-1128.

Collins, W. D., C. M. Bitz, M. L. Blackmon, G. B. Bonan, C. S. Bretherton, J. A. Carton, P. Chang, S. C. Doney, J. J. Hack, T. B. Henderson, J. T. Kiehl, W. G. Large, D. S. McKenna, B. D. Santer, R. D. Smith. 2006. The Community Climate System Model: CCSM3. *Journal of Climate* 19: 2122-2143.

Collins, M., R. Knutti, J. Arblaster, J. L. Dufresne, T. Fichefet, P. Friedlingstein, X. Gao, W. J. Gutowski, T. Johns, G. Krinner, M. Shongwe, C. Tebaldi, A. J. Weaver, and M. Wehner. 2013. Long-term Climate Change: Projections, Commitments and Irreversibility. In: *Climate Change 2013: The Physical Science Basis. Contribution of Working Group I to the Fifth Assessment Report of the Intergovernmental Panel on Climate Change*. Stocker, T. F., D. Qin, G. K. Plattner, M. Tignor, S. K. Allen, J. Boschung, A. Nauels, Y. Xia, V. Bex and P. M. Midgley (eds.). Cambridge University Press, Cambridge, United Kingdom and New York, NY, USA.

Cook K. H., and E. K. Vizzy. 2010. Hydrodynamics of the Caribbean low-level jet and its relationship to precipitation. *Journal of Climate* 23: 1477-1494.

Cook, K. H., E. K. Vizy, Z. S. Launer, and C. M. Patricola. 2008. Springtime Intensification of the Great Plains Low-Level Jet and Midwest Precipitation in GCM Simulations of the Twenty-First Century. *Journal of Climate* 21: 6321–6340.

Croft, P. J., M. Watts, and B. E. Potter. 2001. The analysis of the Haines Index climatology for the eastern United States, Alaska, Hawaii, and Puerto Rico. In 'Fourth Symposium on Fire and Forest Meteorology', Paper No. 8.7. American Meteorological Society, Boston, MA.

Davis R. E., B. P. Hayden, D. A. Gay, W. L. Phillips, and G. V. Jones. 1997. The North Atlantic Subtropical Anticyclone. *Journal of Climate* 10: 728-744.

Dayananda, P.W.A. 1977. Stochastic models for forest fires. *Ecological Modelling* 3: 309-313.

De Groot, W. J., 1988. Interpreting the Canadian Forest Fire Weather Index (FWI) System. In Proc. of Fourth Central Region Fire Weather Committee Scientific and Technical Seminar, Edmonton, Canada.

Deeming, J. E., R. E. Burgan, and J. D. Cohen. 1977. The National Fire-Danger Rating System. The National Fire-Danger Rating System – 1978, General Technical Report INT-39, Intermountain Forest and Range Experiment Station, U.S. Department of Agriculture, Forest Service, Ogden, UT.

Di Luca, Alejandro, R. de Elía, and R. Laprise. 2012. Potential for added value in precipitation simulated by high-resolution nested regional climate models and observations. *Climate dynamics* 38: 1229-1247.

Diaconescu E. P., R. Laprise. 2013. Can added value be expected in RCM-simulated large scales? *Climate Dynamics* 41: 1769-1800.

Diallo I., M. B. Sylla, F. Giorgi, et al. 2012. Multimodel GCM-RCM ensemble-based projections of temperature and precipitation over West Africa for the early 21st century. *International Journal of Geophysics: Article ID 972896*.

Doubler D. L., J. A. Winkler, X. Bian, S. Zhong, and C.K. Walters. 2015. A NARR-derived climatology of southerly and northerly low-level jets over North America and coastal environs. *Journal of Applied Meteorology and Climatology*. In Press

Doubler, D. L., 2013. A NARR derived low-level jet climatology over North America, Michigan State University.

Du Y., and R. Rotunno. 2014. A simple analytical model of the nocturnal low-level jet over the Great Plains of the United States. *Journal of the Atmospheric Sciences* 71: 3674-3683.

Feser, F., B. Rockel, H. von Storch, J. Winterfeldt, and M. Zahn. 2011. Regional climate models add value to global model data: a review and selected examples. *Bulletin of the American Meteorological Society* 92: 1181-1192.

Fischer, G., M. Shah, F. N. Tubiello, and H. Van Velhuizen. 2005. Socio-economic and climate

change impacts on agriculture: an integrated assessment, 1990–2080. *Philosophical Transactions of the Royal Society B: Biological Sciences* 360: 2067-2083.

Flannigan, M. D., B. J. Stokes, and B. M. Wotton. 2000. Forest fires and climate change. *The Science of the Total Environment* 262: 221-229.

Flannigan, M. D., K. A. Logan, B. D. Amiro, W. R. Skinner, and B. J. Stocks. 2005. Future area burned in Canada. *Climate Change* 72: 1-16.

Flannigan, M. D., M. A. Krawchuk, W. J. de Groot, B. M. Wotton, and L. M. Gowman. 2009. Implications of changing climate for global wildland fire. *International Journal of Wildland Fire* 18: 483-507.

Flato, G. M. 2005. The third generation coupled global climate model (CGCM3). <http://www.ec.gc.ca/ccmac-cccma/default.asp?n=1299529F-1> (last accessed 29 October 2013)

Fosberg M. A.. 1978, Weather in wildland fire management: The Fire Weather Index, Conference on Sierra Nevada Meteorology. American Meteorological Society, Lake Tahoe, CA.

Ghan, S. J., X. Bian, and L. Corsetti. 1996. Simulation of the Great Plains Low-Level Jet and Associated Clouds by General Circulation Models. *Monthly Weather Review* 124: 1388–1408.

Gillies R. R., and T. N. Carlson. 1995. Thermal remote sensing of surface soil water content with partial vegetation cover for incorporation into climate models. *Journal of Applied Meteorology* 34: 745-756.

Giorgi, F. 2006. Regional climate modeling: status and perspectives. *Journal de Physique IV France* 139: 101–118.

Golding, N., and R. Betts. 2008. Fire risk in Amazonia due to climate change in the HadCM3 climate model: Potential interactions with deforestation. *Global Biogeochemical Cycles* 22: GB4007.

Goodrick S. L. 2002. Modification of the Fosberg fire weather index to include drought. *International Journal of Wildland Fire* 11: 205–211.

Gordon, C., C. Cooper, C. A. Senior, H. Banks, J. M. Gregory, T. C. Johns, J. F. B. Mitchell, and R. A. Wood. 2000. The simulation of SST, sea ice extents and ocean heat transports in a version of the Hadley Centre coupled model without flux adjustments. *Climate Dynamics* 16:147-168.

Grell, G. A. and D. Devenyi. 2002. A generalized approach to parameterizing convection combining ensemble and data assimilation techniques. *Geophysical Research Letters* 29: 1693-1697.

Haines D. A, W. A. Main, J. S. Frost, and A. J. Simard, 1983. Fire-danger rating and wildfire occurrence in the Northeastern United States. *Forest Science* 29: 679–696.

Haines, D. 1988. A lower atmosphere severity index for wildlife fires. *Fire Weather* 13: 23-27.

- Hayhoe, K., D. Cayan, C. B. Field, P. C. Frumhoff, E. P. Maurer, N. L. Miller, et al.. 2004. Emissions pathways, climate change, and impacts on California. *Proceedings of the National Academy of Sciences of the United States of America* 101: 12422-12427.
- Haylock, M.R., N. Hofstra, A.M.G. Klein Tank, E.J. Klok, P.D. Jones, M. New. 2008: A European daily high-resolution gridded dataset of surface temperature and precipitation. *J. Geophys. Res (Atmospheres)*, 113, D20119, doi:10.1029/2008JD10201
- Heilman, W. E., and X. Bian. 2007. Combining turbulent kinetic energy and Haines Index predictions for fire-weather assessments. In ‘Proceedings of the 2nd Fire Behavior and Fuels Conference’, 159-172. Rocky Mountain Research Station, Fort Collins, CO, US: USDA Forest Service Proceedings RMRS-P-46CD.
- Helfand, H. M., and S. D. Schubert. 1995. Climatology of the simulated Great Plains low-level jet and its contributions to the continental moisture budget of the United States. *Journal of Climate* 8: 784–806.
- Hewitt, C. D. 2005. The ENSEMBLES Project: Providing ensemble-based predictions of climate changes and their impacts. *EGGS newsletter* 13: 22-25.
- Higgins R. W., Y. Yao, E. S. Yarosh, J. E. Janowiak, and K. C. Mo. 1997: Influence of the Great Plains Low-Level Jet on Summertime Precipitation and Moisture Transport over the Central United States. *J. Climate*, 10, 481–507.
- Holton J. R. 1967. The diurnal boundary layer wind oscillation above sloping terrain. *Tellus* 19: 199-205. doi: 10.1111/j.2153-3490.1967.tb01473.x.
- Jones, K. M., C. Maxwell. 1998. A seasonal Haines Index climatology for New Mexico and the significance of its diurnal variations in the elevated Southwest. In ‘Preprints, Second Conference on Fire and Forest Meteorology’, 127-130. American Meteorological Society, Phoenix, AZ.
- Jones, R. G., M. Noguer, D. C. Hassell, D. Hudson, S. S. Wilson, G. J. Jenkins, and J. F. B. Mitchell. 2004. Generating high resolution climate change scenarios using PRECIS. *Met Office Hadley Centre, Exeter, UK*, pp 35.
- Jones, R., S. Wilson. 2002. Hadley Centre for Climate Prediction and Research, PRECIS, Providing Regional Climates for Impact Studies. The Hadley Centre regional climate modelling system, UK, 124–135.
- Kanamitsu M, W. Ebisuzaki, J. Woollen, S.-K. Yang, J. J. Hnilo, M. Fiorino, and G. L. Potter. 2002. NCEP–DOE AMIP-II Reanalysis (R-2). *Bulletin of the American Meteorological Society* 83: 1631–1643. doi: <http://dx.doi.org/10.1175/BAMS-83-11-1631>.
- Kapela, A. F., P. W. Leftwich, and R. Van Ess. 1995. Forecasting the impacts of strong wintertime post-cold front winds in the Northern Plains. *Weather and Forecasting* 10: 229–44.
- Katz, R. W., and B. G. Brown. 1992. Extreme events in a changing climate: variability is more important than averages. *Climatic change* 21: 289-302.

- Keetch, J. J., and G. Byram. 1968 (Revised 1988). A drought index for forest fire control. Research Paper SE-38, U.S. Department of Agriculture, Forest Service, Southeastern Forest Experiment Station, Asheville, NC.
- Kim J., D. E. Waliser, C. A. Mattmann, et al. 2014. Evaluation of the CORDEX-Africa multi-RCM hindcast: systematic model errors. *Climate dynamics* 42: 1189-1202.
- Knapp, E. E., B. L. Estes, and C. N. Skinner. 2009. Ecological Effects of Prescribed Fire Season: A Literature Review and Synthesis for Managers. General Technical Report no. PSW-GTR-224, Pacific Southwest Research Station. U.S. Department of Agriculture, Forest Service, Pacific Southwest Research Station, Albany, CA.
- Knox, J. W., J. A. Rodríguez Díaz, D. J. Nixon, and M. Mkhwanazi. 2010. A preliminary assessment of climate change impacts on sugarcane in Swaziland. *Agricultural Systems* 103: 63-72.
- Kochtubajda, B., M. D. Flannigan, J. R. Gyakum, and R. E. Stewart. 2001. The influence of atmospheric instability on fire behavior in the Northwest Territories, Canada. In 'Fourth Symposium on Fire and Forest Meteorology', 225-232. American Meteorological Society, Reno, NV. Boston, MA.
- Kushnir Y, W.A. Robinson, I. Bladé, et al. Atmospheric GCM response to extratropical SST anomalies: synthesis and evaluation. *Journal of Climate*, 2002, 15(16): 2233-2256.
- Laprise, R., D. Caya, M. Giguère, G. Bergeron, H. Côté, J.-P. Blanchet, G. J. Boer, and N. McFarlane. 1998. Climate and climate change in western Canada as simulated by the Canadian Regional Climate Model. *Atmosphere-Ocean* 36: 119–167.
- Laux, P., G. Jäckel, R. M. Tingem, and H. Kunstmann. 2010. Impact of climate change on agricultural productivity under rainfed conditions in Cameroon—a method to improve attainable crop yields by planting date adaptations. *Agricultural and Forest Meteorology* 150: 1258-1271.
- Lhomme, J. P., R. Mougou, M. Mansour. 2009. Potential impact of climate change on durum wheat cropping in Tunisia. *Climatic Change* 96: 549-564.
- Li B., S. Sain, L. O. Mearns, H. A. Anderson, S. Kovats, K. L. Ebi, M. Y. V. Bekkedal, M. S. Kanared, and J. A. Patz. 2012. The impact of extreme heat on morbidity in Milwaukee, Wisconsin. *Climatic Change* 110: 959–76.
- Li X., Z. Lv, J. Hu, B. Zhang, L. Shi, and S. Feng. 2015. XEarth: A 3D GIS platform for managing massive city information. *Computational Intelligence and Virtual Environments for Measurement Systems and Applications*. IEEE International Conference on. IEEE: 1-6.
- Li, Y., W. Ye, M. Wang, and X. Yan. 2009. Climate change and drought: a risk assessment of crop-yield impacts. *Climate research* 39: 31-46.
- Liang X. Z., L. Li, K.E. Kunkel, M. Ting, and J. X. L. Wang. 2004. Regional climate model simulation of US precipitation during 1982-2002. Part I: Annual cycle. *Journal of Climate* 17:

3510-3529.

Liu, J., V. Hull, M. Batistella, R. DeFries, T. Dietz, F. Fu, T. W. Hertel, et al. 2013. Framing sustainability in a telecoupled world. *Ecology and Society* 18: 26.

Liu X., J. Han, Y. Zhong, et al. 2009. Implementing WebGIS on Hadoop: A case study of improving small file I/O performance on HDFS. *Cluster Computing and Workshops. IEEE International Conference on. IEEE*: 1-8.

Liu, Y., J. A. Stanturf, and S. L. Goodrick. 2010. Trends in global wildfire potential in a changing climate. *Forest Ecology and Management* 259: 685-697.

Liu, Y., S. L. Goodrick, and J. A. Stanturf. 2013. Future U.S. wildfire potential trends projected using a dynamically downscaled climate change scenario. *Forest Ecology and Management* 294: 120-135.

Lu, W., J. Charney, S. Zhong, X. Bian, and S. Liu. 2011. A North American regional reanalysis climatology of the Haines Index. *International Journal of Wildland Fire* 20: 91-103.

Luo, L., Y. Tang, S. Zhong, X. Bian, and W. E. Heilman. 2013. Will Future Climate Favor More Erratic Wildfires in the Western United States? *Journal of Applied Meteorology Climatology* 52: 2410–2417.

Mall, R. K., M. Lal, V. S. Bhatia, L. S. Rathore, and R. Singh. 2004. Mitigating climate change impact on soybean productivity in India: a simulation study. *Agricultural and forest meteorology* 121: 113-125.

Mandallaz, D., and R. Ye, 1997. Prediction of forest fires with Poisson models. *Canadian Journal of Forest Research*, 27, 1685-1694.

Maraun, D., F. Wetterhall, A. M. Ireson, et al. 2010. Precipitation downscaling under climate change: recent developments to bridge the gap between dynamical models and the end user. *Reviews of Geophysics*, 48: RG3003.

McCaw L., P. Marchetti, G. Elliott, and G. Reader. 2007. Bushfire weather climatology of the Haines Index in south-western Australia. *Australian Meteorological Magazine* 56: 75–80.

McKenzie D., Z. Gedalof, D. Peterson, and P. Mote. 2004. Climate change, wildfire, and conservation. *Conservation Biology* 18: 890-902.

Means, L. L. 1954. A study of the mean southerly wind maximum in low levels associated with a period of summer precipitation in the Middle West. *Bulletin of the American Meteorological Society* 35: 166–170.

Mearns L. O., W. J. Gutowski, R. Jones, L. Leung, S. McGinnis, A. M. B. Nunes, Y. Qian. 2009. A regional climate change assessment program for North America. *EOS* 90: 311-312.

Mearns L.O., D.P. Lettenmaier, S. McGinnis. 2015. Uses of Results of Regional Climate Model

Experiments for Impacts and Adaptation Studies: the Example of NARCCAP. *Current Climate Change Reports* 1: 1-9..

Mearns, L. O., R. Arritt, S. Biner, M. Bukovsky, S. Sain, D. Caya, D. Flory, W. Gutowski, R. Jones, W. Moufouma-Okia, R. Leung, Y. Qian, S. McGinnis, L. McDaniel, A. Nunes, J. Roads, L. Sloan, M. Snyder, G. Takle, and R. Laprise. 2012. The North American Regional Climate Change Assessment Program: Overview of Phase I Results. *Bulletin of the American Meteorological Society* 93: 1337-1362.

Mearns, L. O., W. J. Gutowski, R. Jones, L. Leung, S. McGinnis, A. M. B. Nunes, and Y. Qian. 2009. A regional climate change assessment program for North America. *EOS* 90: 311-312.

Mearns, L.O., et al. 2007 (updated 2012). The North American Regional Climate Change Assessment Program dataset, National Center for Atmospheric Research Earth System Grid data portal, Boulder, CO. [doi:10.5065/D6RN35ST] (last accessed 29 October 2013)

Mearns, L.O., F. Giorgi, P. Whetton, D. Pabon, M. Hulme, and M. Lal. 2003. Guidelines for Use of Climate Scenarios Developed from Regional Climate Model Experiments. Intergovernmental Panel on Climate Change Task Group on Data and Scenario Support for Impact and Climate Assessment (TGICA).

Mesinger F., G. DiMego, E. Kalnay, K. Mitchell, P.C. Shafran, W. Ebisuzaki, D. Jovic, J. Woollen, E. Rogers, E.H. Berbery, M. B. Ek, Y. Fan, R. Grumbine, W. Higgins, H. Li, Y. Lin, G. Manikin, D. Parrish, W. Shi. 2006. North American regional reanalysis. *Bulletin of the American Meteorological Society* 87: 343-360.

Millar, C. I., N. L. Stephenson, and S. L. Stephens. 2007. Climate change and forests of the future: Managing in the face of uncertainty. *Ecological Applications* 17: 2145-2151.

Mitchell M.J., R.W. Arritt, and K. Labas. 1995. A climatology of the warm season Great Plains low-level jet using wind profiler observations. *Weather and Forecasting* 10: 576-591.

Mo, K. C., M. Chelliah, M.L. Carrera, R.W. Higgins, and W. Ebisuzaki. 2005. Atmospheric moisture transport over the United States and Mexico as evaluated in the NCEP regional reanalysis. *Journal of Hydrometeorology* 6: 710-728.

Moss, R. H., J. A. Edmonds, K. A. Hibbard, et al. 2010. The next generation of scenarios for climate change research and assessment. *Nature* 463: 747-756.

Nakicenovic, N., J. Alcamo, G. Davis, H.J.M. de Vries, J. Fenhann, S. Gaffin, K. Gregory, A. Grubler, T.Y. Jung, T. Kram, E.L. La Rovere, L. Michaelis, S. Mori, T. Morita, W. Papper, H. Pitcher, L. Price, K. Riahi, A. Roehrl, H-H. Rogner, A. Sankovski, M. Schlesinger, P. Shukla, S. Smith, R. Swart, S. van Rooijen, N. Victor, and Z. Dadi. 2000. Special report on emissions scenarios: a special report of Working Group III of the Intergovernmental Panel on Climate Change. Cambridge, UK: Cambridge University Press.

National Interagency Fire Center, 2013. Total Wildland Fires and Acres (1960-2012). http://www.nifc.gov/fireInfo/fireInfo_stats_totalFires.html (last accessed 29 October 2013)

NOAA (National Oceanic and Atmospheric Administration). 2014. Terms Commonly used in fire weather forecast. <http://www.erh.noaa.gov/okx/glossary.html>(last accessed 18 February 2014).

Olesen, J. E., T. R. Carter, C. H. Diaz-Ambrona, et al. 2007. Uncertainties in projected impacts of climate change on European agriculture and terrestrial ecosystems based on scenarios from regional climate models. *Climatic Change* 81: 123-143.

Pal, J. S., F. Giorgi, X. Bi, et al. 2007. The ICTP RegCM3 and RegCNET: Regional climate modeling for the developing world. *Bulletin of the American Meteorological Society*88: 1395-1409.

Parisien, M. A., V. Kafka, N. Flynn, K. G. Hirsch, J. B. Todd, and M. D. Flannigan. 2005. Fire behavior potential in central Saskatchewan under predicted climate change. PARC Summary Document 05-01, PARC (Prairie Adaptation Research Collaborative), Regina, Saskatchewan.

Parker, W. S.. 2013. Ensemble modeling, uncertainty and robust predictions. *Wiley Interdisciplinary Reviews: Climate Change* 2013: 213-223.

Patz J. A., D. Campbell-Lendrum, T. Holloway, et al. 2005. Impact of regional climate change on human health. *Nature* 438: 310-317.

Peel J. L., R. Haeuber, V. Garcia, et al. 2013. Impact of nitrogen and climate change interactions on ambient air pollution and human health. *Biogeochemistry* 114: 121-134.

Pielke, R. A., W. R. Cotton, R. L. Walko, C. J. Tremback, W. A. Lyons, L. D. Grasso, M. E. Nicholls, M. D. Moran, D. A. Wesley, T. J. Lee, and J. H. Copeland. 1992. A comprehensive meteorological modeling system — RAMS. *Meteorology and Atmospheric Physics* 49: 69–91.p

Pitchford, K. L., and J. London. 1962. The low-level jet as related to nocturnal thunderstorms over Midwest United States. *Journal of Applied Meteorology* 1: 43–47.

Pitman, A. J., G. T. Narisma, and J. McAneney. 2007. The impact of climate change on the risk of forest and grassland fires in Australia. *Climate Change* 84: 383-401.

Porter, J. R., L. Xie, A. J. Challinor, K. Cochrane, S. M. Howden, M. M. Iqbal, D. B. Lobell, and M. I. Travasso. 2014. Food security and food production systems. In: *Climate Change 2014: Impacts, Adaptation, and Vulnerability. Part A: Global and Sectoral Aspects. Contribution of Working Group II to the Fifth Assessment Report of the Intergovernmental Panel on Climate Change*. Field, C.B., V.R. Barros, D.J. Dokken, K.J. Mach, M.D. Mastrandrea, T.E. Bilir, M. Chatterjee, K.L. Ebi, Y.O. Estrada, R.C. Genova, B. Girma, E.S. Kissel, A.N. Levy, S. MacCracken, P.R. Mastrandrea, and L.L. White (eds.). Cambridge University Press, Cambridge, United Kingdom and New York, NY, USA, pp. 485-533.

Preisler, H. K., and A. L. Westerling. 2007. Statistical model for forecasting monthly large wildfire events in Western United States. *Journal of Applied Meteorology and Climatology* 46: 1020–1030.

Preisler, H. K., D. R. Brillinger, R. E. Burgan, and J. W. Benoit. 2004. Probability based models for estimating wildfire risk. *International Journal of Wildland Fire* 13: 133-142.

Qiao L., Z. Pan, R. B. Herrmann, and Y. Hong. 2014. Hydrological variability and uncertainty of lower Missouri river basin under changing climate. *Journal of the American Water Resources Association* 50: 246–60.

Randall, D. A., R.A. Wood, S. Bony, R. Colman, T. Fichefet, J. Fyfe, V. Kattsov, A. Pitman, J. Shukla, J. Srinivasan, R. J. Stouffer, A. Sumi, and K. E. Taylor. 2007. Climate Models and Their Evaluation. In: *Climate Change 2007: The Physical Science Basis. Contribution of Working Group I to the Fourth Assessment Report of the Intergovernmental Panel on Climate Change*. Solomon, S., D. Qin, M. Manning, Z. Chen, M. Marquis, K. B. Averyt, M. Tignor and H. L. Miller (eds.). Cambridge University Press, Cambridge, United Kingdom and New York, NY, USA.

Richter, G. M., and M. A. Semenov. 2005. Modelling impacts of climate change on wheat yields in England and Wales: assessing drought risks. *Agricultural Systems* 84: 77-97.

Rosenzweig C., J. Elliott, D. Deryng, et al. 2014. Assessing agricultural risks of climate change in the 21st century in a global gridded crop model intercomparison. *Proceedings of the National Academy of Sciences* 111: 3268-3273.

Ruane, A. C., L. D. Cecil, R. M. Horton, R. Gordón, R. McCollum, et al. 2013. Climate change impact uncertainties for maize in Panama: Farm information, climate projections, and yield sensitivities. *Agricultural and Forest Meteorology* 170: 132-145.

Salathe, E. P., P. W. Mote, and M. W. Wiley. 2007. Review of scenario selection and downscaling methods for the assessment of climate change impacts on hydrology in the United States Pacific Northwest. *International Journal of Climatology* 27: 1611-1621.

Schlenker, W., and D. B. Lobell. 2010. Robust negative impacts of climate change on African agriculture. *Environmental Research Letters*, 5: 014010.

Schmidt, G. A., R. Ruedy, J. E. Hansen, I. Aleinov, N. Bell, M. Bauer, S. Bauer, B. Cairns, V. Canuto, Y. Cheng, A. Del Genio, G. Faluvegi, A. D. Friend, T. M. Hall, Y. Hu, M. Kelley, N. Y. Kiang, D. Koch, A. A. Lacis, J. Lerner, K. K. Lo, R. L. Miller, L. Nazarenko, V. Oinas, Ja. Perlwitz, Ju. Perlwitz, D. Rind, A. Romanou, G.L. Russell, Mki. Sato, D. T. Shindell, P. H. Stone, S. Sun, N. Tausnev, D. Thresher, and M. Yao. 2006. Present day atmospheric simulations using GISS ModelE: Comparison to in-situ, satellite and reanalysis data. *Journal of Climate* 19: 153-192.

Semenov, M. A. 2009. Impacts of climate change on wheat in England and Wales. *Journal of the Royal Society Interface* 6. 33: 343-350.

Singh, A. K., R. Tripathy, and U. K. Chopra. 2008. Evaluation of CERES-Wheat and CropSyst models for water–nitrogen interactions in wheat crop. *Agricultural Water Management* 95: 776-786.

- Sjostedt, D. W., J. T. Sigmon, and S. J. Colucci. 1990. The Carolina nocturnal low-level jet: Synoptic climatology and a case study. *Weather and Forecasting* 5: 404–15.
- Skamarock, W. C., J. B. Klemp, J. Dudhia, D. O. Gill, D. M. Barker, W. Wang, and J. G. Powers. 2005. A description of the Advanced Research WRF Version 2, NCAR Tech Notes-468+STR, National Center for Atmospheric Research, Boulder, Colorado.
- Song, J., K. Liao, R. L. Coulter, and B. M. Lesht. 2005. Climatology of the low-level jet at the southern Great Plains atmospheric boundary layer experiments site. *Journal of Applied Meteorology* 44: 1593–606.
- Spracklen, D. V., L. J. Mickey, J. A. Logan, R. C. Hudman, R. Yevich, M. D. Flannigan, and A. L. Westerling. 2009. Impacts of climate change from 2000 to 2050 on wildfire activity and carbonaceous aerosol concentrations in the western United States. *Journal of Geophysical Research* 114: D20301.
- Stanton, J. C., R. G. Pearson, N. Horning, P. Ersts, and H. ReşitAkçakaya. 2012. Combining static and dynamic variables in species distribution models under climate change. *Methods in Ecology and Evolution* 3: 349–357.
- Stensrud, D. J. 1996. Importance of low-level jets to climate: A review. *Journal of Climate* 9: 1698–1711.
- Storm, B., J. Dudhia, S. Basu, A. Swift, and I. Giammanco. 2009. Evaluation of the Weather Research and Forecasting model on forecasting low-level jets: implications for wind energy. *Wind Energy* 12: 81-90.
- Takle E. S., M. Jha, E. Lu, R.W. Arritt, and W.J. Gutowski. 2010. Streamflow in the upper Mississippi river basin as simulated by SWAT driven by 20th Century contemporary results of global climate models and NARCCAP regional climate models. *MeteorologischeZeitschrift* 19: 341-346.
- Taylor, K. E., R. J. Stouffer, and G. A. Meehl. 2012. An Overview of CMIP5 and the experiment design. *Bulletin of the American Meteorological Society* 93: 485-498.
- Thiemeßl, M. J., A. Gobiet, and G. Heinrich. 2012. Empirical-statistical downscaling and error correction of regional climate models and its impact on the climate change signal. *Climatic Change* 112: 449-468.
- Thornton, P. K., P. G. Jones, G. Alagarswamy, and J. Andresen. 2009. Spatial variation of crop yield response to climate change in East Africa. *Global Environmental Change* 19: 54-65.
- Thornton P. K., P. J. Ericksen, M. Herrero, et al. Climate variability and vulnerability to climate change: a review. *Global change biology* 20: 3313-3328.
- Todd, M. C., R. Washington, S. Raghavan, et al. 2008. Regional model simulations of the Bodélé low-level jet of northern Chad during the Bodélé Dust Experiment (BoDEx 2005). *Journal of Climate* 21: 995-1012.

Trouet, V., A. H. Taylor, A. M. Carleton, and C. N. Skinner. 2009. Interannual variations in fire weather, fire extent, and synoptic-scale circulation patterns in northern California and Oregon. *Theoretical and Applied Climatology* 95: 349-360.

Tubiello, F. N., J. F. Soussana, and S. M. Howden. 2007. Crop and pasture response to climate change. *Proceedings of the National Academy of Sciences* 104: 19686-19690.

Uccellini L.W., and D. R. Johnson. 1979. Coupling of upper and lower tropospheric jet streaks and implications for the development of severe convective storms. *Monthly Weather Review* 107: 682-703.

MLA

Van Vuuren, D. P., et al. 2011. The representative concentration pathways: an overview. *Climatic change* 109: 5-31.

Van Wagner, C. E., 1970. New development in forest fire danger rating. Canada Department of Fisheries and Forestry, Canadian Forest Service, Petawawa Forest Experiment Station, Information Report PS-X-19. Chalk River, ON.

Vanderwende, B. J., J. K. Lundquist, M. E. Rhodes, E. S. Takle, and S. L. Irvin. 2015. Observing and Simulating the Summertime Low-Level Jet in Central Iowa. *Monthly Weather Review* 143: 2319–2336.

Vinukollu R. K., E. F. Wood, C. R. Ferguson, et al. 2011. Global estimates of evapotranspiration for climate studies using multi-sensor remote sensing data: Evaluation of three process-based approaches. *Remote Sensing of Environment* 115: 801-823.

Wahid, A., S. Gelani, M. Ashraf, and M. R. Foolad. 2007. Heat tolerance in plants: an overview. *Environmental and Experimental Botany* 61: 199-223.

Walters C. K., J. A. Winkler, S. Husseini, R. Keeling, J. Nikolic, and S. Zhong. 2014. Low-level jets in the North American Regional Reanalysis (NARR): a comparison with rawinsonde observations. *Journal of Applied Meteorology and Climatology* 53: 2093–2113.

Walters C. K. 2001. Airflow configurations of warm season southerly low-level wind maxima in the Great Plains. Part II: The synoptic and subsynoptic-scale environment. *Weather and Forecasting* 16: 531-551.

Walters, C. K., J. A. Winkler, R. P. Shadbolt, J. van Ravensway, and G. D. Bierly. 2008. A Long-Term Climatology of Southerly and Northerly Low-Level Jets for the Central United States. *Annals of the Association of American Geographers* 98: 521-552.

Watanabe, T., and H. Seino. 1991. Correlation between the immigration area of rice planthoppers and the low-level jet stream in Japan. *Applied entomology and zoology* 26: 457-462.

Werth D., R. Kurzeja, N. L. Dias, G. Zhang, H. Duarte, M. Fischer, M. Parker, and M. Leclerc.

2011. The simulation of the southern Great Plains nocturnal boundary layer and the low-level jet with a high-resolution mesoscale atmospheric model. *Journal of Applied Meteorology and Climatology* 50: 1497-1513.

Werth, J., and P. Werth. 1998. Haines index climatology for the western United States. *Fire Management Notes* 58: 8–17.

Westerling, A., A. Gershunov, T. Brown, D. Cayan, and M. Dettinger. 2003. Climate and wildfire in the western United States. *Bulletin of the American Meteorological Society* 84: 595-604.

Whiteman, C.D., X. Bian, and S. Zhong. 1997. Low-level jet climatology from enhanced rawinsonde observations at a site in the southern Great Plains. *Journal of Applied Meteorology* 36: 1363-1376.

Wilby, R. L., and T. M. L. Wigley. 1997. Downscaling general circulation model output: a review of methods and limitations[J]. *Progress in Physical Geography*. 21: 530-548.

Williams, J. T. 2004. Managing fire-dependent ecosystems: we need a public lands policy debate. *Fire Management Today* 64: 6–11.

Wilson, S., D. Hassell, D. Hein, R. Jones, and R. Taylor. 2005. Installing and using the Hadley Centre regional climate modeling system PRECIS Version 1.3. Met Office Hadley Centre, Exeter, UK, pp 131.

Winkler, J. A. 2004. The impact of technology upon in situ atmospheric observations and climate science. In *Geography and Technology*, Brunn SD, Cutter SL, Harrington Jr. JW (ed). Springer: Netherlands, 461-490.

Winkler, J. A., B. E. Potter, D. F. Wilhelm, R. P. Shadbolt, K. Piromsopa, and X. Bian. 2007. Climatological and statistical characteristics of the Haines Index for North America. *International Journal of Wildland Fire* 16: 139–152.

Winkler, J. A., G. S. Guentchev, M. Liszewska, Perdinan, and P. Tan. 2011. Climate Scenario Development and Applications for Local/Regional Climate Change Impact Assessments: An Overview for the Non-Climate Scientist. *Geography Compass* 5: 301-328.

Winkler, J.A., R.W. Arritt, and S.C. Pryor. 2014. Climate projections for the Midwest: Availability, interpretation, and synthesis. In: *Climate Change in the Midwest: A Synthesis Report for the National Climate Assessment*, ed. J.A. Winkler, J.A. Andresen, J. Hatfield, D. Bidwell, and D. Brown, 37-63. Island Press: Washington, D.C.

Wood, A. W., L. R. Leung, V. Sridhar, and D. P. Lettenmaier. 2004. Hydrologic implications of dynamical and statistical approaches to downscaling climate model outputs. *Climatic change* 62: 189-216.

Wu Y, Raman S. 1998. The summertime Great Plains low level jet and the effect of its origin on moisture transport. *Boundary-Layer Meteorology* 88: 445-466. doi: 10.1023/A:1001518302649.

- Xiong, W., D. Conway, E. Lin, Y. Xu, H. Ju, J. Jiang, I. Holman, and Y. Li. 2009. Future cereal production in China: the interaction of climate change, water availability and socio-economic scenarios. *Global Environmental Change* 19: 34-44.
- Xiong, W., R. Matthews, I. Holman, et al. 2007. Modelling China's potential maize production at regional scale under climate change. *Climatic change* 85: 433-451.
- Xu, C. 1999. From GCMs to river flow: a review of downscaling methods and hydrologic modelling approaches. *Progress in Physical Geography* 23: 229-249.
- Yang, C., Z. Yu, Z. Hao, J. Zhang, and J. Zhu. 2012. Impact of climate change on flood and drought events in Huaihe River Basin, China. *Hydrology Research* 43: 14-22.
- Yao, F., Y. Xu, E. Lin, et al. 2007. Assessing the impacts of climate change on rice yields in the main rice areas of China. *Climatic Change* 80: 395-409.
- Zhang H., G. H. Huang, D. Wang, X. Zhang. 2011. Uncertainty assessment of climate change impacts on the hydrology of small prairie wetlands. *Journal of Hydrology* 396: 94-103. doi:10.1016/j.jhydrol.2010.10.037.
- Zhang, D. L., S. Zhang, S. J. Weaver. 2006. Low-level jets over the mid-Atlantic states: Warm-season climatology and a case study. *Journal of applied meteorology and climatology* 45: 194-209.
- Zhang, X. C. 2005. Spatial downscaling of global climate model output for site-specific assessment of crop production and soil erosion. *Agricultural and Forest Meteorology* 135: 215-229.
- Zhong, S., J. D. Fast, X. Bian. 1996. A case study of the Great Plains low-level jet using wind profiler network data a high-resolution mesoscale model. *Journal of Applied Meteorology* 124: 785-806.
- ZsoltTorma, C., F. Giorgi, and E. Coppola. 2015. Added value of regional climate modeling over areas characterized by complex terrain. *EGU General Assembly Conference Abstracts*: 709.